Universitat Politècnica de Catalunya

Modelling pathological effects in intracellular calcium dynamics leading to atrial fibrillation

Author:
Miquel Marchena

Supervisor:
Dr. Blas Echebarria

Doctoral program: Computational and applied physics
Department: Physics Department
Research group: Computational Biology and Complex Systems

A thesis submitted for the degree of
Doctor of Philosophy in *Physical Science*

Barcelona, June 2020

Abstract

Modelling pathological effects in intracellular calcium dynamics leading to atrial fibrillation

by Miquel MARCHENA

The beating of the heart is produced by the synchronization of the cardiac cells' contraction. A dysregulation in this mechanism often lies at the subcellular level, where calcium is the most important ion that controls the cell contraction. The regulation of calcium concentration is determined by the ryanodine receptors (RyR), i.e. calcium channels that connect the cytosol and the sarcoplasmic reticulum. RyRs open and close stochastically with calcium-dependent rates. The fundamental calcium release event is known as calcium spark, which refers to a local release of calcium through one or more RyRs. Thus, a deep knowledge on both the spatio-temporal characteristics of the calcium patterns and the role of the RyRs is crucial to understand the transition between healthy to unhealthy cells. The aim of this Thesis has been to study these changes at the submicron scale, which may induce the transition to Atrial Fibrillation (AF) in advanced stages. To address this issue, a subcellular mathematical model of an atrial myocyte has been developed and validated. The model includes the electro-physiological currents as well as the fundamental intracellular structures. The high resolution of the model has allowed the study of the spatio-temporal calcium features that arise from both stimulated and resting conditions. Simulations show the relevance of the assembly of RyRs into clusters, leading to the formation of macro-sparks for heterogeneous distributions. These macro-sparks may produce ectopic beats under pathophysiological conditions. The incorporation of RyR-modulators into the model produces a nonuniform spatial distribution of calcium sparks, a situation observed during AF. In this sense, calsequestrin (CSQ) has emerged as a key calcium buffer that modifies the calcium handling. The lack of CSQ produces an increase in the spark frequency and, during calcium overload, it also promotes the appearance of global calcium oscillations. Finally, I have also characterized the effect of detubulation, a common issue in cells with AF and heart failure. Thus, the present work represents a step forward in the understanding of the mechanisms leading to AF, with the development of computational models that, in the future, can be used to complement in vitro or in vivo studies, helping find therapeutic targets for this disease.

Keywords: calcium modeling, atrial cells, intracellular calcium signaling, calcium release unit, ryanodine receptor, atrial fibrillation

Acknowledgements

This PhD Thesis is the most recent work of a challenging adventure, which has been a truly life-changing experience for me and it would not have been possible to do without the support and guidance that I received from many people. It is difficult to list all the people that have walked with me in this journey because the memory is not always trustworthy. For that, I would like to start expressing all my gratitude to those who have intervened in this Thesis.

First and foremost I want to thank my advisor Prof. Blas Echebarria. I am extremely grateful to him for his valuable guidance, for his patience, persistence, dedication and immense expertise on cardiac modeling. He has a very wide knowledge including subcellular biophysics and accurate physical intuition. His scientific vision helped me in all the time of research always looking for the excellence. Without his careful and bright guidance, I could not have completed this work.

The next person whom I would like to thank is Dr. Leif Hove-Madsen at the Biomedical Research Institute Barcelona (CSIC-IIBB), at Hospital Sant Pau. He has been a source of inspiring knowledge in the experimental field that helped me to understand the biological mechanism involved in the subcellular cardiac contraction.

My sincere thanks to Prof. Yohannes Shiferaw, from the California State University in Northridge (CSUN), for the pleasant reception I received in the two visits that I did at the Physics Department of CSUN. He provided me an opportunity to join their team as an intern. I will not forget our daily strong meetings during those months which he gave me advice and encouragement.

In these years I have had the opportunity to work with Prof. Enric Alvarez-Lacalle. I really enjoyed the deep talks about calcium dynamics and biophysical modeling. I also would like to thank all the people of Physics Department at EPSEB, in particular for all the coworkers I have met during these years: Francesc, Martí, David, Eduardo, Miquel, Thomas and Gustavo.

Finally, without the support of all members of my family and my friends, I would never finish this Thesis and I would never find the courage to overcome all these difficulties during this work. I would like to thank to my sister Mireia, who has designed the cover of the Thesis. I would specially thank to my girlfriend, Marina. I am indebted with you for all your love and support.

Funding: The studies included in this PhD-Thesis were supported by the financial support provided by the Fundació La Marató de TV3, under grant number 20151110 that also provided funding for my PhD fellowship, and from the Spanish Ministerio de Economía y Competitividad (MINECO) under grant number SAF2014-58286-C2-2-R.

Preface

Preface

The heart is a complex multi-scale organ that pumps blood throughout the body by a coordinated contraction. The correct operation of the heart requires a carefully orchestrated activity across all the scales (from single cell to full tissue), which includes the establishment of synchronized behavior of the cardiac myocytes, from which different spatio-temporal patterns transiently arise.

The heart is, and will remain in the future, a crucial organ that determines the quality of life of the population. Cardiovascular diseases (CVD) are the leading cause of death in the developed world and account for about a third of all deaths [188, 1]. CVD may occur due to problems (1) in the veins or arteries (arteriosclerosis) and/or (2) in the disruption of the proper contraction of the ventricles and atria. These dysfunctions are associated with a number of arrhythmias (i.e., abnormal or irregular heart rhythm) including atrial (AF) and ventricular (VF) fibrillation and ventricular tachycardia (VT). CVDs are responsible for over 17.3 million deaths per year worldwide and are the leading causes of death in the world [205] (Fig. 1).

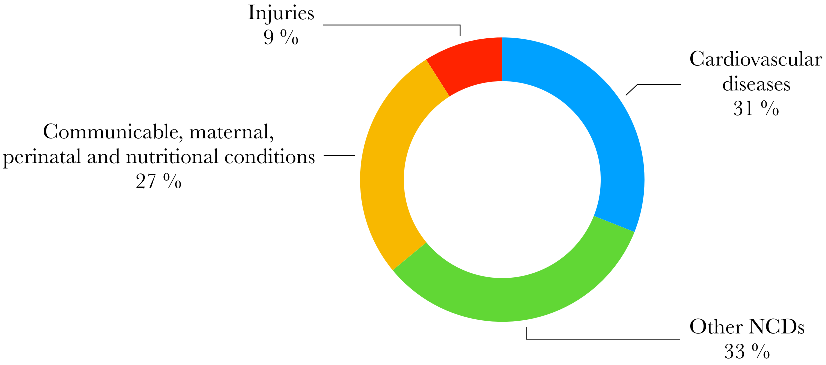

FIGURE 1: **Distribution of major causes of death including CVDs.** NCD: Noncommunicable Diseases. Data obtained from [188].

In this Thesis, I study a diverse range of structural and biochemical dysfunctions produced during AF, by means of different applications of a novel model developed on purpose. The model simulates a single cell by taking into account the calcium dynamics. The main motivation for modeling in cardiology is nicely summarized in a short introduction written by J. Jalife for a series of articles on recent advances in computational cardiology in the leading journal Circulation Research [129]: *"Of all the cardiac arrhythmias seen in clinical practice, atrial fibrillation (AF) and ventricular tachycardia/fibrillation (VT/VF) are among the leading causes of morbidity and mortality in the developed world. AF is the most common sustained arrhythmia and is associated with an increased risk of stroke, heart failure, dementia, and* *death. In developed nations overall prevalence of AF is 0.9% and the number of people affected is projected to more than double over the next 2 decades. VT/VF is the most important immediate cause of sudden cardiac death (SCD). Incidence of SCD is estimated to be 4 to 5 million cases per year worldwide. Thus, arrhythmias and SCD are among the most significant manifestations of cardiovascular diseases worldwide, but their underlying mechanisms remain elusive."*

Nowadays, the incorporation of available experimental data permits the development of detailed and realistic models of the heart at all scales: from a single membrane channel of a cell to the full heart dynamics. The adequate representation of the normal function of the heart and of various forms of CVDs presents big challenges for mathematical modeling and simulations. A second equally formidable task is the integration of largely different spatial and temporal scales in cardiac modeling. This is achieved by the development of powerful computers that allow us to improve resolution, increase the capability of prediction and enhance the accuracy of the results.

Structure of Thesis

The structure of the Thesis is the following: the main text is divided into four parts, each of which is in turn subdivided into several chapters. Part I introduces the biological framework of the Thesis (chapter 1) as well as the main models that have been developed previously by other authors (chapter 2). We dedicate part II to present a new model of calcium handling in atrial cells. In chapter 3 the cell geometry, fluxes and buffers are described highlighting their most important features. This part also incorporates the validation of the model with previous reported data (chapter 4). The model has been used to study several effects on calcium handling. All these applications are exposed in part III. In particular, the effect of size and distribution of the RyR2s clusters has been studied in chapter 5. The biochemical alterations produced during AF have been investigated in chapter 6. In chapter 7 I explain the consequences of detubulation in atrial cells, another modification produced during AF. Finally, in chapter 8 I analyze the appearance of calcium spontaneous oscillations in atrial cells from a theoretical point of view. In part IV, one can find the conclusions of the Thesis.

Regarding the chapters, they are short enough to be easy-to-read but still they hold self-consistent results. In this way, the reader can jump from one chapter to the other without losing the thread. However, reading them one after the other provides a more comprehensive overview of the subject. All chapters have the same inner structure. First, an introduction to the specific area of interest where a more broad framework is given to the reader. Second, one will find the material, method and analysis of the specific methodology developed to address that section. Third, the main results and finally the conclusions.

Contents

Abstract iii

Acknowledgements v

I Introduction 1

1 Physiology 3
- 1.1 Calcium-induced calcium release 4
- 1.2 Atrial Fibrillation 8

2 State of the art: models 11
- 2.1 Common-pool models 11
- 2.2 RyR2 models 13
- 2.3 Spatial models 14
- 2.4 Beyond the cell level 15
- 2.5 Motivation of the Thesis 16

II Methods 19

3 Subcellular calcium model 21
- 3.1 Geometry 21
- 3.2 Model equations 23
- 3.3 Calcium fluxes 23
  - 3.3.1 SR release flux 24
  - 3.3.2 LCC flux 26
  - 3.3.3 NaCa exchanger 27
  - 3.3.4 SERCA pump 27
- 3.4 Buffers 28
  - 3.4.1 Cytosolic buffers 28
  - 3.4.2 Fluorescence buffers 28
  - 3.4.3 Calsequestrin 28
- 3.5 Stochastic gating 30

4 Model validation 31
4.1 Stimulated cell 31
4.2 Calcium wave propagation 33
4.3 Spark analysis in non-paced cells 36
4.3.1 Spark properties 37
4.3.2 Characterization of the experimental noise 40

III Applications 45

5 Changes in CaRU size and distribution 47
5.1 Effects of cluster size and spatial distribution 47
5.2 Effects of a heterogeneous distribution of RyR2s per CaRU 50
5.2.1 Analysis 53
5.2.2 Results 55
5.3 Discussion 61

6 RyR2 activity modulators during AF 65
6.1 Calsequestrin 65
6.1.1 Methods 66
6.1.2 Results 68
6.2 Phosphorylation 70
6.2.1 Methods 70
6.2.2 Results 71
6.3 Effects of pathological conditions during AF 73
6.3.1 Discussion 76

7 Detubulation 79
7.1 Analysis 82
7.2 Results 82
7.2.1 Calcium transients 82
7.2.2 Inward propagation 86
7.2.3 Local dynamics 89
7.3 Discussion 92

8 Calcium oscillations 97
8.1 Materials and methods 98
8.1.1 Detailed subcellular calcium model 99
8.1.2 Reduced calcium model 99
8.2 Results 102
8.2.1 Results from the subcellular model 102
8.2.2 Minimal model without calsequestrin 105
8.2.3 Minimal model with calsequestrin 108
8.2.4 Robustness of the results 115
8.3 Discussion 118

IV Conclusions **121**

9 General conclusions **123**

10 Perspectives **127**

Bibliography **129**

V Appendixes **153**

A Model parameters **155**

B Deterministic compartment model of a CaRU **157**

List of Figures

1 Distribution of major causes of death including CVDs vii

1.1 Relation between action potential, calcium and contraction 5
1.2 Experimental RyR2 distribution 6
1.3 Basic components of the calcium cycle process 7
1.4 Ventricular vs. atrial myocytes 8
1.5 Diastolic Ca^{2+}-handling abnormalities underlie DADs 10

2.1 Different types of RyR2 models 14
2.2 Outline of the main models 15

3.1 Subcellular structure of the model 22
3.2 Qualitative scheme of the calcium currents used in the our model . . 24
3.3 Markov models 25
3.4 Stochastic behavior of the RyR2s 30

4.1 Global calcium traces 32
4.2 Behaviors as function of the pacing period 33
4.3 Heterogeneity in the spatial calcium profiles 34
4.4 Longitudinal line scan 35
4.5 Spatial profiles at different times of the pacing period 36
4.6 Spatial line-scans during a stimulation 37
4.7 Characterization of the calcium waves 38
4.8 Diagram of the procedure employed in the model to label the opened RyR2s into the same event 39
4.9 RyR2 distribution and local calcium traces 40
4.10 Spark properties 41
4.11 Experimental noise characterization 42
4.12 Local calcium traces with the addition of noise 43
4.13 Experimental local trace 43
4.14 Spark frequency measured with the experimental software 44

5.1 Spatial CaRU distributions 48
5.2 Spatial characteristics of the configurations 49
5.3 Spark characteristics 50
5.4 Outline of the CaRU distributions 52

5.5 Schematics of the protocol used for the creation of the heterogeneous distribution in the model 53
5.6 Spatial distribution of the CaRUs for the heterogeneous distribution 54
5.7 Geometrical characteristics of the configurations 55
5.8 Spatial distribution of the firing CaRUs 56
5.9 Calcium sparks as function of the number of RyR2s 57
5.10 Variability of the local traces 58
5.11 Spark properties 59
5.12 Correlation between spark properties and the number of RyR2s . . . 60
5.13 Influence of CaRU structure on local calcium concentrations 61

6.1 Modeling of CSQ as a RyR2-modulator 68
6.2 Spark properties for no AF and AF conditions due to the lack of calsequestrin 69
6.3 Spark frequency as function of the distance to membrane 69
6.4 Modeling of phosphorylation as a RyR2-modulator 71
6.5 Average spark properties due to RyR2-phosphorylation 72
6.6 Spark frequency as function of the distance to membrane 72
6.7 Number of sparks as function of the opened RyR2s 73
6.8 Spark properties for no AF and AF conditions 74
6.9 Correlation between the spark properties and the RyR2s 75
6.10 Spatial distribution of sparks for no AF and AF conditions 76

7.1 Characteristics of the t-tubule network 81
7.2 Ca^{2+} transient characteristics as a function of F.A. 84
7.3 Dependence on the pacing period 85
7.4 Effect of a dysfunctional SERCA pump 86
7.5 Spatial Ca^{2+} profiles 87
7.6 Inhomogeneity in release as a function of t-tubule density 88
7.7 Effect of axial tubules 89
7.8 Statistical measures of RyR2 activity 91

8.1 Structure of the simplified model 100
8.2 Calcium profiles obtained with the subcellular model 103
8.3 Subcellular model with SR luminal dependence on the RyR2 104
8.4 Oscillations in the subcellular model 105
8.5 Time traces of the different calcium concentrations for different values of total calcium concentration, $\bar{c}_T$, and calsequestrin concentration set to zero ($B_{SQ} = 0$) 106
8.6 Plot of the function $f(c_i)$ for different values of the $\bar{c}_T$ concentration 107
8.7 Solutions for cytosolic calcium concentration, c_i, as a function of total calcium concentration, $\bar{c}_T$ 108
8.8 Stability of the fixed points and the oscillations 109
8.9 Fixed points as function of CSQ 110

8.10 Structure of the nullclines at different values of $\bar{c}_T$ indicated in the title of each panel . . . 111
8.11 Structure of the nullclines at different values of $\bar{c}_T$ indicated in the title of each panel . . . 112
8.12 Dependency of the onset of oscillations with buffer parameters . . . 113
8.13 Structure of the nullclines . . . 114
8.14 Solutions as a function of total calcium concentration $\bar{c}_T$, with calsequestrin concentration set to zero when the fast dyadic approximation is used . . . 115
8.15 Structure of the nullclines at different values of $\bar{c}_T$ indicated in the title of each panel . . . 116
8.16 Stochastic effects on the minimal model . . . 117

B.1 Role of inactivation in the onset of oscillations . . . 160

List of Tables

A.1 Parameters of the subcellular model (part 1). 155
A.2 Parameters of the subcellular model (part 2). 156

B.1 Parameters of the model. 160

List of Abbreviations

RyR2	**Ry**anodine **R**eceptor type-2
CaRU	**Ca**lcium **R**elease **U**nit
LCC	**L**-type **C**alcium **C**hannel
SR	**S**arcoplasmic **R**eticulum
EC	**E**xcitation-**C**ontraction
CICR	**C**a^{2+}-**I**nduced **C**a^{2+} **R**elease
NCX	**N**a^{+} / **C**a^{2+} e**x**changer
SERCA	**S**arco/**E**ndoplasmic **R**eticulum **C**a^{2+}-**A**TPase
TnC	**T**roponi**n** **C**
CaM	**Ca**lcium-**M**odulated protein, Calmodulin
SR binding	**SR** binding site buffer
CSQ	**C**al**s**e**q**uestrin
AP	**A**ction **P**otential
SA	**S**ino**a**trial node
AF	**A**trial **F**ibrillation
VF	**V**entricular **F**ibrillation
HF	**H**eart **F**ailure
VT	**V**entricular **T**achycardia
CVD	**C**ardio**v**ascular **D**iseases

Physical Constants

Faraday constant	$F = 96\,485.3365\,\mathrm{C\,mol^{-1}}$
Ideal gas constant	$R = 8.31\,\mathrm{J\,K^{-1}\,mol^{-1}}$

List of Symbols

General parameters

Δt	time step	ms
Δx	spatial step	μm
L_x	cell x-length	μm
L_y	cell y-length	μm
v_i	cytosol volume fraction	
v_{sr}	SR volume fraction	
T	Temperature	K
V_{rest}	Resting potential	mV
V_{max}	Maximum potential	mV
T_s	stimulation period	ms
c_i	calcium concentration	μM
c_{sr}	calcium concentration in the SR	μM
$c_{b,TnC}$	calcium concentration bounded to troponin C buffer	μM
$c_{b,CaM}$	calcium concentration bounded to calmodulin buffer	μM
$c_{b,SR}$	calcium concentration bounded to SR binding site buffer	μM
$c_{b,CSQ}$	calcium concentration bounded to calsequestrin buffer	μM
D_i	diffusion coefficient in the cytosol	μm^2/ms
D_{sr}	diffusion coefficient in the SR	μm^2/ms

Release parameters

J_{rel}	Release flux	μM/ms
g_{rel}	Single channel strength	ms^{-1}
N_{RyR}	Number of RyR per CaRU	
O_{RyR}	Fraction of opened RyRs in a single CaRU	
k_{oc}	Closing rate (O → C)	ms^{-1}
k_{co}	Opening rate (C → O)	ms^{-1}
k_a	Opening rate parameter	μM^{-2} ms^{-1}
k_{oi}	Inactivation rate (O → I_1)	ms^{-1}

k_c	Transition rate parameter between opened and inactivated states	μM^{-1} ms^{-1}
k_{io}	Opening rate from the inactivated state ($I_1 \rightarrow O$)	ms^{-1}
k_{i1i2}	Transition rate between inactivated states ($I_1 \rightarrow I_2$)	ms^{-1}
k_{i2i1}	Transition rate between inactivated states ($I_2 \rightarrow I_1$)	ms^{-1}
k_b	Transition rate parameter between inactivated states	μM^{-2} ms^{-1}
k_{ic}	Recovery rate ($I_2 \rightarrow C$)	ms^{-1}
k_{ci}	Inactivation rate from closed state ($C \rightarrow I_2$)	ms^{-1}
Max_{SR}	Maximum value of $\mathrm{k_{CaSR}}$	
Min_{SR}	Minimum value of $\mathrm{k_{CaSR}}$	
H	Exponent in SR calcium lumenal dependence	
EC_{50-SR}	Threshold concentration of SR calcium	μM

LCC parameters

J_{CaL}	L-type channel flux	μM/ms
g_{CaL}	Single channel strength	ms^{-1}
N_{LCC}	Number of LCC per cluster	
O_{LCC}	Fraction of opened LCCs in a single cluster	
a_{ij}	Transition rates from state i to state j	
K_{LCC}	Threshold Ca-induced transition	μM

SERCA parameters

J_{up}	SERCA flux	μM/ms
g_{up}	Maximum uptake SERCA	μM/ms
K_i	Half occupation of cytosolic calcium binding states	μM
K_{sr}	Half occupation of SR calcium binding states	μM

NCX parameters

J_{NCX}	Ex-changer flux	μM/ms
g_{NCX}	Uptake strength exchanger	μM/ms
$\mathrm{[Ca]_o}$	Extra cellular Ca concentration	μM
$\mathrm{[Na]_o}$	Extra cellular Na concentration	μM
$\mathrm{[Na]_i}$	Intra cellular Na concentration	μM

k_{sat}	Saturation constant	
η	Voltage sensitivity constant	
K_{mNao}	External sensitivity constant for Na	μM
K_{mCao}	External sensitivity constant for Ca	μM
K_{mNai}	Internal sensitivity constant for Na	μM
K_{mCai}	Internal sensitivity constant for Ca	μM

Buffer parameters

B_{TnC}	Troponin C concentration	μM
$k_{on,TnC}$	Troponin C binding rate	μM^{-1}ms^{-1}
$k_{off,TnC}$	Troponin C unbinding rate	ms^{-1}
B_{CaM}	Calmodulin concentration	μM
$k_{on,CaM}$	Calmodulin binding rate	μM^{-1}ms^{-1}
$k_{off,CaM}$	Calmodulin unbinding rate	ms^{-1}
B_{SR}	SR-bound buffer concentration	μM
$k_{on,SR}$	SR-bound buffer binding rate	μM^{-1}ms^{-1}
$k_{off,SR}$	SR-bound buffer unbinding rate	ms^{-1}
B_{Rhod}	Rhod-2 buffer concentration	μM
$k_{on,Rhod}$	Rhod-2 buffer binding rate	μM^{-1}ms^{-1}
$k_{off,Rhod}$	Rhod-2 buffer unbinding rate	ms^{-1}
B_{CSQ}	Calsequestrin buffer concentration	μM
K_{CSQ}	Calsequestrin dissociation constant	μM

Part I

Introduction

Chapter 1

Physiology

The heart is situated at the chest cavity, between the right and left lungs, and supported by a membranous structure. It is the muscle that pumps blood throughout the body by a coordinated contraction, triggered by an electrical impulse that propagates along cardiac tissue. The heart is separated in two halves and has four main chambers. The lower chambers are the ventricles, while the smaller upper chambers are called atria. The cardiac muscle, or myocardium, constitutes the bulk of the heart. It is composed by millions of cells with a length of 80-100μm and a diameter of 10-20μm. Myocytes present dynamical regulation and processes at different temporal and spatial scales. The proper functioning of the heart requires a synchronized activity at all these scales. The oscillatory dynamics of the heart is led by the sinoatrial node (SA), which is a natural pacemaker that generates the action potential (AP) that spreads out to drive the contraction cycle within the atrial and ventricular cells [24]. The AP travels throughout the heart very fast provoking a cascade effect of single cell contractions that ends up with a coordinated contraction. This process is called excitation-contraction (EC) coupling [26, 24], where calcium itself exerts important direct regulatory effects during EC coupling.

In cardiac cells, calcium provides the link between the electrical signal and the contraction of heart, among other ions. Beyond the cardiac cells, calcium is also one of the most important intracellular messengers, and thus the mechanisms that control the intracellular free calcium concentration are of fundamental physiological importance [23]. For instance, Ca^{2+} takes part in oocyte activation at fertilization [211], axonal growth [28], cell migration [119], gene expression [12], formation of nodules in plant root hairs [68], development of muscle [78], release of cytokines from epithelial cells [135], cell death [228, 76], and excitation-contraction coupling in muscle cells [74].

In cardiomyocytes, calcium dysregulation has been related to the appearance of contractile dysfunction, arrhythmias and sudden cardiac death in pathophysiological conditions [213]. In particular, calcium can modulate EC coupling by activation of kinases and phosphatases, which can modulate gene expression responsible for hypertrophic signaling and heart failure (HF) [24]. A life-threatening arrhythmia, fibrillation, results when an electrical wavebreak induces reentry and triggers a cascade of new wavebreaks. Ventricular fibrillation (VF) is the most common cause of sudden death, whereas atrial fibrillation (AF), the most prevalent clinical arrhythmia, accounts for nearly one third of strokes in the elderly [298]. Clinically, AF duplicates the mortality rate and increases the risk of ictus (in which poor blood flow to the brain results in cell death) 5-fold. In spite of this, the treatment of AF remains deficient or inefficient, because of the incomplete knowledge of the complex pathophysiology of this disease. Often, AF has been linked to a dysregulation in the dynamics of intracellular calcium, thus the importance of a good knowledge of calcium handling dynamics in the cell. On the other hand, in the last ten years, the refinement of the experimental techniques, such as STED and dSTORM [107, 125, 249] has provided, for instance, a link between the calcium handling microstructure and the occurrence of cardiac diseases, as AF [175], prompting the quest for more detailed models of calcium handling, able to mechanistically explain this relation.

1.1 Calcium-induced calcium release

Cell contraction in the heart is mediated by the periodic increase of calcium in the cytosol. At rest conditions, the levels of calcium inside and outside the cell are about 0.1μM and 1mM, respectively. In addition, inside the cell there is a membrane-bound structure called Sarcoplasmic Reticulum (SR) that extends throughout the cell. The main function of the SR is to store calcium in high levels (1mM).

The dynamical properties of the myocytes are heavily determined by the membrane (a phospholipid bilayer) properties. This membrane presents a selective permeability, allowing some ions (Na^+, K^+, Ca^{2+}, etc.) to flow between the extracellular and intracellular media through a set of specific ion channels. The resulting charge imbalance produces a transmembrane potential difference, whose evolution is governed by the balance between the electrical and chemical gradients across the membrane of the cell. The potential at which chemical and electrical forces are in equilibrium is called the reversal or Nernst potential, and is specific to each ion. The potential at which the cell is at rest is known as the resting potential, and in cardiac cells its value is typically around -85 mV. If a sufficiently large stimulus is given to the cell, the transmembrane potential rises above a threshold potential and an active response occurs, giving rise to a series of events that result in the contraction of the cell (Fig. 1.1). The amplitude of the cardiac AP is of the order of 100 mV. This increase in the AP produces a small influx of calcium through the L-type calcium channels (LCC). This current triggers Ca^{2+} release from the SR network via the Ryanodine Receptors (RyR, [81]) when a threshold calcium concentration in the cytoplasm is achieved. Thus, the stimulus for release of calcium by RyRs is controlled by the local nanodomains of Ca^{2+} generated by nearby LCCs, rather than the global cytosolic Ca^{2+} [258]. According to that, the control of macroscopic SR calcium release is achieved by graded statistical recruitment of individual, autonomous and stochastic calcium release events.

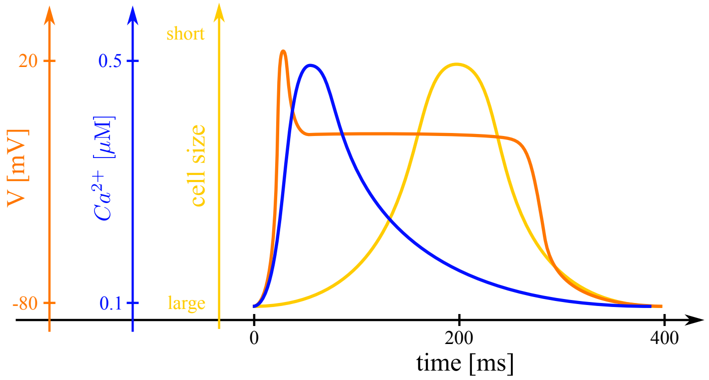

FIGURE 1.1: **Relation between action potential, calcium and contraction.** Dynamics of the membrane action potential (orange), the concentration of calcium (blue) and contraction of the myocyte (yellow).

RyRs are homotetramers with a total molecular mass of >2 MDa (each subunit is >550 kDa) [121, 150]. RyRs are modulated directly or indirectly by macromolecular complexes (dihydropyridine receptor, also known as L-type Ca^{2+} channel), ions (Ca^{2+}, Mg^{2+}), proteins (kinase) and binding proteins (calmodulin, calsequestrin). All these elements contribute to the dynamics of a single RyR. There are three known mammalian isoforms of RyR: RyR1, which was first found in skeletal muscle [265], RyR2, which was first detected in cardiac cells [196], and RyR3, which was found in brain cells [104]. Since we are studying cardiac cells, I will refer always to the second isoform of the RyRs (RyR2s).

RyR2s open and close collectively in clusters forming functional units known as Calcium Release Units (CaRU), which are often confronted to a cluster of LCCs. Functionally, the RyR2 serves as an intracellular Ca^{2+} channel in the SR membrane. A cardiac myocyte contains about 20.000 CaRUs. These clusters are densely localized in z-lines distributed periodically in planes perpendicular to the cell longitudinal direction, at distances of about 1.5-2 μm [82]. It has been possible to determine the intracellular structure and the CaRU positions in cardiac cells using confocal microscopy [250, 251]. This spatial organization is shown in Fig. 1.2 where the RyR2 clusters are labeled in red.

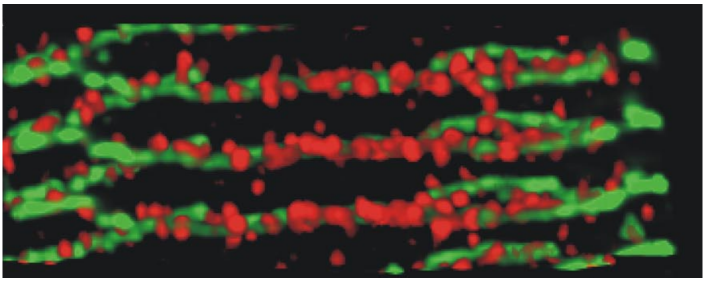

Figure 1.2: **Experimental RyR2 distribution.** Longitudinal distribution of RyR2 clusters (red) and its relationship to actinin labeling (green), a marker for the location of z-planes, in a rat ventricular myocyte. Image obtained from Soeller et al. (2007) [250].

In each CaRU the number of RyR2s and LCCs is small (of the order of 10-100 of the former and 5-10 of the latter), thus its dynamics is intrinsically stochastic. CaRUs are distributed inside the cell, resulting in random and discrete Ca^{2+} release events, known as Ca^{2+} sparks [44]. A Ca^{2+} spark has been considered as the unitary dynamical element which produces the cellular Ca^{2+} dynamics, such as Ca^{2+} waves and oscillations [75]. The (seemingly deterministic) global calcium signal appears from the coordination of several tens of thousands of these CaRUs. The resultant excess of calcium in the cytosol produces an increment of the calcium bound to the protein Troponin C, which in turn, binds to the myofilaments that produce cardiac contraction (see Fig. 1.3). Contraction, therefore, depends on the amount of Ca^{2+} bound to troponin C. The end of this process culminates in the cell contraction (Fig. 1.1). All this process is called Ca^{2+}-induced Ca^{2+} release (CICR) [73, 22, 49] and is the fundamental mechanism that produces the heart beating when, globally synchronized, takes place in all the cells. After the excitation process, Ca^{2+} removal allows relaxation of the cardiac muscle. This requires Ca^{2+} transport out of the cytoplasm by several pathways. The concentration in the SR is recovered by the active pumping of calcium from the cytoplasm to the SR carried out by the Sarcoplasmic Reticulum Ca^{2+}-ATPase (SERCA), an active transport where consumption of ATP allows calcium to flow in the inverse direction from the cytosol to the SR. Moreover, the Na-Ca exchanger pumps Ca^{2+} out of the cell. This process is summarized in Fig. 1.3. CaRUs not just couple SR and cytoplasm Ca^{2+} concentrations via Ca^{2+} release, but they are also correlated due to the Ca^{2+} diffusion in both domains. Therefore, the behavior of a single CaRU depends on the behaviors of the neighboring CaRUs.

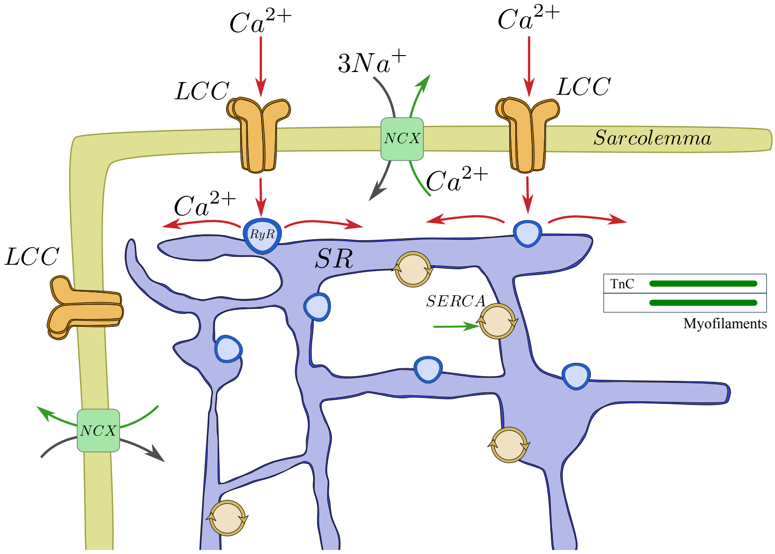

FIGURE 1.3: **Basic components of the calcium cycle process.** In yellow, the cell membrane where the LCCs (orange) and the NCX pump (green) are present. In blue, the SR where the RyR2s (blue) and the SERCA pump (yellow) are present. Calcium enters through the LCCs, stimulating release from the RyR2s and in turn producing the contraction of the myofilaments. Then, calcium is reuptaken into the SR by SERCA and taken out of the cell by the sodium-calcium exchanger.

Even though the same mechanism (CICR) triggers the transient elevation of Ca^{2+} in both ventricular and atrial myocytes, there are substantial spatio-temporal differences in Ca^{2+} transients [266, 293], due to the dissimilar intracellular structures. In ventricular cells, the membrane has deep penetrations into the cytosolic space called transversal tubules (t-tubules) [248] (Fig. 1.4a). The presence of t-tubules implies, directly, a presence of LCCs in the internal space of the cell and, thus, a simultaneous calcium release when depolarization takes place. The t-tubular system in atrial cells is significantly less developed or even entirely absent [118, 20] producing inhomogeneties in the spatio-temporal calcium patterns when the CICR occurs (Fig. 1.4b). In particular, the excitation starts at the cell membrane and then propagates inward, resulting in a delay in activation time between the subsarcolemma and the cell interior. This is a key difference between atrial and ventricular cells. In the latter, the opening of LCC channels along the t-tubules triggers the release of calcium from the SR, resulting in a homogenized calcium pattern. In the former, this trigger is due to the inward calcium wave.

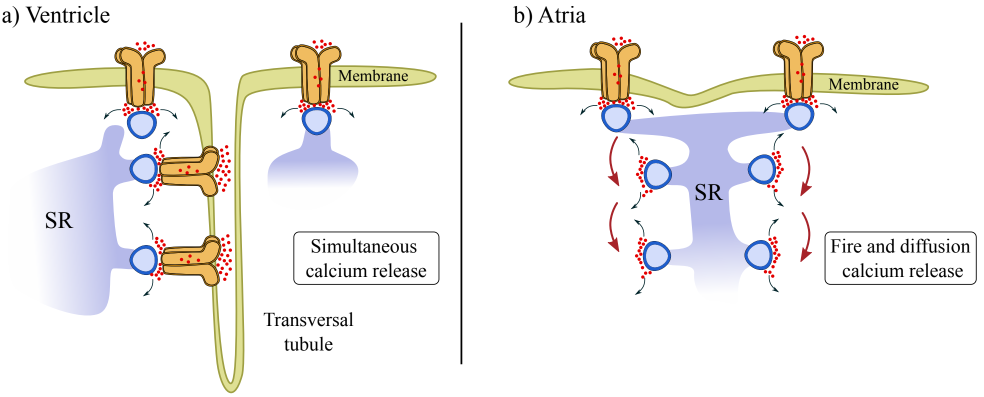
a) Ventricle
b) Atria
Membrane
SR
Simultaneous calcium release
Transversal tubule
Membrane
SR
Fire and diffusion calcium release

FIGURE 1.4: **Ventricular vs. atrial myocytes.** Comparison of the mechanism of excitation–contraction coupling and SR Ca^{2+} release in ventricular and atrial myocytes.

1.2 Atrial Fibrillation

AF is the most prevalent clinical arrhythmia, accounting for nearly one third of strokes in the elderly [298]. Many studies suggest that AF has a prevalence of approximately 1% [71]. This value is highly dependent on the population characteristics. For instance, in 2010, the number of individuals with AF in the European Union over the age of 55 years was estimated to be 8.8 million but this is expected to double to 17.9 million by 2060 [148].

HF, hypertensive heart disease, valvular disease and ischemic heart disease are major contributors to AF-occurrence. A variety of extracardiac conditions can affect AF-occurrence. Heavy alcohol consumption promotes AF [194], hyperthyroidism is a well-recognized factor [10] and obesity is increasingly recognized as an AF risk-factor [232]. Above these factors, advancing age is the most prominent risk factor for AF [207]. There are other risk factors that contribute to increase the AF propensity. They can be grouped into modifiable or non-modifiable risk factors [8]. Modifiable risk factors include body mass index, diabetes, obstructive sleep apnea, among others. The non-modifiable risk factors include genetics, gender, ethnicity, and of course, age.

AF causes an increase on the risk for stroke and related heart problems. Often, fibrillation is produced by the propagation of ectopic waves through the cardiac tissue provoking a cascade of wavebreaks. These ectopic waves, if persistent, may produce reentry, a type of tachycardia where the cause of the arrhythmia is due to the electric signal not completing the normal circuit, but rather an alternative circuit looping back upon itself.

Typically, the propensity to have fibrillation due to wavebreak and reentry has traditionally been related to tissue heterogeneities caused by structural and electrical remodeling associated with disease processes. Problems with the AP propagation over the cardiac tissue can create spirals and rotors [3, 56]. The study of these waves in terms of velocity of propagation, wavelength and periodicity was a hot topic in the early twentieth century [191]. Mines et al. [190] developed the notion that the wavelength of the cardiac wave must be less than available circuit dimensions for reentry to occur based on visual observation, electrocardiographic recording and selective electrical stimulation. Later on, in 1946, Wiener et al. [300] showed that the wavelength is the magnitude that determines the likelihood of reentry.

However, recent evidences indicate that dynamic factors (properties of the AP and Ca^{2+} handling) cooperate with tissue heterogeneities to promote AF [299]. That is, a crucial factor that determines the spontaneous automatic activity is the balance between inward and outward currents during the AP. Especially, a modulation of the currents carried by Na^{+} and Ca^{2+} can cause ectopic firing. Any persistent change in atrial structure or function is known as atrial remodeling and the first to introduce this concept was Wijffels et al. [301], who proved that the maintenance of AF is promoted by these structural and physiological changes ("AF begets AF"). The dynamic factors can vary in different regions of the heart and aggravate tissue heterogeneities.

All these effects at tissue level have a correspondence at subcellular level, which are related to a Ca^{2+} mishandling. Under normal conditions, regulation of contractile force is controlled by the AP, meaning that the Ca^{2+} transient is effectively slaved to the AP. However, CICR constitutes an excitable system in its own right and can exhibit independent dynamics. For instance, it has been shown that, during arrythmia episodes with an elevated pacing period, the beat to beat response is altered due to a previous alteration of the SR content [59]. In human atrial cells, these alterations in the calcium transients may produce spatial irregularities [159]. Focal ectopic activity may also result from delayed afterdepolarizations (DADs) occurring after full repolarization. DADs are thought to be the predominant cause of focal atrial ectopic firing. DADs are caused by a diastolic Ca^{2+} leak from the SR via RyR2s. RyR2s are sensitive to both cytosolic and luminal SR Ca^{2+} concentrations. A rise in diastolic release can result from SR Ca^{2+}-overload or when oversensitive RyR2s have an abnormally low Ca^{2+}-threshold for Ca^{2+}-release. This excess of cytosolic Ca^{2+} is handled by the NCX pump, generating net inward Na^{+} current that depolarizes the cell, producing a DAD (see path 1 on Fig. 1.5). This overabundance of cytosolic Ca^{2+} can be produced by an enhancement of RyR2 Ca^{2+}-sensitivity [291, 285]. Another crucial mechanism is the binding-unbinding process between SR calcium and calsequestrin (CSQ), which is the principal Ca^{2+}-storage buffer of the SR. A lack of CSQ expression increases free SR Ca^{2+}-concentration and promotes diastolic RyR2 Ca^{2+}-release [171] (see path 2 on Fig. 1.5). All these non-linear processes result from the combination of many single pathways that are, at the same time, cause and consequence of an AF episode. For instance, in persistent AF it is common to have an over-expression of NCX [291], a reduction of the LCC current [307, 281] and an up-regulation of the potassium currents [89, 215]. Moreover, AF itself causes upregulation in transcriptions factors, in particular by increasing cellular Ca^{2+}-loading and thereby activating a variety of signaling systems [197].

These electrophysiological and genetic alterations promote in turn the development of more AF episodes [115].

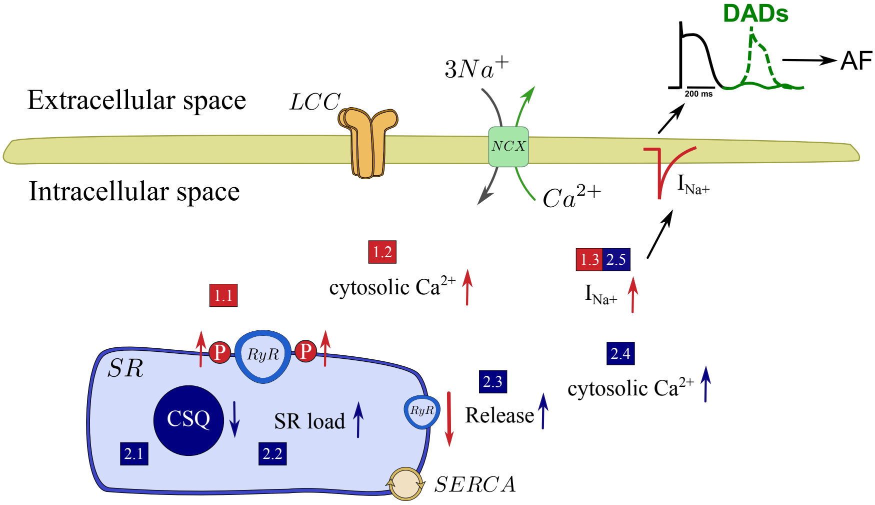
DADs
AF
200 ms
$3Na^+$
Extracellular space
LCC
NCX
Intracellular space
Ca^{2+}
I_{Na+}
1.2
cytosolic Ca^{2+}
1.1
1.3
2.5
I_{Na+}
2.4
cytosolic Ca^{2+}
SR
P
RyR
P
CSQ
SR load
2.3
Release
RyR
2.1
2.2
SERCA

FIGURE 1.5: **Diastolic Ca^{2+}-handling abnormalities underlie DADs.** Spontaneous SR Ca^{2+} releases through RyR2 elevate cytosolic Ca^{2+}, which is exchanged for extracellular Na^+ by the exchanger, producing depolarizing transient inward current. Inappropriate diastolic RyR2 Ca^{2+}-release is promoted by RyR2-hyperphosphorylation (red path) or decreased SR Ca^{2+}-binding to CSQ (blue path). P symbol: RyR2-phosphorylation.

Chapter 2

State of the art: models

The principal aim of a computational model is to represent an experimental system in a simplified way. It should meet two criteria often contradicting each other: on the one hand, it has to describe the features of interest as adequately as possible. On the other hand, it should be simple enough to be tractable and interpretable. There would be a set of parameters that must be fitted with the experimental results. This process would be more or less complicated depending on the model. At the end, there is a trade-off between the detail of the model (number of parameters) and the capability to fit these parameters with the physiological knowledge.

Cell physiology has been comprehensively studied during many years. Mathematical description of the corresponding biological processes has made possible to thoroughly understand the relevant mechanisms that play a characteristic role in the CICR course. The result is a huge pool of models that fit experimental findings in a wide range of spatio-temporal scales, going from single channels, to individual cells and finally to the whole heart.

2.1 Common-pool models

The first whole myocyte model was published in 1962 by Noble [200]. It modeled the cell dynamics using a modification of the Hodgkin–Huxley equations [112] applied to pace-maker and Purkinje fibre action potentials. It is a deterministic model and it assumes homogeneous global concentrations through the cell, what is known as the "common-pool" approximation. Subsequently, the model was expanded [184, 58] by introducing a more detailed description of the transmembrane currents.

Later on, a model for the ventricular myocyte was developed by Beeler and Reuter in 1977 [17]. The aim of this first work was to reproduce the action potential of mammalian cardiomyocytes measured experimentally. The model was formulated again as an extension of the Hodgkin-Huxley equations. It incorporates inward and outward currents carried by different ions as potassium, sodium or calcium, among others. After the publication of this model, many enhancements were incorporated to make it more realistic. In particular, Luo and Rudy [167] incorporated the dynamics of the external concentrations of calcium and potassium, and they also rectified the expression of the time-independent potassium current. It was the first published biophysically detailed model of the ventricular cell. Up until that moment, the models only simulate the ionic current through the membrane. The first models that included dynamical equations for ionic calcium concentration were developed by Luo and Rudy [165, 166]. The model produces robust action potential wave trains under a number of experimental protocols. For instance, this model is able to predict that, under pathological conditions of fast pacing, the AP amplitude is reduced due to the incomplete reactivation of the potassium currents between beats. These more recent models included, beyond the description of ionic currents, empirical descriptions of calcium dynamics.

In 1998, Jafri et al. [127] presented a novel model to describe the calcium concentration during excitation-contraction coupling. This model incorporates the SR calcium release via the RyR2 in the dyadic space, a proper description of the LCC channels to simulate the discrete-state time-dependent dynamics and calcium buffering due to calmodulin and calsequestrin. This generic formulation established the basis of many of the models that followed, including those developed for mouse, rat, dog or rabbit [29, 304, 238]. These models included the description of the calcium concentration in the closeness of the LCCs and the RyR2s, where calcium is released. This small subspace is called "dyadic space". Furthermore, this was the first model to go beyond the Hodgkin-Huxley approach by introducing a novel concept, the Markov state representations for the LCCs as well as the RyR2s.

The first atrial cardiomyocyte model was developed in 1987 by Hilgemann et al. [110]. It simulates the main pathways that play a role in the CICR process, such as Ca^{2+} influx through L-type calcium channels, SR Ca^{2+} release and Ca^{2+}-dependent activation of NCX. It is able to reproduce the calcium dynamics in the presence of premature stimulations. Later, the model was used to describe the sinoatrial node activity [57]. Rasmusson et al. [218] presented a computational model for bullfrog atrial cardiomyocytes providing insights into the contribution of individual ion currents to atrial AP initiation, repolarization and resting membrane potential. As in ventricular models, the first models of atrial cells were based on the Hodgkin-Huxley formulations. Following with this idea, Ramirez et al. [217] developed a model for canine atrial cardiomyocytes. They incorporated heterogeneity in the ion currents expression allowing the reproduction of major experimentally observed AP features, notably AP shortening and loss of rate adaptation. The model was enhanced by Kneller et al. [142], which included the effects of atrial tachycardia.

The possibility to obtain experimental data of human atrial mycoyte motivated the development of the first two computational models of these particular myocytes in 1998 by Nygren et al. [202] and Courtemanche et al. [54]. Both are common-pool models, using a compartmental description of the subcellular spaces and are based, again, on the Hodgkin–Huxley ion-channel formulation. These models have been widely using during many years to study the atrial cellular electrophysiology as well as multicellular simulation studies. The Nygren model was later improved by incorporating charge conservation for the stimulus current [126]. Even though both the Nygren and Courtemanche models were based on the same experimental data, they show important differences in AP morphology and pacing rate dependence [45]. Furthermore, the expressions for Ca^{2+} fluxes were taken from old ventricular models yielding to unphysiological results such that the Ca^{2+} peak under basal conditions [302] or the rate-dependent behavior [46].

Newer attempts have been done to trustworthy reproduce the Ca^{2+} handling as, for example, by Grandi et al. [94]. This is, again, a common-pool model of an atrial mycoyte that has been validated with experimental data obtained in isolated human atrial myocytes at physiological temperature. It incorporates the Ca^{2+} handling developed by Shannon et al. [238], which has been presented above as the first to introduce the subspace description of the dyadic cleft and the Markov RyR2 representation presented by Stern et al. [259]. This model is able to reproduce the Ca^{2+} dynamics in both normal situations and AF being the first atrial model to accurately represent the Ca^{2+} homeostasis of a human atrial cell. For instance, the model reproduces the appearance of arrhythmogenic EADs when the ultra fast potassium current is blocked.

2.2 RyR2 models

In the previous section I have explained the relevant features of the main models that have been developed with the aim to model ventricular and atrial myocytes. Now, I want to focus on how is modeled the RyR2s dynamics. The first models were based on deterministic representations of the ion channels. As a result, once the RyR2s in the common pool models are activated by trigger calcium, the strong positive feedback of CICR ensures that the release units fully activate, displaying an all-or-none calcium response. However, experimental findings suggest that calcium release follows a graded response to calcium triggering [13]. The first to explain this dynamics was Stern [258], who proposed that calcium sparks terminate by inactivation of the RyR2s. More physiological models were later developed [219] and corroborate that Ry2s have an inherent stochastic dynamics. The local control of the RyR2s through the calcium concentration in the dyadic space was the main idea of those novel models and it is currently accepted.

In order to reproduce the stochastic activity of the RyR2s, many schemes have been proposed. In Fig. 2.1 I present four schemes that have been fitted to experimental data. These schemes have different states that take into account the different conformations that a RyR2 can present. In the decade of the nineties many attempts were made to fit these models to the experimental data. In this sense, many models were proposed with a wide range of states and connections between them. All of them assume that calcium is the crucial ion that determines the transition among states, that is, the basis of the CICR mechanism. For instance, Keizer et al. in 1996 [139] proposed a four state model with three connections (see Fig. 2.1a); Keizer et al. in 1998 [140] proposed a six state model with six connections (see Fig. 2.1b). Later on, Sobie et al. [247] propose a two state model which agrees with the experimental findings (see Fig. 2.1d). In our models, we use a four state model with four connections (see Fig. 2.1c), based on Stern et al [259] such that it incorporates inactivation of the RyR2.

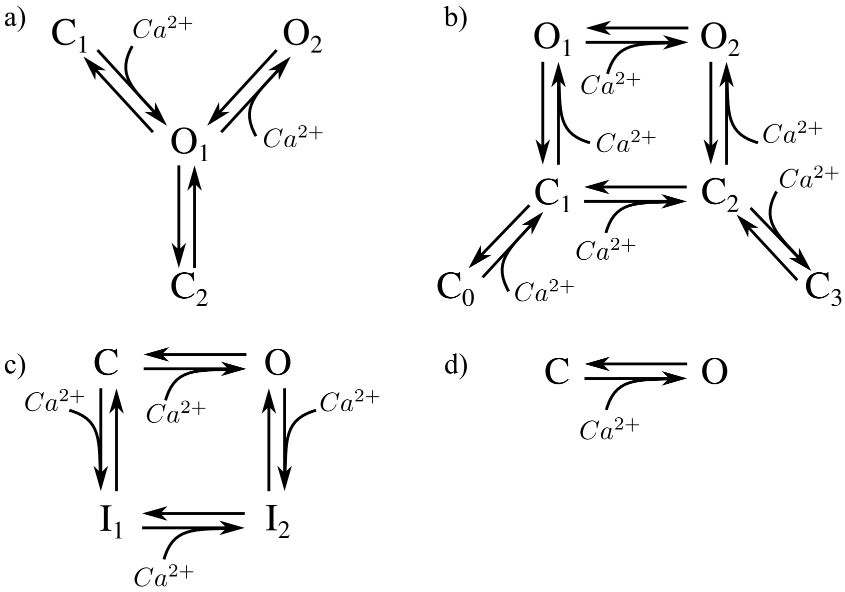

FIGURE 2.1: **Different types of RyR2 models.** a) Four state model with three connections proposed by Keizer et al. [139]. b) Six state model with six transitions proposed by Keizer et al. [140]. c) Four state model with four transitions proposed by Stern et al. [259]. d) Two state model with one connection proposed by [247].

2.3 Spatial models

All the models presented above are common-pool models, where the calcium concentration is considered to be homogeneous in each of several compartments (SR, cytosol, dyadic space, etc.). One of the first models that took into account inward wave propagation in atrial models was by Koivumäki et al. [146] in 2011, where the bulk cytoplasm and SR spaces were divided into several compartments, being thus a one-dimensional model, allowing for centripetal but not lateral diffusion. This model was used to study the effect of both subsarcolemmal and central release sites in AP and whole-cell Ca^{2+} transient. The model was broadly compared with the common-pool model developed by Grandi et al. [94] in terms of electrophysiological properties [302]. A similar model was also used by Li et al. [155], showing the presence of alternans. However, this one-dimensional approach has some limitations in terms of calcium wave propagation. A model allowing for both centripetal and lateral diffusion, as well as stochastic RyR2 gating was developed by Voigt et al. [290] in 2013 using the Grandi model [94], in order to study the mechanisms of EADs and triggered activity in paroxysmal atrial fibrillation. The model presented by Shannon et al in 2004 [238] was used as the basis for a subcellular, three-dimensional model, by Nivala et al. [198]. They could replicate the well-known Ca^{2+} local calcium events (sparks and macrosparks), as well as, the effects of detubulation on the appearance of Ca^{2+} alternans [199]. Calcium wave initiation and propagation

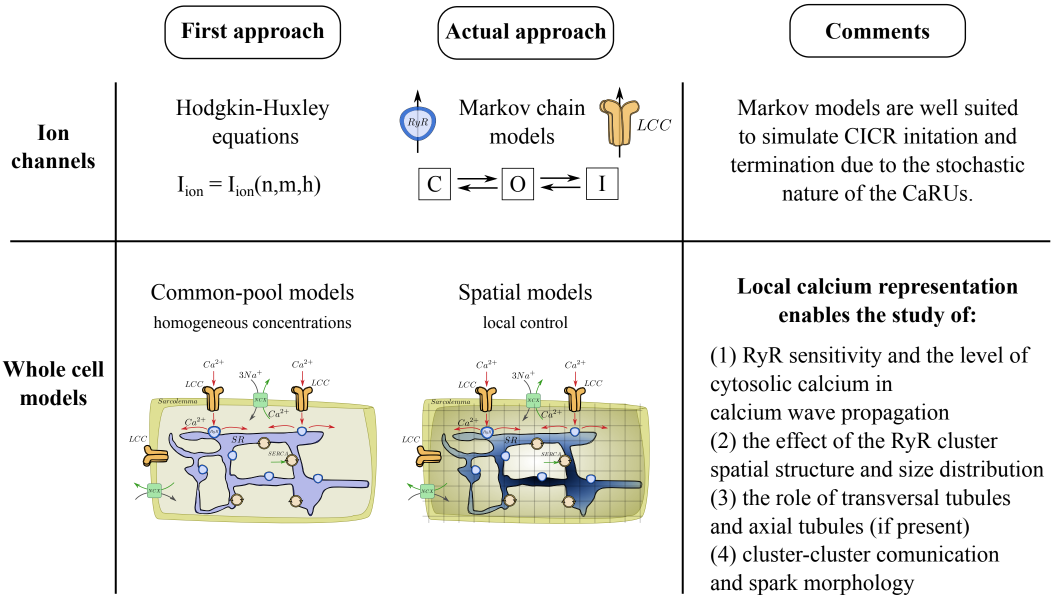
First approach
Actual approach
Comments
Ion channels
Hodgkin-Huxley equations
$I_{ion} = I_{ion}(n,m,h)$
RyR
Markov chain models
LCC
C
O
I
Markov models are well suited to simulate CICR initation and termination due to the stochastic nature of the CaRUs.
Whole cell models
Common-pool models
homogeneous concentrations
Spatial models
local control
Ca2+
3Na+
LCC
NCX
Sarcolemma
SR
SERCA
Local calcium representation enables the study of:
(1) RyR sensitivity and the level of cytosolic calcium in calcium wave propagation
(2) the effect of the RyR cluster spatial structure and size distribution
(3) the role of transversal tubules and axial tubules (if present)
(4) cluster-cluster comunication and spark morphology

FIGURE 2.2: **Outline of the main models.** Schematic overview of the most important groups of models at ion channels and whole cardiomyocyte levels. The right column gathers the relevant features of the actual approach.

has been considered by Thul et al. [271] in a three-dimensional geometry, assuming a diffuse and fire model for calcium release. This model proposes "ping waves", consisting of rotating waves of partial SR Ca^{2+} releases. It is important to note that this mechanism is only explicable in 2D and 3D. In the following work, Thul et al. [272], proved that small variations in the stochastic positions of the RyR2s produce highly different results in the Ca^{2+} handling.

Recently, efforts are under way to approach more realistic Ca^{2+} handling representations by including sophisticated ultra-structures to the models. For instance, Macquaide et al. [175] developed a detailed three-dimensional bidomain model of calcium propagation to study intra-CaRU cluster interactions, supporting the idea that cluster fragmentation and redistribution sustains atrial fibrillation through the enhancement of calcium release. Another relevant study has been done by Colman et al. [52, 51], who included realistic SR and t-tubule geometries to study their role on intracellular calcium waves and alternans. The most important modeling approaches are summarized in Fig. 2.2.

2.4 Beyond the cell level

The development of multiscale mathematical models of the heart is one of the most important topics in the biophysics area. It may contribute to the understanding of the main processes of cardiac function helping in the development and improvement of novel therapies and prognostic methods. For instance, the improvement of a human AP propagation model in real cardiac structures [203] has achieved by integrating clinical data. These models are being used to test and generate hypotheses that are difficult to address experimentally.

However, the transition through all the spatio-temporal scales is an extremely tough task when trying to grab all these behaviors in a coupled multiscale model [91]. Models describing ion channels on the cell membrane and the EC mechanism are typically systems of ordinary differential equations that are solved for each individual cell (length scales of μm) and can have time scales of 10^{-4} ms. On the other hand, mechanical contraction of the tissue and fluid dynamics (length scales of cm) are nonlinear partial-differential equations with time scales of 10^{-1} ms. The approach to the multiscale problem is not unique and many attempts have been done to find computationally efficient methods [201, 276]. With this in mind, in the last decade, advancements on mathematical modeling and computational resources allow now to solve highly complex, tightly coupled, multi-physics models. They perform reliable in silico studies, useful for patient risk stratification, therapy planning, or in silico clinical trials, among others [284, 86, 224]. The execution of these models are only achievable by using the super-computing centers.

These full-heart models are increasingly being used to develop specific and personal analysis for patients with pathologies in the electrical conduction system of the heart [189, 229, 267]. The combination of these models together with studies from population-based statistics allow to calculate the parameters and their interval of confidence in the physiological range. The patient-specific model is then obtained by adjusting relevant parameters so that model simulation results are in agreement with clinical recordings. The application of these novel techniques in real situations requires a multidisciplinary team. On one hand, the medical/biological profile is needed to provide physiological data as well as previous knowledge of the patient, whereas the physical/mathematical perspective will formulate the problem and will develop the programming software.

2.5 Motivation of the Thesis

Mathematical modeling has been a common thread during my undergraduate degree and masters. The bachelor's degree in Engineering Physics taught me to apply the basic principles of physics and mathematics to a wide scope of multidisciplinary environments. Thus, I gained knowledge about biotechnology and biological systems as well as other key emerging technologies such that photonics or nanotechnology. In this dissertation I have been able to apply these powerful techniques to real and actual cardiac health problems. In recent years, the multidisciplinary team approach has emerged as a collaborative way to deal with biophysical problems. The development of this Thesis has been possible working together with people with different backgrounds. In this sense, I have learned a lot with the meetings with Dr. Leif Hove-Madsen. Given my profile as engineering physicist, it has been utterly necessary to further in the biological knowledge about the cardiac subject and, at the same time, it has been really motivating to learn and research in this area. The contribution to CVD research has been a deep motivation to enjoy the preparation of this work.

Part II

Methods

Chapter 3

Subcellular calcium model

In the following I will present a detailed description of the subcellular calcium model developed in this Thesis. I will present the geometry considered, the equations that govern the dynamics, and the different fluxes and buffers that are present.

This model follows the spirit of earlier bidomain models [128, 137], defining at each point in space both cytosolic and SR calcium concentrations, with given volume fractions [138]. The model presents some important characteristics: 1) a very fine discretization, making it possible to describe (even if coarsely) the RyR2 cluster structure; 2) incorporation of the cell structure with distinction between z-lines and normal cytosol in terms of the volume ratio of SR and cytosolic volumes, diffusion constants and presence of buffers; 3) freedom to set the RyR2 clusters arbitrarily, that do not need to be disposed in an homogeneous regular grid.

3.1 Geometry

The computational model describes calcium dynamics at the single cell level and is based on homogenization [90]. Although it is well known that the SR forms a branching network (largely interconnected), with an interior that is distinct from the cell cytoplasm, this fact has largely been ignored, with most models making the a priori assumption that a Ca^{2+} concentration for both the SR and the cytoplasm can be defined at each point in space. So that, the cytoplasm and the SR are assumed to coexist at every point in space. For this reason, a fraction of each voxel is occupied by the cytoplasm (v_i) and the complementary fraction by the SR (v_{sr}), given that $v_i + v_{sr} = 1$.

The cardiac cell is modeled as a two dimensional domain with $L_x = 80$ μm and $L_y = 12$ μm. The spatial grid belongs to the submicron scale and it is defined as $dx = dy = 0.1\mu$m. There are points of the grid with and without RyR2s. A typical RyR2 has a size of 30nm x 30nm. The RyR2s are transmembrane proteins located at the surface of the SR, so they form a 2D grid. Thus, in each of our grid points I locate a maximum of 10 RyR2s.

A collection of grid points presenting RyR2s forms a cluster, i.e., a CaRU. In atrial cells, CaRUs are arranged periodically in the longitudinal and transversal directions, with some -seemingly Gaussian- dispersion [41]. In our model, we place the centers of the clusters on the perimeter following an exact periodic distribution

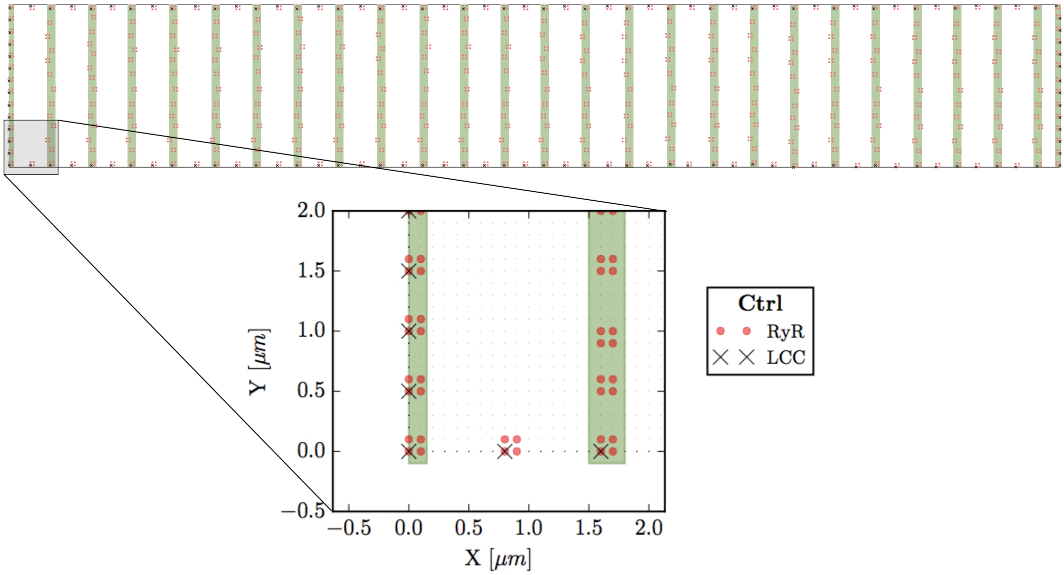

FIGURE 3.1: **Subcellular structure of the model.** Circles (red) represent points with RyR2s, black crosses are LCC groups, green stripes indicate the z-line region (domain Ω_{sr}), and small dots the sarcomere (Ω_c). The zoomed figure is the bottom left corner of the whole cell.

with a period $\bar{T}_x = \bar{T}_y = 0.5$ μm (see Fig. 3.1). In front of all these exterior CaRUs there are LCC groups. Inside the cell, CaRUs are placed following a Gaussian distribution centered at the z-lines and with a fixed dispersion σ. We take $\sigma = 0.4$ μm as standard value. So that, the average distance between CaRUs is $T_x = 1.6$ μm and $T_y = 0.5$ μm. Experimental data shows that the SR domain coincides with these z-lines [250]. In this sense, we identify the z-lines with periodic narrow strips (0.3 μm width) with a predefined period (T_x). Let be Ω_c the sarcomere domain, that is, the zone between z-lines and let be Ω_{sr} the zone contained in z-lines and all the contour ($\partial\Omega$). Notice that $\Omega_c \cap \Omega_{sr} = \emptyset$. Besides, we consider the presence of Ca^{2+} buffers: troponin (TnC), calmodulin (CaM) and SR Ca-binding sites. The TnC buffer affects the cytoplasmic concentration of calcium in the Ω_c domain. The other buffers, calmodulin and SR, affect also c_i but in all the cell, $\Omega_c \cup \Omega_{sr}$. We also consider a buffer in the SR space: calsequestrin (CSQ). We assume that all the buffers are immobile.

We define c_i, c_{sr} and c_{bi} as the concentration of calcium in the cytoplasm, the SR, and the concentration of calcium bound to buffers. This description assumes that there exist effective diffusion coefficients $D_i = D_i(v_i)$ and $D_{sr} = D_{sr}(v_{sr})$ that, in an average sense, incorporate the effect of that complex geometry. Although in principle these coefficients could be calculated knowing the SR structure [90], we will take the same relation as used in [90]. Since both fractions, v_i and v_{sr}, vary in different parts of the cell, this implies that both diffusion coefficients are functions of the position, $D_i = D_i(\mathbf{r})$ and $D_{sr} = D_{sr}(\mathbf{r})$. In our simulations we take the values $D_i \sim 250\ \mu\mathrm{m}^2/\mathrm{s}$ and $D_{sr} \sim 90\ \mu\mathrm{m}^2/\mathrm{s}$, that are within the upper range considered in the literature [161, 27].

3.2 Model equations

Because of the homogenization coarse grain, we define $c_i(\mathbf{r}, t)$ (free calcium concentration), $c_{sr}(\mathbf{r}, t)$ (calcium concentration in the SR) and $c_{bi}(\mathbf{r}, t)$ (calcium attached to buffers: TnC, CaM and SR buffer) in all points. Therefore, we state the problem with the following set of partial differential equations (PDEs).

$$\begin{aligned} \frac{dc_i(\mathbf{r},t)}{dt} &= J_i(\mathbf{r},t) + \nabla \cdot [D_i(\mathbf{r})\nabla c_i(\mathbf{r},t)] - J_{bi}(\mathbf{r},t) && (3.1)\\ \frac{dc_{sr}^{tot}(\mathbf{r},t)}{dt} &= \frac{v_i(\mathbf{r})}{v_{sr}(\mathbf{r})} J_{sr}(\mathbf{r},t) + \nabla \cdot [D_{sr}(\mathbf{r})\nabla c_{sr}(\mathbf{r},t)], && (3.2)\\ \frac{dc_{bi}(\mathbf{r},t)}{dt} &= J_{bi}(\mathbf{r},t), && (3.3) \end{aligned}$$

where J_i and J_{sr} are the fluxes into the cytosol and the SR spaces, respectively, J_{bi} accounts for the binding of free calcium to the different buffers. In order to relate the fluxes between the cytoplasm and the SR we have multiplied by the volume fraction v_i/v_{sr}, that depends on $\mathbf{r}$, that is, on the domain Ω_c and Ω_{sr}. In addition, each point could have different components (RyR2 or not, LCC or not) and could belong to the membrane or not. The fluxes that may contribute to the total flux into the cytosol J_i are the SR release flux, J_{rel}, the SERCA pump, J_{up}, the L-type calcium flux, J_{CaL}, and the sodium-calcium exchanger flux, J_{NaCa}. All these fluxes are represented in Fig. 3.2, where the bidomain framework is outlined with the two layers (cytosol and SR). The release flux J_{rel} carries Ca^{2+} ions from the SR to the cytoplasm through the RyR2s. Thus, it exists only on those points that have a CaRU, indicated by a red dot in Figs. 3.1 and 3.2. J_{up} pumps calcium from the cytoplasm to the SR and it is present in all cell domain $(\Omega_c \cup \Omega_{sr})$. The sum of these two fluxes (when appropriate) constitute the total flux from the SR. Then, J_{CaL}, the inward L-type calcium flux, depends on the LCC clusters, so that it will act on those points that contain this channel, indicated by a cross in Figs. 3.1 and 3.2. Indeed, LCCs appear only in some points of the cell membrane, $\partial\Omega$ (those that also have a CaRU). Finally, the NaCa exchanger, J_{NaCa}, acts along all the perimeter $\partial\Omega$. The explicit of each flux will be presented in the following sections.

3.3 Calcium fluxes

In the previous section I have presented the principal equations that govern the calcium dynamics. The particular expressions of currents J_i and J_{sr} have to be split up in cases. In particular, for the already defined regions (Ω_c, Ω_{sr} and $\delta\Omega$) we have that:

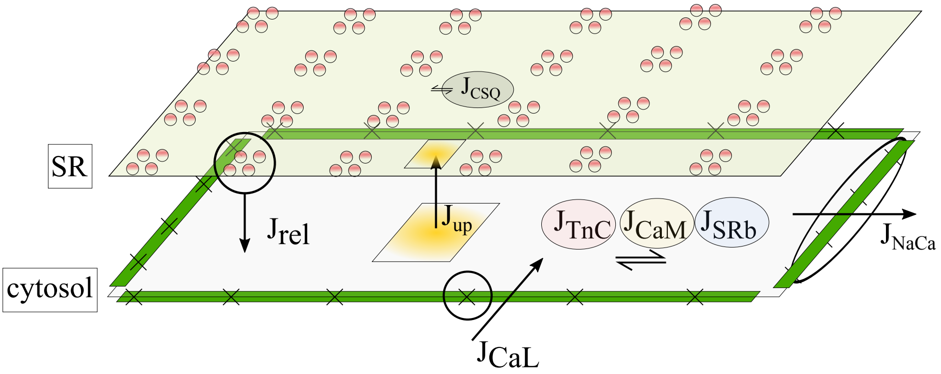

FIGURE 3.2: **Qualitative scheme of the calcium currents used in the our model.** The bidomain description is represented with both the SR and cytosol layers. The currents are represented with arrows which indicate the direction of the calcium flow.

- Inter z-planes space ($\mathbf{r} \in \Omega_c$):

$$J_i(\mathbf{r},t) = -J_{sr}(\mathbf{r},t) = -J_{up}(\mathbf{r},t) \tag{3.4}$$

  These currents are defined in internal points without RyR2.

- Internal cytosolic space along the z-lines ($\mathbf{r} \in \Omega_{sr} \setminus \delta\Omega$):
  - without RyR2:

$$J_i(\mathbf{r},t) = -J_{sr}(\mathbf{r},t) = -J_{up}(\mathbf{r},t) \tag{3.5}$$

  - with RyR2:

$$J_i(\mathbf{r},t) = -J_{sr}(\mathbf{r},t) = J_{rel}(\mathbf{r},t) - J_{up}(\mathbf{r},t) \tag{3.6}$$

- Submembrane space ($\mathbf{r} \in \delta\Omega$):
  - without RyR2:

$$J_i(\mathbf{r},t) = J_{NaCa}(\mathbf{r},t) - J_{up}(\mathbf{r},t), \tag{3.7}$$

$$J_{sr}(\mathbf{r},t) = J_{up}(\mathbf{r},t) \tag{3.8}$$

  - with RyR2 (so, with LCC):

$$J_i(\mathbf{r},t) = J_{NaCa}(\mathbf{r},t) + J_{rel}(\mathbf{r},t) - J_{CaL}(\mathbf{r},t) - J_{up}(\mathbf{r},t), \tag{3.9}$$

$$J_{sr}(\mathbf{r},t) = J_{up}(\mathbf{r},t) - J_{rel}(\mathbf{r},t). \tag{3.10}$$

3.3.1 SR release flux

As shown in Fig. 3.1, we consider each CaRU formed by several grid points containing RyR2s. As standard for a CaRU, we consider one containing 36 RyR2s, divided equally among 4 grid points, each one containing 9 RyR2s. We will change this configuration in sections 5.1 and 5.2 to consider larger CaRUs, maintaining fixed the total number of RyR2s in the cell, to account to the situation found in cells presenting AF [175].

Following Stern et al. [259] each RyR2 can be in one of four different states: close C, open O, and two inactivated states I_1, I_2 (Fig. 3.3). Calcium release from the SR to the cytoplasm is taken to be proportional to the concentration difference and the number of RyR2 in the open state, O_{RyR},

$$J_{rel} = g_{rel} O_{RyR} (c_{sr} - c_i). \tag{3.11}$$

This flux is only present in those points that present RyR2s (highlighted in red in Fig. 3.1). An effective cooperativity of RyR2 Ca^{2+} activation is incorporated by transition rates depending on c_i^3. Besides, RyR2 inactivation is also considered to depend on Ca^{2+} concentration. Therefore, four transition rates are calcium dependent (see Fig. 3.3):

$$k_{co}(c_i) = k_a \frac{c_i^n}{1+\left(\frac{c_i}{c_i^*}\right)^n} \qquad k_{i2i1}(c_i) = k_b \frac{c_i^n}{1+\left(\frac{c_i}{c_i^*}\right)^n} \qquad k_{oi} = k_c c_i \tag{3.12}$$

where the value of $c_i^* = 20\mu$M is a threshold value that prevents the RyR2s to over-release calcium. The value of the exponent n has been set at 3 and 2 for chapters 5-6 and 7-8, respectively. The other rates are constant with the following properties $k_{oc} = k_{i1i2}$, $k_{oi} = k_{ci}$. Detailed balance implies $k_{io} = k_{ic}(k_a/k_b)$. A luminal SR calcium dependence has been implemented as in [238]:

$$k_{CaSR} = Max_{SR} - \frac{Max_{SR} - Min_{SR}}{1 + (EC_{50-SR}/Ca_{SR})^H_{SR}} \tag{3.13}$$

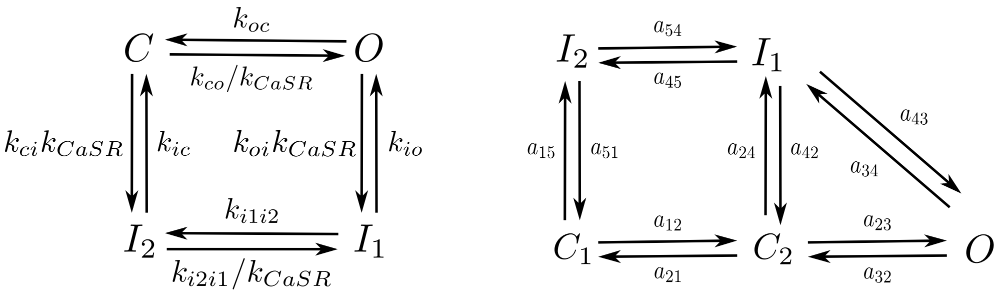

FIGURE 3.3: **Markov models.** Markov models of the RyR2 (left) and LCC channels (right).

3.3.2 LCC flux

The inward current of calcium from the extracellular medium towards each CaRU is dependent on the number of LCC channels in the open state O_{LCC}, the voltage, and the average local calcium concentration in these points, which are close to the membrane, according to [165]:

$$I_{CaL} = g_{CaL} O_{LCC} 4 z_m \frac{e^{2z} c_i - [Ca]_0}{e^{2z} - 1}, \tag{3.14}$$

where $z = VF/(RT)$ and $z_m = 0.341zF$. The current I_{CaL} is converted to the flux J_{CaL}, with units of μM/ms, through:

$$J_{CaL} = \frac{I_{CaL}}{2Fv_{myo}}, \tag{3.15}$$

where v_{myo} is the volume of the cytosol and F the Faraday constant. We have used the LCC model described in [176] with some changes in the parameters as in [7]. We consider the presence of 5 LCC channels in each CaRU (located all in the same grid point) with five possible states (Fig. 3.3): two closed states (C_1 and C_2), two inactivated states (I_1 and I_2) and one open state (O). The transition rates a_{ij} (see Fig. 3.3) are given by:

$$\begin{aligned}
&a_{12}(V) = p_\infty, \quad a_{21}(V) = 1 - p_\infty, \quad p_\infty = \frac{1}{1 + e^{-(V-15)/8}},\\
&a_{15}(V) = p_0/\tau_0, \quad a_{51}(V) = (1 - p_0)/\tau_0,\\
&p_0 = \frac{1}{1 + e^{-(V+40)/10}}, \quad \tau_0 = (\rho_0 - 450) p_{0f} + 450,\\
&\rho_0 = 10 + 4954 e^{V/15.6}, \quad p_{0f} = 1 - \frac{1}{1 + e^{-(V+40)/4}},\\
&a_{45}(V) = (1 - p_{if})/3, \quad p_{if} = \frac{1}{1 + e^{-(V+40)/3}}.
\end{aligned} \tag{3.16}$$

Notice that these rates depend on voltage. When the membrane depolarizes, that is $V \sim 10$mV, the LCC transitions to the open state. Moreover, there are rates dependent on cytoplasmic calcium concentration:

$$\begin{aligned}
&a_{24} = 0.00413 + 0.024 f_{ca}, \quad a_{34} = 0.00195 + 0.01826 f_{ca},\\
&\text{with } f_{ca} = \frac{1}{1 + (K_{LCC}/c_i)^3},
\end{aligned} \tag{3.17}$$

providing the inactivation of the LCC. Detailed balance also requires:

$$\begin{aligned}
a_{43} &= a_{34}(a_{23}/a_{32})(a_{42}/a_{24}),\\
a_{54} &= a_{45}(a_{51}/a_{15})(a_{24}/a_{42})(a_{12}/a_{21})
\end{aligned} \tag{3.18}$$

This current is present in those points that include a LCC group (all of them located in the cell membrane).

3.3.3 NaCa exchanger

The Na-Ca exchanger flux is given by

$$J_{NaCa} = \frac{g_{NaCa}}{1 + (K_{da}/c_i)^3} \frac{e^{\eta z}[Na]_i^3[Ca]_0 - e^{(\eta-1)z}[Na]_0^3 c_i}{S(c_i)(1 + k_{sat}e^{(\eta-1)z})}, \tag{3.19}$$

with $z = VF/(RT)$, V the membrane potential, F the Faraday constant, R the constant of gases and T the temperature. It depends on extracellular calcium and sodium concentrations $[Na]_0$, $[Ca]_0$, and on intracellular sodium $[Na]_i$, which we take as a parameter. The function $S(c_i)$ reads as:

$$\begin{aligned} S(c_i) = &[Na]_0^3 c_i + K_{mNa0}^3 c_i[1 + (c_i/K_{mCai})] \\ &+ K_{mCa0}[Na]_i^3 + [Na]_i^3[Ca]_0 \\ &+ K_{mCai}[Na]_0^3[1 + ([Na]_i/K_{mNai})^3]. \end{aligned} \tag{3.20}$$

The pump reaches the equilibrium in a time scale controlled by the value of K_{da}. In that case, the cytosolic calcium equilibrium concentration of the exchanger depends on the transmembrane voltage and is given by:

$$c_i^{eq} = \frac{[Na]_i^3[Ca]_0}{[Na]_0^3} e^z. \tag{3.21}$$

This pump will be present all along the cell membrane.

3.3.4 SERCA pump

The flux associated to the SERCA pump is considered to be:

$$J_{up} = g_{up} \frac{(c_i/K_i)^2 - (c_{sr}/K_{sr})^2}{1 + (c_i/K_i)^2 + (c_{sr}/K_{sr})^2}. \tag{3.22}$$

The flux J_{up} can be outward or inward depending on the relative concentrations in the SR and the cytosol. We say that J_{up} is an inward flux when it increases the concentration in the SR. Otherwise, it will be outward. Since the denominator is always positive, an inward flux is achieved when:

$$\left(\frac{c_i}{K_i}\right)^2 - \left(\frac{c_{sr}}{K_{sr}}\right)^2 > 0 \to \frac{c_i}{K_i} > \frac{c_{sr}}{K_{sr}}, \tag{3.23}$$

where K_i and K_{sr} represent the local equilibrium concentration of cytoplasmic and SR, respectively. Since we are considering an homogenized model, the SERCA pump is set in the whole cell.

3.4 Buffers

Inside the cell, the majority of Ca^{2+} ions are bound to proteins, known as calcium buffers, and only a minor part diffusive freely. To give an order of magnitude, for every free Ca^{2+} ion, 100 to 200 are bound to buffers [21, 273]. The effects of buffers on the calcium dynamics depends on the kinetics with which they bind and unbind Ca^{2+}. In general, a buffer is said to be fast if the time scale is smaller than the release time scale. Otherwise, the buffer is said to be slow. A very fast buffer in the cytosol will decrease the amplitude of the Ca^{2+} transient and retard its decay. If, however, the buffer binds Ca^{2+} more slowly, the initial amplitude of the Ca^{2+} transient will be large but will decay with a rate given by the binding of Ca^{2+} to the buffer [60]. In some cases, there are genetic mutations that affect the calcium buffering resulting, for instance, in an increase of Ca^{2+} binding to Troponin C. This increases both diastolic Ca^{2+} and the probability of triggered Ca^{2+} waves [231]. In the model we consider to have three buffers in the cytosol (Troponin C, Calmodulin and SR binding site buffer) and another one in the SR (Calsequestrin).

3.4.1 Cytosolic buffers

All the buffers in the cytosol are considered immobile and the binding to Ca^{2+} is modeled as a linear reaction of the form

$$\mathrm{c}_i + \mathrm{b}_j \underset{\mathrm{k_{off,j}}}{\overset{\mathrm{k_{on,j}}}{\rightleftharpoons}} \mathrm{c}_{bj}$$

where b_j is the free concentration of the $j-$th buffer and c_{bj} is the concentration of calcium bounded to $j-$th buffer: Troponin C, Calmodulin and SR binding site buffer. Let be B_{Tj} the total concentration of the $j-$th buffer, then the ODE associated to the previous reaction is

$$\frac{dc_{bj}}{dt} = -k_{off,j}c_{bj} + k_{on,j}c_i(B_{Tj} - c_{bj}) \equiv J_{bj} \tag{3.24}$$

3.4.2 Fluorescence buffers

The most used method for quantifying intracellular calcium is based on a family of fluorescent calcium indicators introduced by Tsien et al. [277, 96]. These indicators are visible when the cell is observed with a confocal microscope. The addition of these indicators has an implication in calcium handling, since these indicators act as any other calcium buffer. Thus, in order to compare our results with the experimental ones, we have included in the simulations the dynamics of the Rhod-2 fluorescence buffer [70]. It is simulated as immobile calcium buffer with an associated ODE that follows Eq. (3.24).

3.4.3 Calsequestrin

Calsequestrin (CSQ) is the main calcium ion buffering in the SR of both skeletal and cardiac myocytes. It was first isolated by Maclennan et al. [172]. At that time, the protein was believed to sequester Ca^{2+} and thus was named, calsequestrin [173]. The dynamics of CSQ has been incorporated to the model. It is a buffer that affects the calcium on the SR and is considered to be fast based on their rate constants [222, 38] compared with the release time scale [64]. For that reason, we have applied the rapid buffer approximation (RBA) to CSQ. Let be q the amount of free CSQ, that is, $q = B_{CSQ} - c_{b,CSQ}$. The reaction that governs this process is

$$\mathrm{c}_{sr} + \mathrm{q} \underset{\mathrm{k_{off,CSQ}}}{\overset{\mathrm{k_{on,CSQ}}}{\rightleftharpoons}} \mathrm{c_{b,CSQ}}$$

and the ODE that describes this reaction is

$$\frac{d[c_{b,CSQ}]}{dt} = -k_{off,CSQ}[c_{b,CSQ}] + k_{on,CSQ}[c_{sr}][q] \tag{3.25}$$

Since we assume that the CSQ buffering binding process is faster than release, Eq. (3.25) can be taken to be in steady state. Then,

$$0 = -k_{off,CSQ}[c_{b,CSQ}] + k_{on,CSQ}[c_{sr}][q] \tag{3.26}$$

The total concentration of CSQ in the SR is

$$B_{CSQ} = q + c_{b,CSQ} \tag{3.27}$$

Combining both equations, one can obtain an equation for the free concentration of CSQ

$$q = \frac{B_{CSQ}K_{CSQ}}{K_{CSQ} + c_{sr}} \tag{3.28}$$

where K_{CSQ} is the dissociation constant and it is defined as $K_{CSQ} \equiv k_{off,CSQ}/k_{on,CSQ}$. The concentration of buffer bound to CSQ is

$$c_{b,CSQ} = B_{CSQ} - q = B_{CSQ}\left(1 - \frac{K_{CSQ}}{K_{CSQ} + c_{sr}}\right) = \frac{B_{CSQ}c_{sr}}{K_{CSQ} + c_{sr}} \tag{3.29}$$

The total concentration of calcium in the SR is the sum of the free calcium and the calcium bound to CSQ

$$c_{sr}^{tot} = c_{sr} + c_{b,CSQ} = c_{sr}\left(1 + \frac{B_{CSQ}}{K_{CSQ} + c_{sr}}\right) \tag{3.30}$$

and the inverse relation is

$$c_{sr} = \frac{1}{2}\left[c_{sr}^{tot} - K_{CSQ} - B_{CSQ} + \sqrt{(c_{sr}^{tot} - K_{CSQ} - B_{CSQ})^2 + 4c_{sr}^{tot}K_{CSQ}}\right] \tag{3.31}$$

In the simulation, we solve the PDE for c_{sr}^{tot} and then we calculate the free calcium in the SR applying the Eq. (3.31). Computationally, with this procedure the numerical error of the simulations in the RBA of CSQ is negligible.

3.5 Stochastic gating

In the following I will reefer to both RyR2s and LCCs as "channels". Both type of channels are described using a Markov chain with calcium and voltage dependent rates (see Fig. 3.3). The activity of these channels has been often modeled as continuous-time discrete-state Markov chains [53]. These Markov chains have four and five states, respectively, and are irreducible, meaning that it is possible to move from any state to any other state via one or more transitions. To solve the stochastic dynamics I have used the Gillespie algorithm [88]. The transition rates for each channel are determined by their gating schemes and their dependence on local Ca^{2+} level.

In order to illustrate the stochasticity of the model, I have solved the dynamics of a CaRU with 36 RyR2s represented each one by a Markov chain. This simulation of a single CaRU has been done for fixed values of c_i and c_{sr}. The time evolution of the RyR2 states is shown in Fig. 3.4a. In addition, I have calculated the number of open RyR2s in steady state for a broad range of c_i and c_{sr} values. These results have been assembled in Fig. 3.4b. For low values of c_i the number of opened RyR2s tends to 0 and it increases as c_i increases. The increment is produced by the $C \rightarrow O$ rate, k_{co}, which is proportional to c_i^2. On the other hand, for low values of c_{sr} the number of opened RyR2s is also low due to luminal SR calcium lock down. As c_{sr} increases the number of opened RyR2s tends to the maximum, 36 RyR2s.

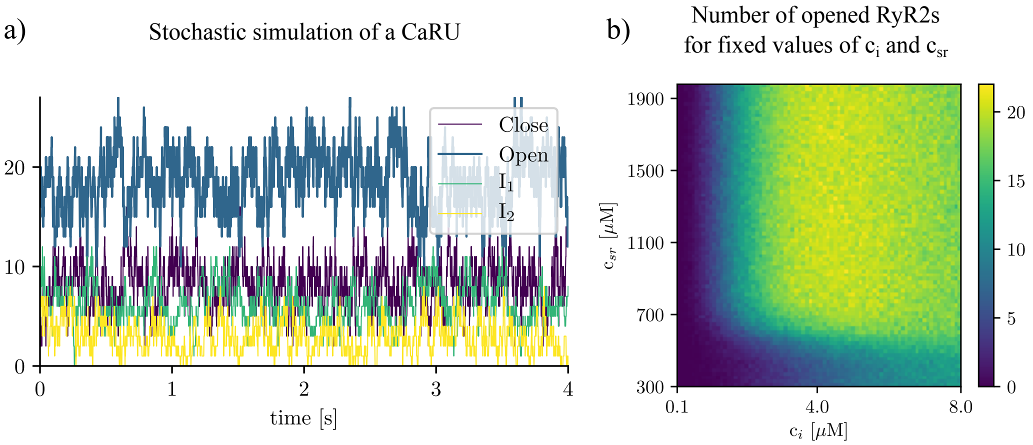

FIGURE 3.4: **Stochastic behavior of the RyR2s.** a) Temporal evolution of number of RyR2s in the close, open inactivated 1 and 2 states, respectively. b) Number of opened RyR2s in steady state as function of c_i and c_{sr}. Each point has been averaged with 20 realizations.

Chapter 4

Model validation

Once I have described the subcellular calcium model, I will present results regarding the global and local calcium traces, when an external stimulation is introduced, and of spontaneous release events, when there is no stimulation. Part of these results have been already published in [180]. The novelty in the current Thesis is the incorporation of the CSQ dynamics to the model with respect to the paper. For that reason figures may differ from the ones that are already published.

4.1 Stimulated cell

First I consider the case where the cell is stimulated periodically with an AP clamp. The calcium trace results from the sum of calcium at different sites. Since in our model the volume fraction changes from site to site, we have to define the average calcium concentrations as:

$$\langle c_i \rangle = \frac{\sum_{\mathbf{r}} v_i(\mathbf{r}) c_i(\mathbf{r},t)}{\sum_{\mathbf{r}} v_i(\mathbf{r})}, \quad \langle c_{sr} \rangle = \frac{\sum_{\mathbf{r}} v_{sr}(\mathbf{r}) c_{sr}(\mathbf{r},t)}{\sum_{\mathbf{r}} v_{sr}(\mathbf{r})} \tag{4.1}$$

Fig. 4.1 shows typical traces of the average calcium over all the cell in both domains: cytoplasm and SR. The model reproduces the experimentally calcium increment during the upstroke of the global Ca^{2+} transient [170]. We also show in Fig. 4.1 the four cytoplasmic fluxes, corresponding to the sodium-calcium exchanger (J_{NaCa}), the L-type calcium flux (J_{CaL}), SR release (J_{rel}) and SERCA (J_{up}). Due to the small number of LCC channels, the L-type calcium flux is particularly stochastic.

Depending on the pacing period, the model shows different behaviors. We have quantified this effect by calculating the calcium peak and the calcium basal level in the cytoplasm and in the SR domain (Fig. 4.2). To assure that the system is close to the steady state, I have first paced the cell for 50s at each pacing period, and then taken the average over the next 10 stimulations. As the pacing period decreases, the cytosolic calcium peak increases moderately, up to a pacing period of $\sim 200 - 300$ ms, beyond which it decreases, due to the decrease in SR calcium content and fractional release. This behavior agrees qualitatively with the observed change in the contractile force as a function of pacing period observed in atrial cells [177, 233], that shows a peak at a period of $\sim$ 500 ms, beyond which it decreases.

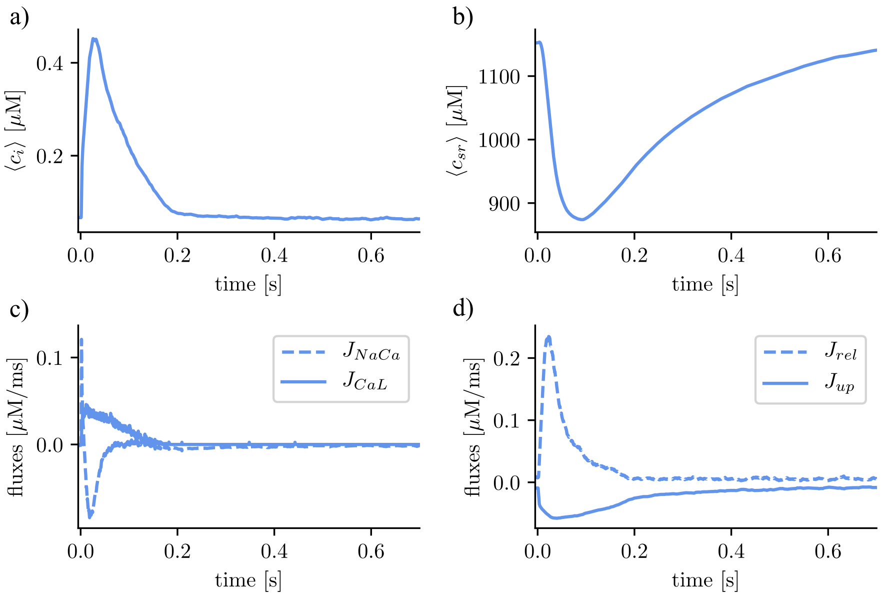

FIGURE 4.1: **Global calcium traces.** a) and b) Temporal profiles of [Ca^{2+}] for both domains, cytoplasm and SR. c) inward and outward cell currents of J_{NaCa} (dashed line) and J_{CaL} (solid line). d) SERCA pump flux (solid line) and release flux (dashed line) in the cytoplasm at a pacing period of 800 ms.

In order to compare the spatial variations within the cell, I have considered longitudinal sections at the central and peripheral regions, averaged over a 1 μm width. The complete CaRU distribution is shown in Fig. 4.3, where the longitudinal sections are plotted in green and blue. Simulations suggest strong differences between calcium levels in the subsarcolemmal space and the center of the cell (see Fig. 4.3), as well as a delay between release at the peripheral and central regions. This finding fits with the experimental results in atrial myocytes [31], although it depends sensitively on the density of the transverse and axial tubule (TAT) network. A more detailed discussion on the effects of TATS on calcium transients will be done in chapter 7.

The spatio-temporal and local correlation between c_i and c_{sr} calcium is shown in the line scan profiles on Fig. 4.4. The four profiles correspond to the same beat. In the subsarcolemmal region the presence of LCCs and CaRUs results in an important release activity causing a relevant SR depletion while, in the central region, calcium does not penetrate, and the local activity is scarce. Still, there is a depletion of the SR content (visible also in Fig. 4.3) due, not so much to release, which at the central region is almost negligible, but to diffusion of SR calcium to the periphery.

The spatio-temporal Ca^{2+} dynamics in the cytoplasm allows us to clearly understand how the standard inward wave propagation occurs when the cell is paced.

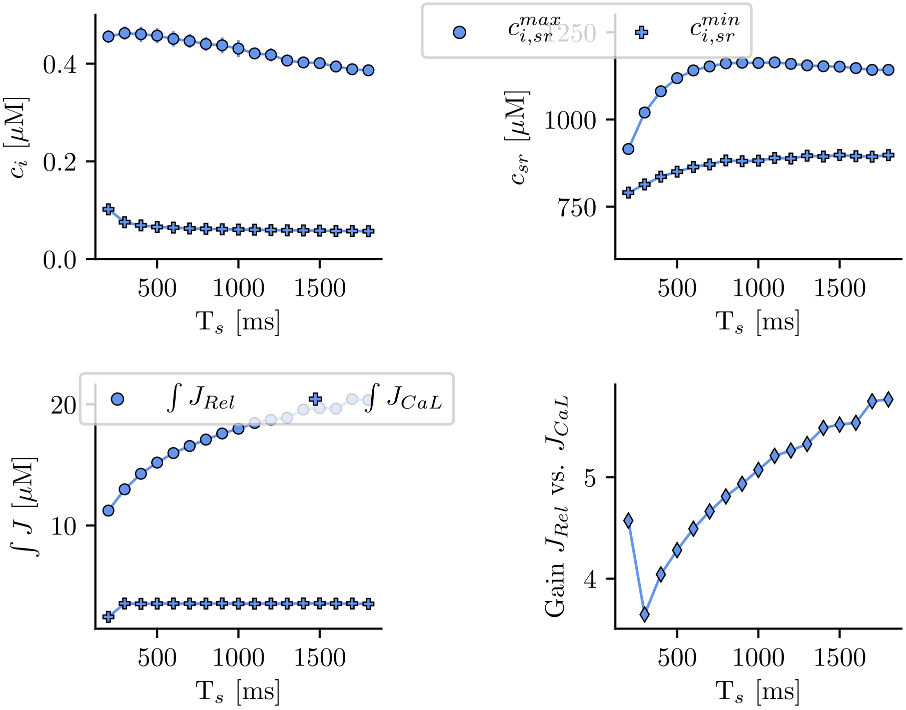

FIGURE 4.2: **Behaviors as function of the pacing period.** Ca^{2+} peak and Ca^{2+} basal level as function of the pacing period (T_s) in both domains: cytoplasm and SR. Each point has been averaged over 10 beats.

Fig. 4.5 shows spatial profiles at different times during a single beat. Under normal conditions, the calcium wave starts on the cell membrane and propagates to the center but this propagation does not reach the central region. This situation is observed experimentally [31] and it can be understood more clearly by averaging the calcium concentration over the longitudinal direction, so we can observe the average inward propagation of the calcium wave (Fig. 4.6). Typically, the inward wave propagates 4 or 5μm in the transversal direction. From the figure, we can estimate an inward wave velocity of roughly 150 μm/s, that agrees well with typical observed calcium wave velocities of $\sim$ 100 μm/s [124].

4.2 Calcium wave propagation

Calcium waves in cardiac myocytes have been implicated in pathologies such as arrhythmias [257, 263, 95]. The spatio-temporal properties of calcium waves have been investigated experimentally to understand the propagation mechanisms [163]. The wave velocity has been estimated to be between 100-200 μm/s [263, 275, 174]. Experimentally, calcium wave propagation has been measured by applying a local

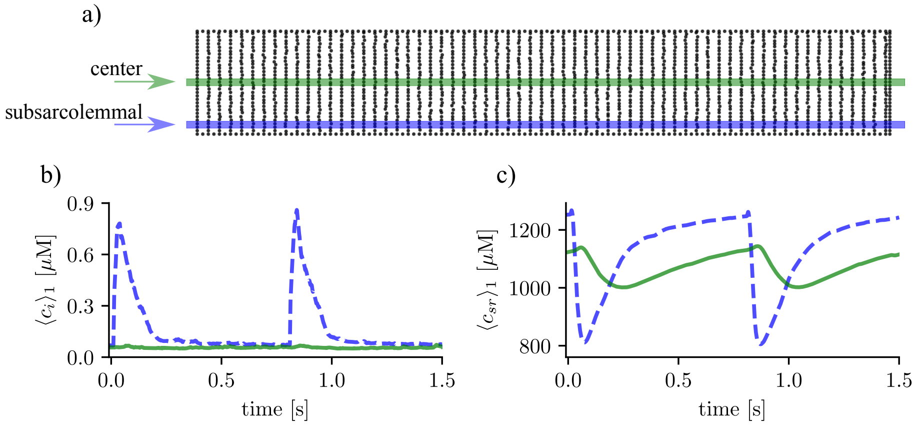

FIGURE 4.3: **Heterogeneity in the spatial calcium profiles.** a) Spatial distribution of the CaRU. Black dots show the position of the CaRUs. The green and blue lines indicate longitudinal lines at the cell center and periphery. b and c) Local Ca^{2+} measured in the subsarcolemmal space (blue dashed lines) and the center of the cell (solid lines) for both cytoplasm and SR domains at a pacing period of 800 ms. All traces have been averaged over a longitudinal section of 1 μm width.

concentration of caffeine, an agonist of RyR2s that accelerates the release of calcium from the SR [209]. The experiments were made under resting conditions and the concentration of intracellular calcium was imaged with confocal microscopy [275]. The local excitation produces a local increase of calcium that then propagates along the cell as a Ca^{2+} wave. In the experiments, as the wave travels trough the cell, it decreases both its amplitude and velocity.

These experimental results have been used as a further validation of the model. To reproduce them, the model is set under resting conditions and I impose that the RyR2s that are at less than 4 microns from the left side of the cell remain in the open state during the first 0.6 seconds. To compare to the experimental results, I have measured not the free calcium concentration but the calcium bound to Rhod-2 buffer (Ca_b), a common calcium indicator used in experiments [70]. The time duration of a single wave is about 0.5 s [275] which is comparable to what it is found with our computational model (Fig. 4.7a), where the wave propagates through the cell in ∼500 ms. In Fig. 4.7a, we can also appreciate that the width of the wave front has a magnitude around tens of microns. Moreover, in the region between the cell left side and the wave front, the RyR2s can not reopen due to two effects: inactivation and SR luminal shut down. The transition between the inactivated state and the closed state is determined by the k_{ic} rate (see Fig. 3.3). Thus, the mean time of this transition is about 200 ms (see Appendix A). The temporal scale of the SR recovery is also abotu 200 ms, and it is determined by the strength of the SERCA pump, which depends on the rates between the calcium concentrations on the cytosol and the SR and the equilibrium values defined in

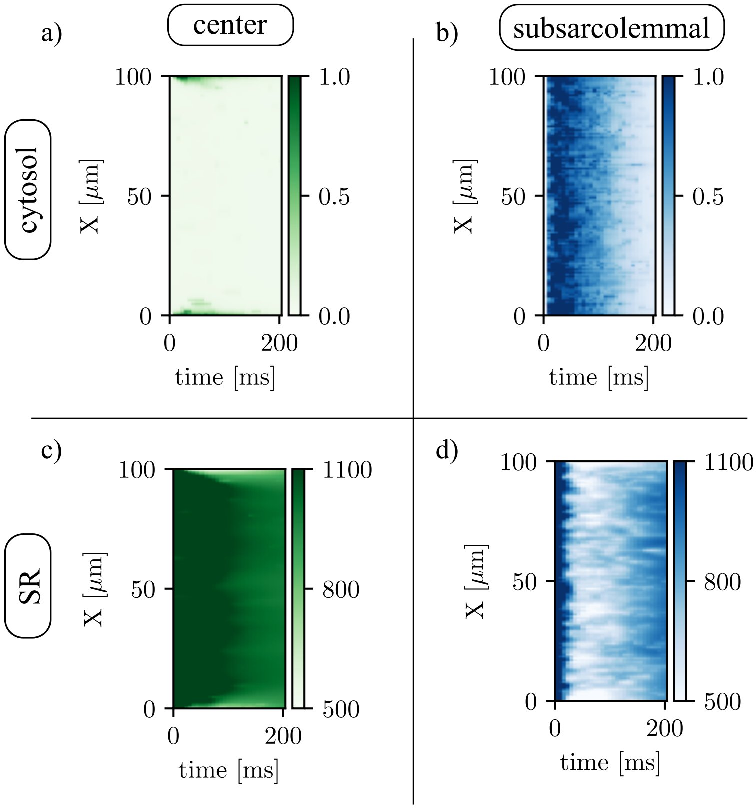

FIGURE 4.4: **Longitudinal line scan.** Longitudinal line scan during a single beat on the subsarcolemmal and the central region at a pacing period of 800 ms for cytosolic (top) and SR (bottom) calcium. The colorbar corresponds to calcium concentration in μM.

Appendix A. The consequence of these two effect is the lack of local stochastic calcium activity (sparks) in the region between the cell left side and the wave front, as can be seen by comparing the frames of Fig. 4.7a.

Local traces of calcium at different points of the cell are shown in Fig. 4.7b. Each local trace corresponds to the average calcium concentration bound to Rhod-2 in the colored region following the color scale. Each region has a height of 10 μm and a width of 2 μm. The peak of Ca_b is almost constant through the cell as the wave propagates. The time of arrival of the wave at these regions is estimated by measuring the time at which Ca_b reaches the 90% of the maximum value of that region. Then, the velocity at region i is calculated from difference of time of arrival regions $i-1$ and $i+1$ separated by 4 μm. The propagation velocity as function of position along the cell is showed in Fig. 4.7c. The velocity has been averaged with 7 realizations of the same simulation. The calcium wave is spread through the cell with a constant velocity around ~200 μm/s. This result fits with the experimental findings [275, 174] even though it is in the upper range. This could be because the calcium diffusion coefficient and the RyR2 open probability are rather larger

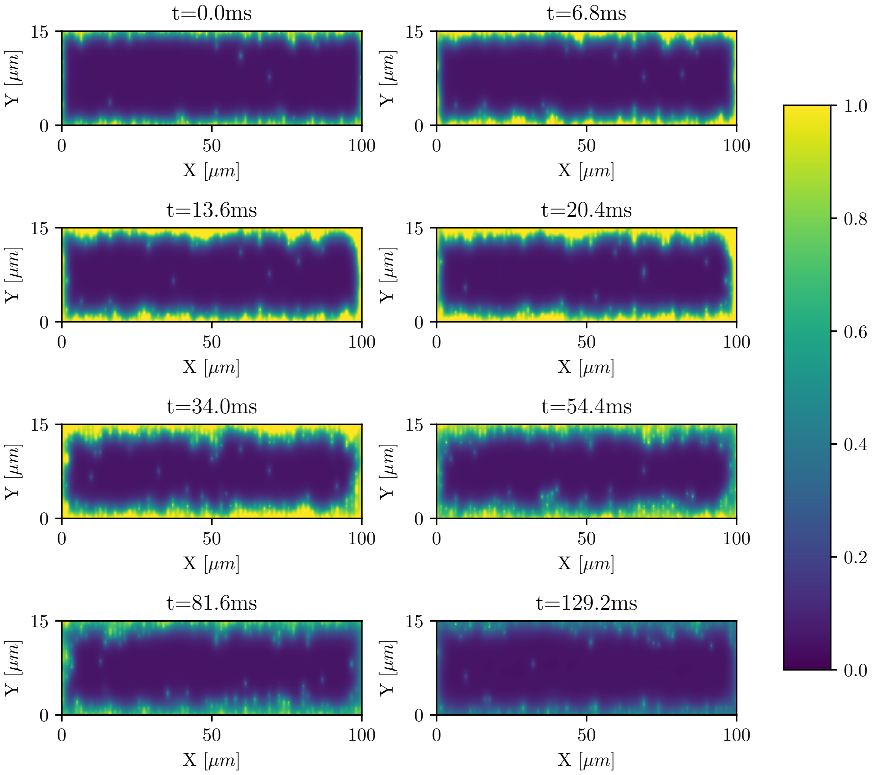

FIGURE 4.5: **Spatial profiles at different times of the pacing period.** Inward wave propagation at a pacing period of 800 ms. The colorbar corresponds to calcium concentration in μM.

in our model. The dispersion of the velocity through the cell increases as the wave propagates due to the stochastic behavior of the calcium domain (see gray lines in Fig. 4.7c).

4.3 Spark analysis in non-paced cells

Sparks have been widely studied since their discovery in 1993 [43]. In no-paced myocytes, a Ca^{2+} spark reaches its peak of about 2-fold increase with respect to the baseline within 20 ms, and dissipates in another 40 ms. Typically, it has a radius of 2 μm. The appearance of calcium sparks is not subjected to the opening of LCCs but it depends on both cytosolic and luminal local calcium concentrations. The stochastic nature of these events produces a wide variability in the spatio-temporal properties. Now I will explain how we measure these events as well as the proper way to compare our results with experiments.

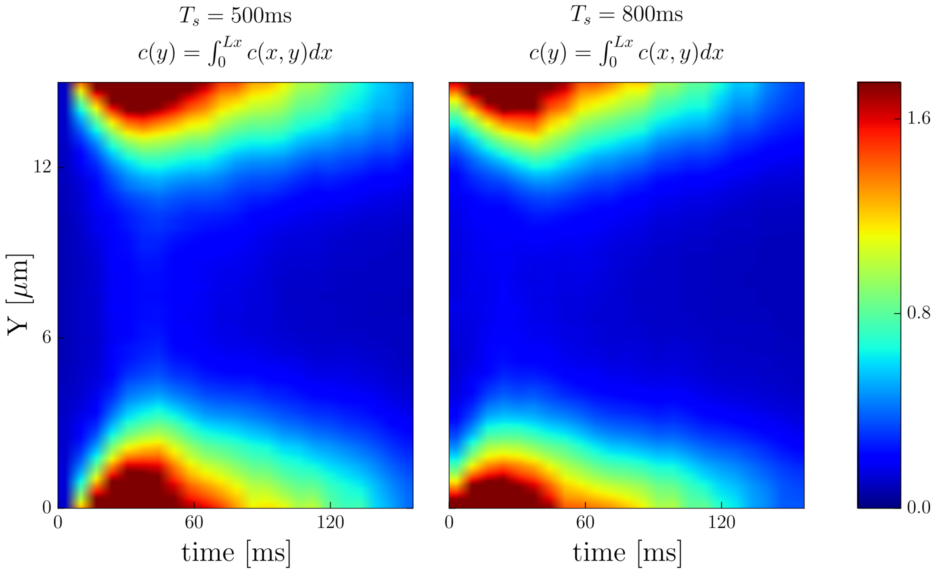

FIGURE 4.6: **Spatial line-scans during a stimulation.** Line scans averaged over the longitudinal direction at pacing periods of 500 and 800ms. The colorbar corresponds to calcium concentration in μM.

4.3.1 Spark properties

Probably the most important part of this Thesis has been the study of the local dynamics due to the stochastic nature of the RyR2s. The collective activity of these channels produce local calcium events which are named calcium sparks. The characterization of these sparks in terms of their spatio-temporal properties it's still a hot topic. A complete knowledge in this field will lead the scientific community to understand the onset of many cardiac problems (DADs, alternans, tachycardias, among others) as well as to suggest novel therapies to prevent CVDs. Although experimental techniques are already able to determine the calcium activity in resting conditions, they are still unable to record the channel activity of each RyR2 during a calcium release event.

In this respect, because of the high resolution of our model, we are able to characterize the calcium release events in terms of the number of RyR2s that have been opened as well as the spatio-temporal properties of the local calcium trace. In order to characterize these events, iterations over the opened RyR2s are done to cluster them, that is, to group the openings of the RyR2s that belong to the same calcium event. To do so, those openings that are close enough in time ($\leq$10ms) and space ($\leq 1\mu$m) are grouped into the same event. This process is summarized in Fig. 4.8a. Thus, calcium sparks are the result of the collective activity of several RyR2s. In the model, the cooperativity between RyR2s is given by the local calcium concentration. If one RyR2 opens produce a local rise of calcium which will increase the probability of the neighboring RyR2s, producing a cascade

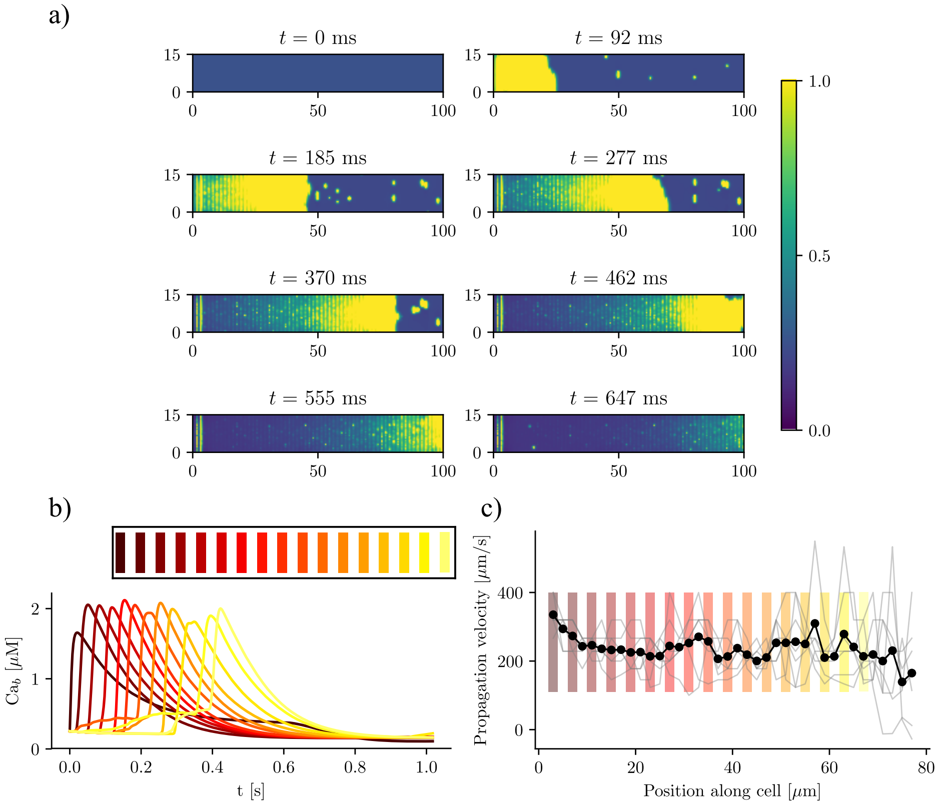

FIGURE 4.7: **Characterization of the calcium waves.** a) Calcium bound to Rhod-2 spatial profiles at different times for the same wave. b) Local Ca$_b$ traces at different points of the cell. The color regions have a width of 2 μm and a height of 10 μm. The inner figure indicates the position of each color along the cell. c) Propagation velocity of the wave as a function of distance along the cell (black line) averaged with 7 realizations (gray lines). The color scale has been overlapped to identify each region.

effect of new openings. Once the openings of each spark are grouped together, the "region of interest" (ROI) for each one can be defined getting the local calcium trace as

$$c_i^{ROI} = \frac{1}{n(ROI)} \sum_{(x,y)\in ROI} c_i(x,y) \tag{4.2}$$

where $n(ROI)$ is the number of pixels that belong to the ROI. In Figs. 4.8b and c a typical local calcium trace is shown in time and space. From this trace, the spark can be characterized by measuring several features, such as

- baseline (c_o): level of cytosolic calcium before the first opening.
- amplitude: relative amplitude with respect to the baseline $amp = \frac{\Delta c}{c_o}$.

- full duration at half maximum (FDHM): time lapse during the calcium trace is above the half f the maximum.
- full width at half maximum (FWHM): it is the width of the calcium signal measured above half the maximum amplitude.
- time to peak: time lapse between the first opening and the time where the calcium reaches its maximum amplitude.

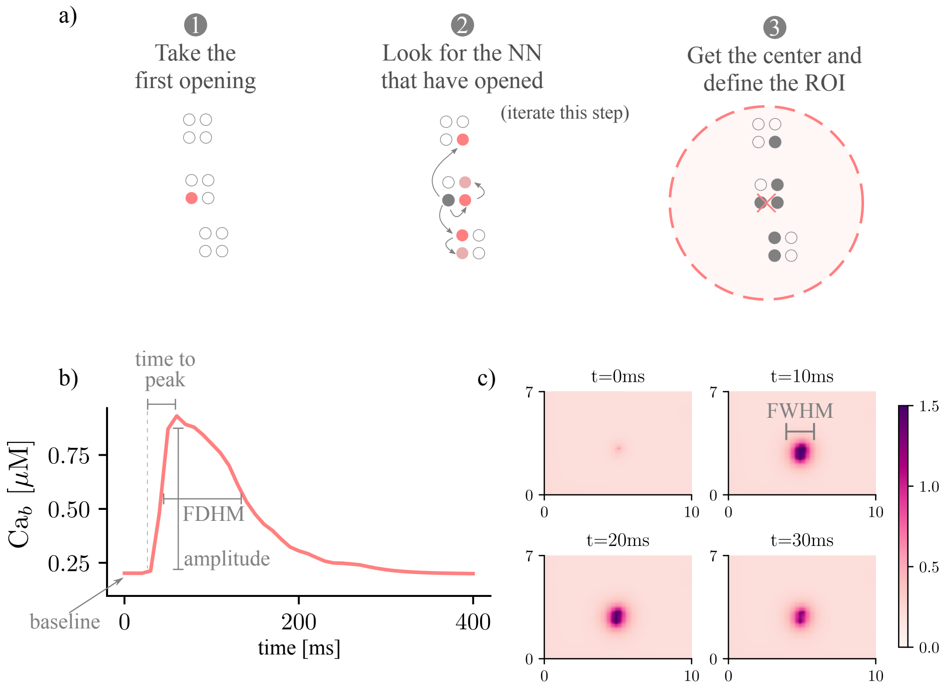
a)
①
Take the first opening
②
Look for the NN that have opened
(iterate this step)
③
Get the center and define the ROI
b)
time to peak
FDHM
amplitude
baseline
Ca_b [μM]
0.25
0.50
0.75
0
200
400
time [ms]
c)
t=0ms
t=10ms
t=20ms
t=30ms
FWHM
7
0
10
1.5
1.0
0.5
0.0

FIGURE 4.8: **Diagram of the procedure employed in the model to label the opened RyR2s into the same event.** a) In the first subplot the red dot represents the first opened RyR2. In the second subplot, the RyR2s opened in the next frame are shown in red, and the RyR2s opened in the third frame in pink which are, in turn, near neighbors of the opened RyR2s of the second frame. Nearest neighbors RyR2s are defined as the RyR2s at a maximum distance of 1μm that have been opened 10 ms after the previous RyR2s. The circle in the third subplot represents the Region of Interest for this spark. b) Example of a spark trace with the relevant characteristics that we measure. c) Spatial profiles of a spark at different times. The measure of the FWHM is depicted in the second frame.

Local calcium traces are shown in Fig. 4.9. We have zoomed in these traces to appreciate the calcium rise and decay during a calcium spark. The stochasticity of the model produces different types of sparks regarding their amplitude and duration.

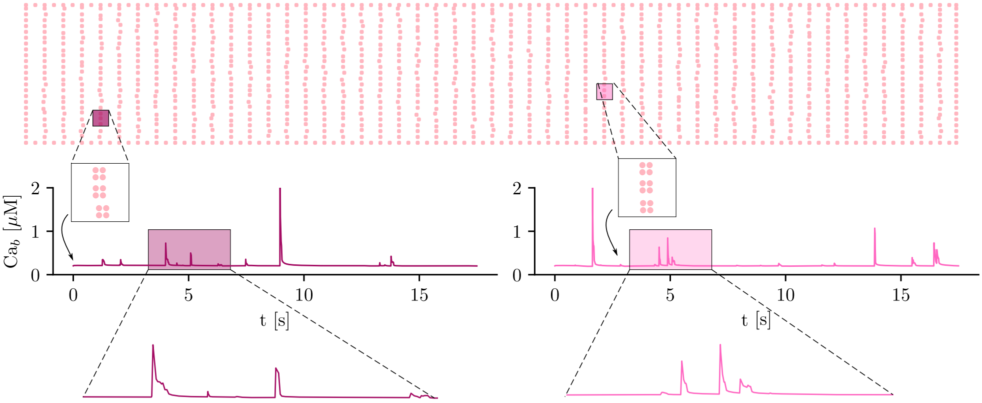

FIGURE 4.9: **RyR2 distribution and local calcium traces.** The local calcium traces correspond to the spatial averages over regions of 2.9 μm^2.

The characterization of these sparks in terms of their properties is shown in Fig. 4.10a. The mean value of these distributions fits with the previous knowledge about calcium sparks. For instance, the duration and time to peak have been measured to be around 20 ms and 10 ms [175, 239], respectively. The mean value of the FWHM has been measured to be about 2 μm [308]. The mean value of the amplitude is not comparable with the experiments since this magnitude is heavily affected by the noise. This issue will be addressed in the next section.

4.3.2 Characterization of the experimental noise

The spatio-temporal profiles of calcium obtained with the model are not comparable directly with the experimental data. First, experiments do not measure calcium concentrations but they measure fluorescence, i. e. the amount of calcium bond to Rhod-2 (for more details go to section 3.4.2). On the other hand, one has to include to the model the intrinsic noise in the calcium profiles. This noise is produced in the experimental setup due to random fluctuations in the photomultiplier. The addition of noise to the simulated data hides the small and short sparks in terms of amplitude and time duration. Nowadays, these small sparks are not measurable and they are supposed to be the leading cause of passive calcium leak [236, 36].

To compare our results with experiments, the intrinsic noise of the experimental data has been characterized. This experimental data has been obtained from the research group leaded by Leif Hove-Madsen at the Biomedical Research Institute Barcelona IIBB-CSIC, at Hospital de Sant Pau (Barcelona). The noise distribution is shown in Fig. 4.11a, where the average time between fires (T_p) of a single pixel has been computed. This data follows an exponential distribution with a mean time between peaks of 103ms. Finally, the average number of pixels that fire with respect to the total number of pixels (S_{xy}) has been calculated. It follows a Gaussian distribution with a mean density of 3.92%. We have already checked that the

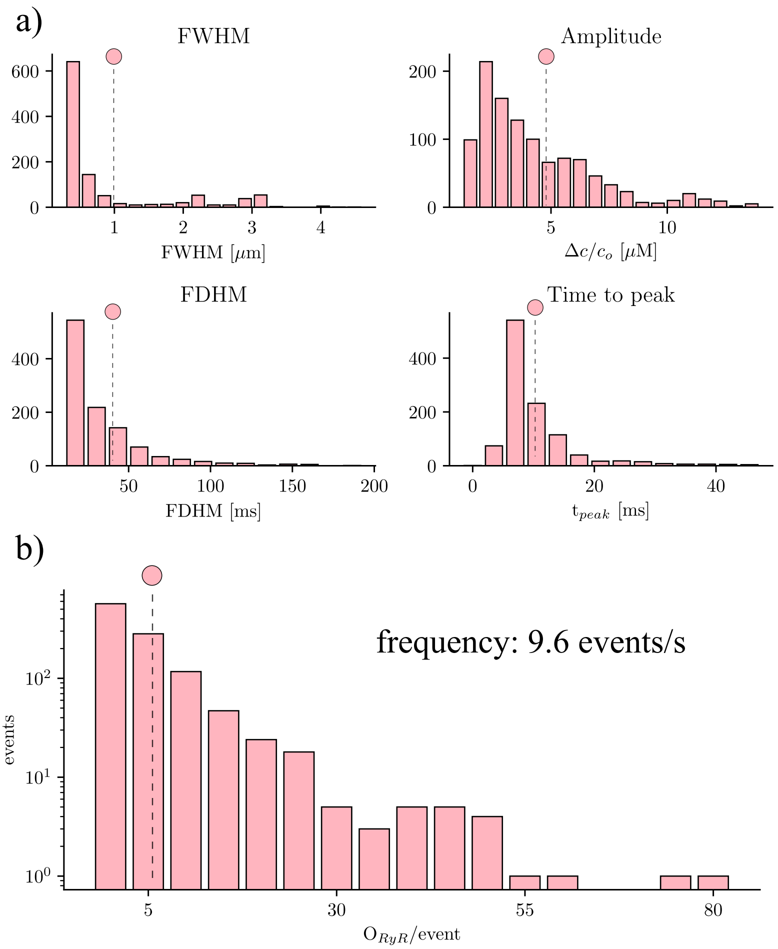

FIGURE 4.10: **Spark properties.** a) Distribution of the spark properties. Dots represent the mean value of each distribution. b) Frequency events as function of the number of opened RyR2s.

experimental noise is spatially uncorrelated. We have created synthetic noise with the same statistical properties as experimental noise. The features of the noise are shown in Fig. 4.11b.

As it is shown in Fig. 4.11, the experimental noise has no zero mean. In order to compare the simulated data with the experimental one, I have followed these three steps:

- Remove the basal level of the calcium signal: $\tilde{c}_i(x,y) = c_i(x,y) - \langle c_i(x,y) \rangle$
- Generate synthetic noise: $S(x,y)$. The mean value of the noise will be proportional to its amplitude
- Add the generated noise to the normalized calcium signal: $\tilde{c}_{s,i}(x,y) = \tilde{c}_i(x,y) + S(x,y)$

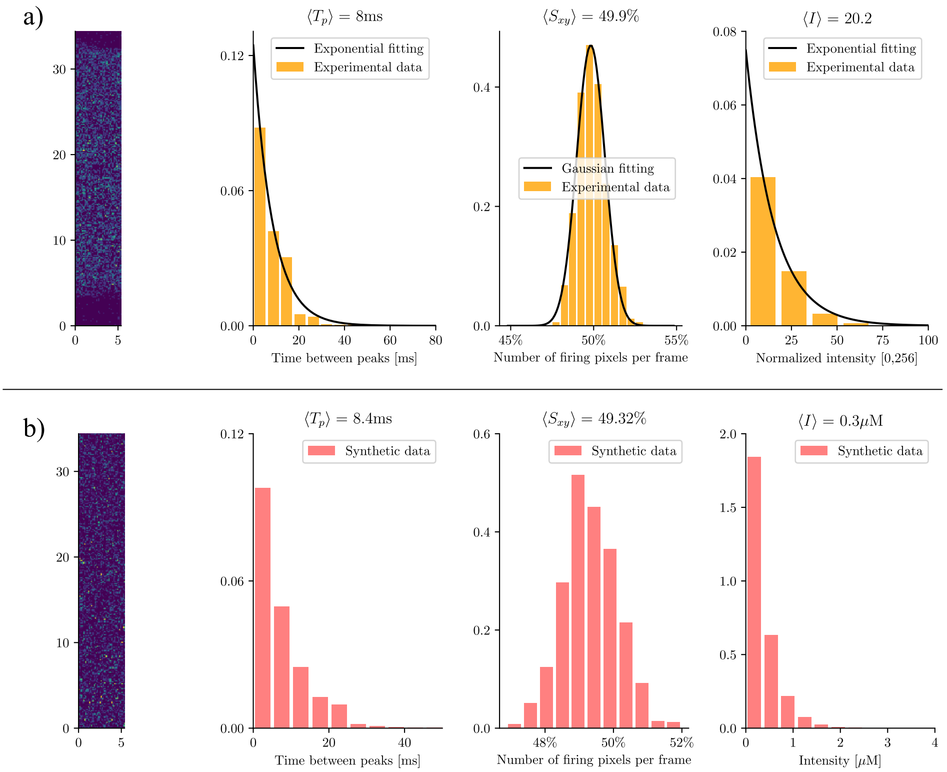

FIGURE 4.11: **Experimental noise characterization.** a) Spatial profile of an experimental frame with noise. Statistical distribution of the time lapses between peaks, density of fires per frame and distribution of intensities. b) Analysis of the synthetic data created with the statistical distributions of the experimental data.

Thus, the baseline of the new signal will be completely determined by the mean value of the noise which, in turn, is determined by its amplitude. For instance, in Fig. 4.12 I show a local calcium fluorescence trace with and without added noise. The addition of noise modifies the baseline of the signal masking the small sparks while the larger ones are still visible. Moreover, it utterly determines the spark properties such that the relative amplitude, which will be lower if the baseline increases due to the addition of noise.

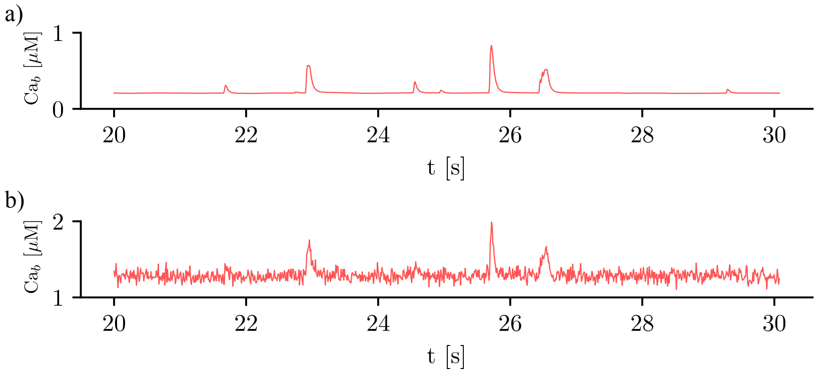

FIGURE 4.12: **Local calcium traces with the addition of noise.** a) Fluorescence calcium concentration obtained directly from the simulation. b) The same calcium trace with the addition of synthetic noise characterized from experiments. Both signals have been averaged over the same region of 2.5 μm^2.

In the experimental lab of Prof. Hove-Madsen, they use an imaging software to detect calcium events [18], a program patented under the name "Method for detecting local events of intracellular calcium release", which we usually call SPARKSIMPLE. This software processes the data obtained from the confocal microscopy characterizing the spark properties of the local calcium events, which are spatial averages over a ROI. One of these calcium traces obtained from the experiments is shown in Fig. 4.13. Visually, the traces obtained from the model are comparable.

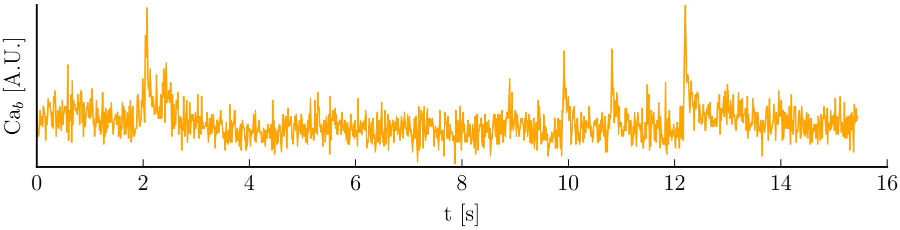

FIGURE 4.13: **Experimental local trace.** The experimental traces are obtained with the SPARKSIMPLE software, which averages calcium concentrations over a Region of Interest (ROI). The y-axis given by the confocal microscopy is measured in a binned scale of integer values between 0 and 255.

SPARKSIMPLE has been used with the data obtained with the model in order to characterize the synthetic calcium events. Using this software, we are able to check if our sparks are detectable under different filtering parameters. In Fig. 4.14a the spark frequency for two filtering sets and two levels of noise is shown. The number of false positives, that is, the number of events that have counted artificially since they do not correspond to any opening of a RyR2 is shown in

Fig. 4.14b. First, Sparksimple discards several calcium sparks due to its spatio-temporal characteristics. The fraction of discarded events is 15-60% depending on the level of restriction. However, when noise is added to the simulations, many events are hidden due to its small amplitude and/or short duration and, thus, the frequency of visible events decreases.

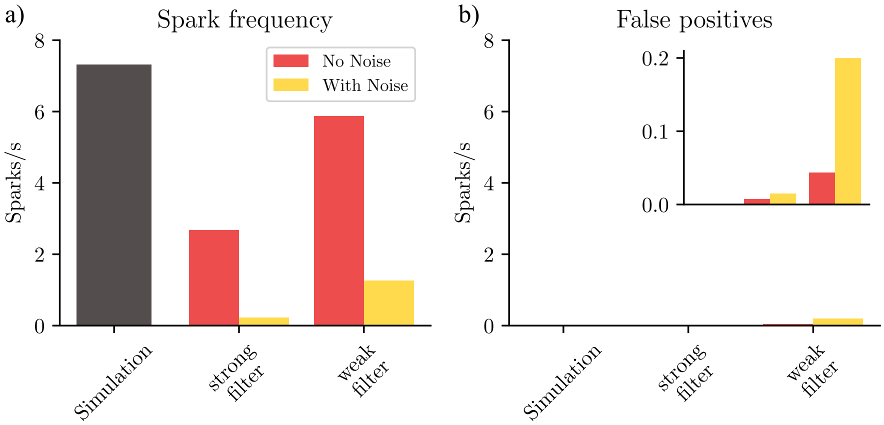

Figure 4.14: **Spark frequency measured with the experimental software.** a) Spark frequency obtained directly from the simulations (black) and using Sparksimple with two filtering sets and two levels of noise. The filtering sets are defined as a group of intervals for each spark property. The strong filter typically discards small events, while the weak filter is able to detect the small sparks. b) Frequency of false positives.

Part III

Applications

Chapter 5

Changes in CaRU size and distribution

The appearance of single-molecule super resolution imaging like the Stochastic Optical Reconstruction Microscopy (STORM) and related techniques, has greatly advanced insight in cell biology over the last decade. With this new technical advancements, the visualization of macro structures like the RyR2 channels has been possible. In particular, it has been feasible to analyze the geometrical structure of the RyR2s at the subcellular scale as well as how they group into clusters, previously defined as Calcium Release Units (CaRU). When a CaRU is triggered, it produces a local release of calcium from the SR. These local release events are called calcium sparks. A good understanding of their temporal and spatial characteristics and frequency, as well as the morphology of the CaRU is, thus, very important to properly characterize the process of CICR. Due to the fine discretization of our model, we can observe their detailed spatio-temporal profiles. In this chapter, I have studied the effect of the cell microstructure in the properties and frequency of sparks.

5.1 Effects of cluster size and spatial distribution

We have first modified the microstructure, changing the size and distribution of the CaRUs. This is particularly important since it has been observed that the RyR2 distribution is modified in a specific manner under conditions of AF [175]. We have then calculated the spark frequency under resting conditions for different configurations defined by the Gaussian distribution of position sites and size of the CaRUs. For the standard size of the CaRU (36 RyR2s divided equally among 4 grid points, each one containing 9 RyR2s), I have considered three values of the dispersion in the Gaussian distribution, the standard value of $\sigma = 0.4$ μm, and two cases with larger dispersion of $\sigma = 2$ and 3.6 μm, see Fig. 5.1. Besides, I also consider the effect of a change in the CaRU size, considering CaRUs with 54 RyR2s, divided equally among 6 grid points, each one containing 9 RyR2s (Fig. 5.1 down right), but maintaining fixed the total number of RyR2s in the cell. Since the total number of RyR2s is the same, this means that there are larger, but less CaRUs in the cell.

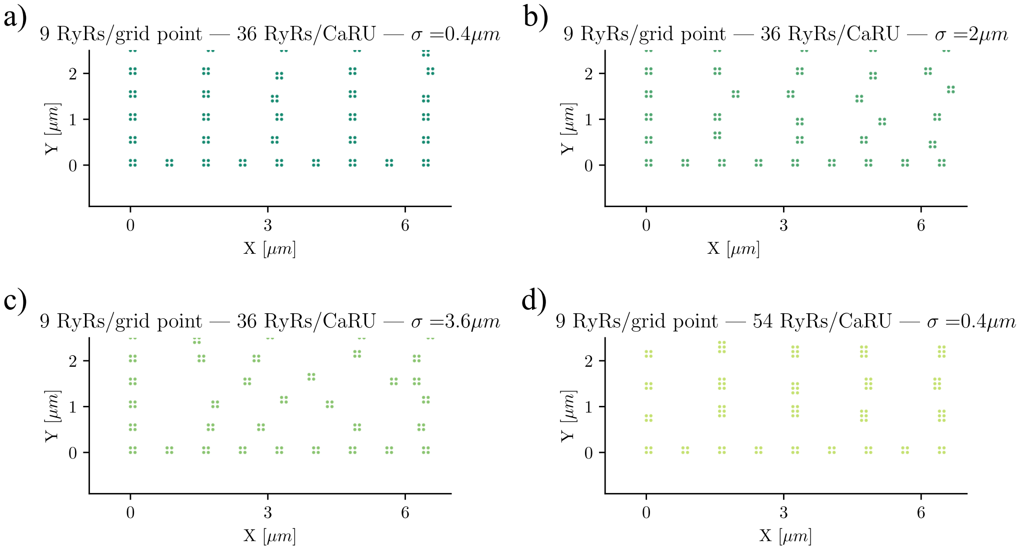

FIGURE 5.1: **Spatial CaRU distributions.** Different RyR2 distributions considered in the text. The bottom left corner of the whole cell is displayed. The green dots represent grid points with RyR2s. a) control configuration, with standard dispersion in the position of the RyR2s $\sigma = 0.4$ μm. b) increased dispersion of σ to 2 μm. c) $\sigma = 3.6$ μm. d) New configuration, where each grid point contains 9 RyR2s and a CaRU is formed by 6 grid points, so that, each CaRU represents 54 RyR2s. The total number of RyR2s remains constant but now, in the new structure, they are more grouped, that is, the CaRUs are bigger. The dispersion is the same as in the standard case: $\sigma = 0.4$ μm.

In Fig. 5.2A the mean CaRU size is shown. To define the size of a CaRU, I follow the results by Macquaide et al [175], that showed using a computational model that clusters closer than 150 nm act together functionally as a single CaRU. We thus assume that a group of clusters belong to the same CaRU if they are separated, at most, by 0.15 μm edge to edge from each other. By definition, there is a random component in the structure, so that, there is a nonzero dispersion on the distance with respect to the z-line (Fig. 5.2C). Finally, the mean nearest neighbor distance is shown in Fig. 5.2B. In the new structure, since the RyR2s are more grouped, the total number of CaRUs is smaller, so that, the mean distance among them increases.

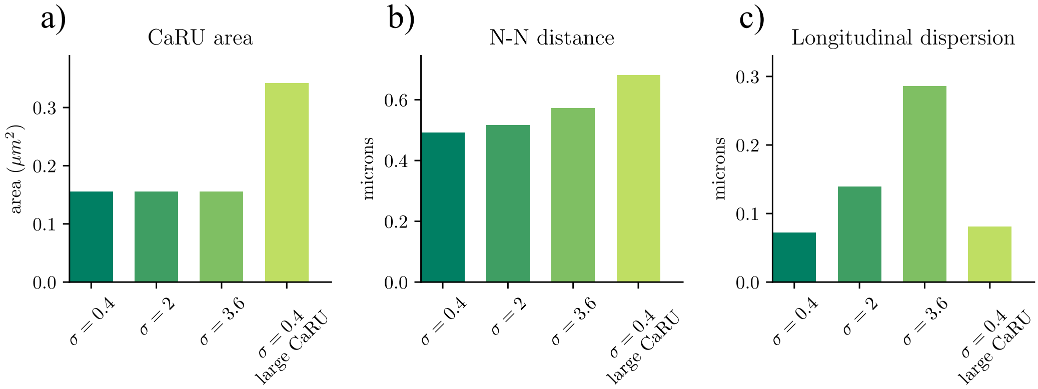

FIGURE 5.2: **Spatial characteristics of the configurations.** a) Mean area occupied by a CaRU. b) Nearest-neighbor distance among CaRUs, measured from the center of each CaRU. c) Longitudinal dispersion, measured as the mean distance between the RyR2s and the center of the z-line. Same color coding as in Fig. 5.1.

The spark frequency is one of the most important indicators of the stochastic activity at resting potential. The total number of spontaneous calcium sparks has been recorded. As shown in Fig. 5.3a, we observe that the frequency decreases with the longitudinal dispersion meaning that the cluster-cluster communication plays an important role in stochastic activity. On the other hand, when the CaRUs are bigger, the spark frequency increases twofold with respect to the distribution with 36 RyR2s and low longitudinal dispersion of the RyR2s. Besides the global frequency of calcium release events, one can measure the spatio-temporal characteristics of each spark. In Fig. 5.3a I also show the amplitude of the sparks with respect to the baseline, the time to reach the peak, which is the lapse time between the firing of the first RyR2 and the time at which is achieved the peak of calcium, and the full duration at half maximum, the lapse of time at which the calcium level is above half of the peak.

The model allows us to determine the number of RyR2s that have been opened during a single calcium event. This calculation is shown in Fig. 5.3b. The cluster size is fixed to 36 RyR2s, meaning that most of the calcium events are produced by the coordinated spatio-temporal activation of several CaRUs. The increment of the CaRU size (54 RyR2s) produces larger events in terms of the number of opened RyR2s. Alterations in RyR2s organization have been measured in patients with AF and they have been related to the appearance of large sparks [175, 239].

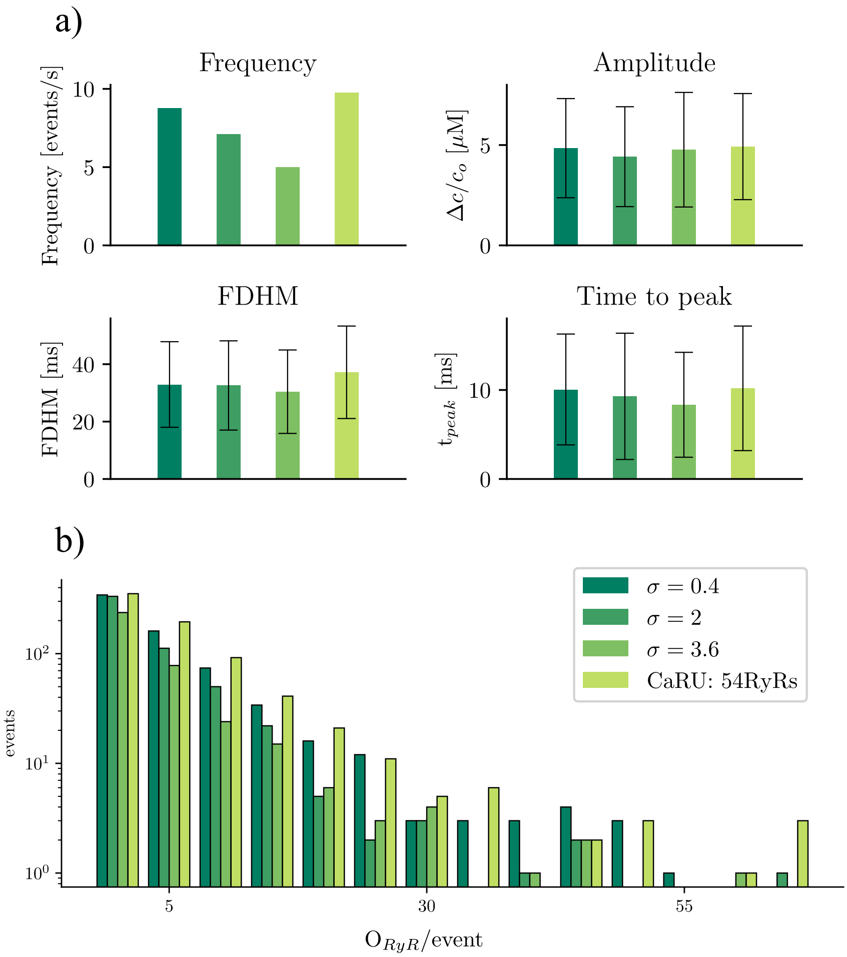

FIGURE 5.3: **Spark characteristics.** a) Spark frequency, amplitude, time to peak and FDHM, for the four different configurations, $\sigma = 0.4$, 2, 3.6 (with 36 RyR2s) and $\sigma = 0.4$ with large CaRUs (54 RyR2s). b) Spark frequency as function of the opened RyR2s for both assemblies.

5.2 Effects of a heterogeneous distribution of RyR2s per CaRU

It is widely accepted that the size of the CaRUs is heterogeneous through the cell. In general, the cardiac myocytes have plenty of small clusters with 1-10 RyR2s and few of them with more than 100 RyR2s. However, beyond that general rule, there are severe discrepancies in how could be this distribution of RyR2s per CaRU. For instance, Soeller et al. [250] measured the cluster size in rat ventricular myocytes and found a mean value of 182 RyR2s with an asymmetric Gaussian distribution. However, strong assumptions were done to calculate the cluster size. In particular, they assume circularity and complete filling of the junction yielding to a overestimation of the cluster size. Baddeley et al. [11] studied the RyR2 distribution in the periphery of the rat ventricular cell. They showed that, in average, the CaRUs have 14 RyR2s and the distribution follows an exponential. Moreover, the stochastic assembly of RyR2s makes it possible to have macroclusters, which are defined as the groups of clusters which are close enough to act functionally as one CaRU. Later, they studied the internal CaRUs [114] where they found that the cluster sizes exhibit a near-exponential distribution with a mean size of 63 RyR2s. This result is similar to what has been found in [55] with a mean value of 43 RyR2s in mouse dyadic couplings. Recently, more efforts have been made to prove the existence of that exponential distribution [130]. However, other recent studies have found that the distribution is Gaussian with a mean value of 84 RyR2s [85]. Galice et al. [85] use the relative F-FKBP fluorescence intensity to provide a direct quantitative relation of the number of RyR2s within a given local cluster. On the other hand, there are several studies which state that RyR2 distribution has a bimodal shape, formed by the sum of a Gaussian and Exponential distributions. In that respect, Macquaide et al. [175] studied the structural properties in sheep atrial mycyotes and they obtained that the mean cluster size is about 15 RyR2s. The relationship is well fit with the sum of an exponential for small clusters and a Gaussian function for larger clusters. This indicates that small and large RyR2 clusters belong to two sub-populations. In addition, they showed that in persistent AF the organization of the CaRUs is more fragmented, with more clusters that are in close proximity to each other. It has also been shown that the organization of RyR2s follows a bimodal distribution in rabbit atrial myocytes [262]. All these experimental findings are summarized in Fig. 5.4. Despite the strong discrepancies on which is the CaRU distribution, it has to be said that the experimental resolution is not fine enough to do an exact definition of a CaRU in terms of the maximum distance between the subsets that conform a CaRU. For that reason, one finds this huge variability on the results.

For simplicity, in all results presented until now, I have used an homogeneous distribution where all the CaRUs have the same size (36 RyR2s). To be more precise, the model actually incorporates dispersion in the position of the CaRUs, so there exists a non-zero probability to have macro clusters built by single CaRUs. However, beyond that fact, we can say that the distribution is homogeneous. To analyze the effect of the CaRU organization, I have incorporated to the model an algorithm to construct heterogeneous distributions. To do so, I follow [175, 262] to consider a probability density distribution of the form

$$f(N) = \frac{1}{2}\left[\frac{1}{N_o}e^{-N/N_o} + \frac{1}{\sigma\sqrt{2\pi}}e^{-\frac{(N-\mu)^2}{\sigma^2}}\right] \tag{5.1}$$

where $f(N)$ is the probability density function to have a cluster of N RyR2s, N_o is the mean value of the exponential distribution and μ and σ are the parameters of the Gaussian distribution. Then, taking the cumulative distribution function of Eq.

Reference	**Type of myocyte**	**Experimental technique**	**RyR2 distribution**	**Mean size**	**Outline**
Soeller, et al. PNAS, 2007	Rat ventricle	Confocal microscopy	Asymmetric Gaussian	182	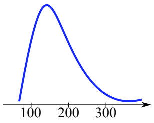
Baddeley, et al. PNAS, 2009	Rat ventricle	Single-molecule localization microscopy	Exponential	14	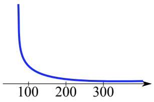
Hayashi, et al. J. Cell Sci., 2009	Mouse ventricle	Confocal microscopy	*Not studied*	43	*Not studied*
Hou, et al. J. Mol Cell Cardiol, 2015	Rat ventricle	Single-molecule localization microscopy	Exponential	63	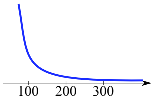
Macquaide, et al. Cardiovasc. Res., 2015	Sheep atria	STED microscopy	Exponential & Gaussian	15	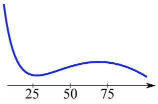
Sutanto, et al. Front Physiol, 2018	Rabbit atria	Confocal microscopy	Exponential & Gaussian	*Not studied*	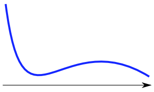
Galice, et al. J. Am. Heart Assoc., 2018	Rat ventricle	Confocal microscopy	Gaussian	84	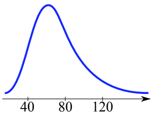
Jayasinghe, et al. Cell Rep., 2018	Rat ventricle	DNA-PAINT	Exponential	8.8	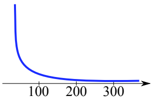

FIGURE 5.4: **Outline of the CaRU distributions.** Overview with the different experiments and results that have been done to measure the CaRU distribution.

(5.1) one can numerically invert the function. That is, let be U a random number between 0 and 1, then one can obtain the cluster size N by solving

$$U = \frac{1}{4}\left[1 + \mathrm{erf}\left(\frac{N-\mu}{\sigma\sqrt{2}}\right)\right] + \frac{1}{2}\left(1 - e^{-N/N_o}\right) \tag{5.2}$$

To construct the full cell CaRU distribution, one has to follow these three steps: 1) take as many random numbers as needed to achieve the value of 65000-70000 RyR2s, 2) place the clusters over the z-lines, considering that we have the same number of clusters in all z-lines, 3) apply the same dispersion criteria as the one presented in section 3.1. In Fig. 5.5 I have summarized these three steps.

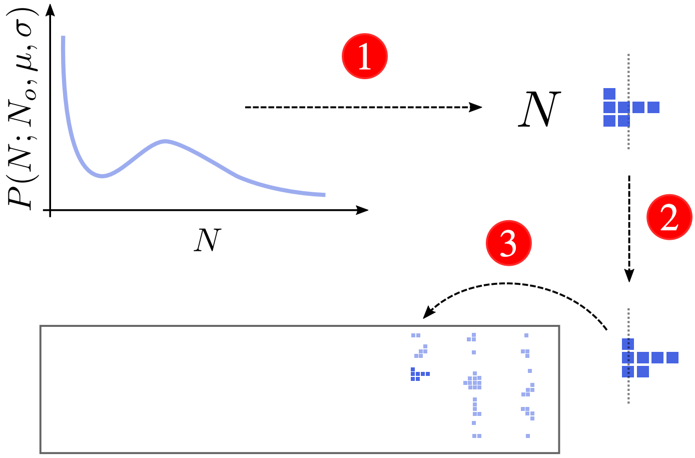

FIGURE 5.5: **Schematics of the protocol used for the creation of the heterogeneous distribution in the model.** 1) The cluster size is a random number obtained from a bimodal probability distribution (exponential and Gaussian). The cluster shape is formed by using a growth isotropic algorithm. 2) The cluster is shifted with respect to the z-line using Gaussian noise. 3) The cluster is placed along the z-lines.

5.2.1 Analysis

In the stochastic algorithm to assembly the RyR2s into clusters, one has to fit the parameters (N_o, μ, σ) to have physiological results. From [175] we know that the mean cluster size is 15-20 RyR2s and the Gaussian peak is close to 50 RyR2s. With that, one can construct the algorithm to simulate an heterogeneous CaRU distribution. In Fig. 5.6 I show an example of the RyR2 distribution, where we can appreciate the heterogeneity in the cluster size. Again, the CaRUs are placed over z-line forming somehow straight lines that cross the cell through the transversal axis.

In the following, I will compare the results obtained using this novel distribution with the results presented in previous sections that are based in an homogeneous

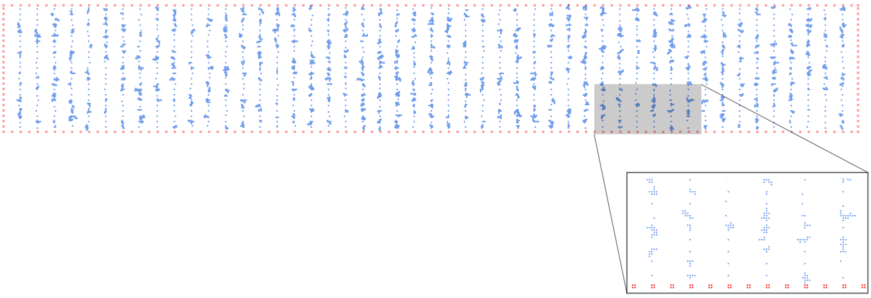

FIGURE 5.6: **Spatial distribution of the CaRUs for the heterogeneous distribution.** RyR2 configuration using the distribution presented in Eq. 5.1. In blue the internal RyR2s and in red the RyR2 placed in the membrane. A region of the cell has been zoomed to appreciate the variability of the CaRUs.

distribution. The number of RyR2s per CaRU is plotted in Fig. 5.7a. We can observe a population of CaRUs with very few RyR2s, meaning that an important part of the clusters are small while, on the other hand, another population at around 50 RyR2s are big clusters and, eventually, can form macro clusters. These macro clusters are huge assemblies of RyR2s with more than 50 RyR2s and appear due to the tail of the Gaussian distribution. The mean cluster size is 32 RyR2s. On the other hand, we have the homogeneous distribution (Fig. 5.7d) which is a discrete delta function centered at the number of 36 RyR2s per CaRU. The novel heterogeneous distribution allows the model to fit the experimental findings recorded by Macquaide et al. [175] and Sutanto et al. [262]. The distribution of the closest distance between clusters is plotted in Fig. 5.7b and d. The mean value in both cases is 0.49 μm. For the heterogeneous distribution it looks like a Gaussian distribution with a longer tail in comparison with the homogeneous distribution. Both configurations have a similar number of CaRUs (see Fig. 5.7c and f).

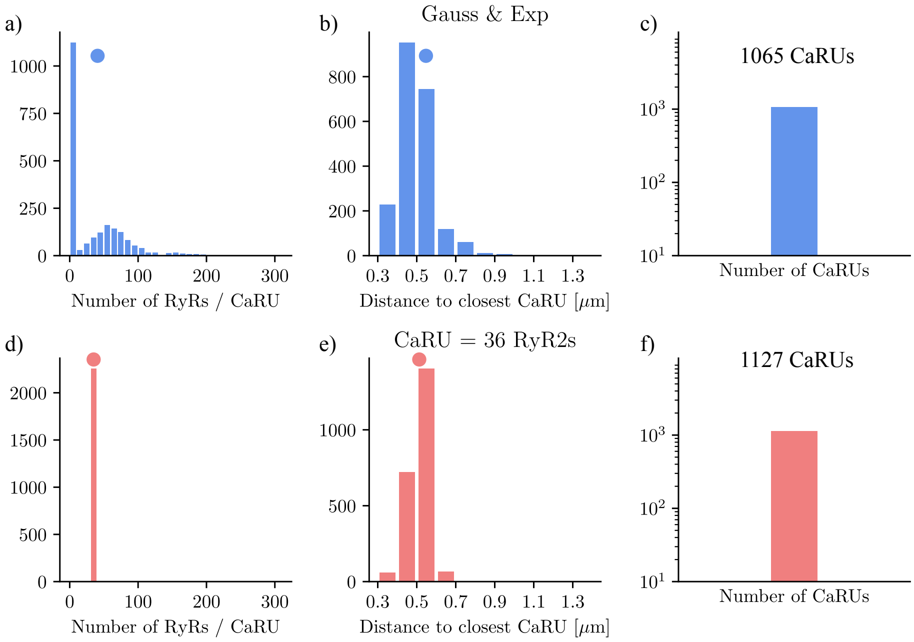

FIGURE 5.7: **Geometrical characteristics of the configurations.** a and d: number of RyR2s per cluster for the heterogeneous and homogeneous distribution, respectively. A cluster is defined as the group of RyR2s that are grouped when edge-to-edge distances are $\leq$ 150 nm. b and e: closest distance center-to-center between clusters for the heterogeneous and homogeneous distribution, respectively. c and f: number of CaRUs in the cell for the heterogeneous and homogeneous distribution, respectively. The filled dots represent the mean value of each distribution.

5.2.2 Results

With this new assembly of RyR2s, simulations without external stimulation have been performed, that is, the membrane potential is set at -85 mV. By setting the proper initial conditions, it is ensured that the system is at the steady state. All this leads to a post rest framework where one can study the spark frequency and all the properties related to the calcium release events. Other than the RyR2 number distribution, both systems have the same parameters and the same initial conditions. The CaRU distribution together with the calcium activity of each CaRU is shown in Fig. 5.8. The spark activity is focused on those CaRUs which have a sufficient number of RyR2s, while small clusters have less activity. This qualitative figure gives us an idea of how much relevant is the intrinsic structure and distribution of the RyR2s into CaRUs.

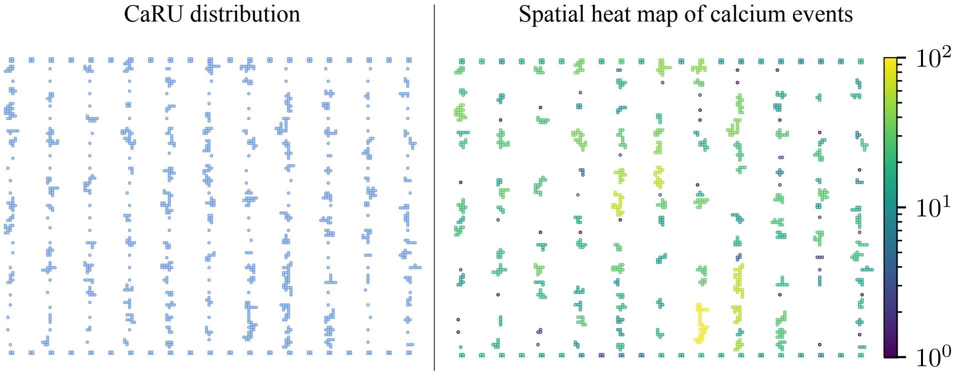

FIGURE 5.8: **Spatial distribution of the firing CaRUs.** CaRU distribution for an heterogeneous assembly of RyR2s (left) matched with the activity of each cluster (left). The current distribution represents a section of 12x15 μm^2 of the cell. The colorbar shows the number of events in each CaRU in a logarithmic scale.

This correlation between the events and the opened RyR2s allows us to clearly understand the local calcium activity. In Fig. 5.9 I show three representative calcium events for different number of total opened RyR2s. First, I show the number of opened RyR2s as function of time. In the second subfigure I show the free calcium concentration and, third, I show the calcium attached to Rhod-2, the fluorescence indicator used in experiments. For the small event ($N_{RyRs} = 5$), the amplitude is much smaller than for the large events ($N_{RyRs} = 38, 71$), whereas no significant differences in terms of amplitude are shown between these larger events. This suggests that SR local load is completely depleted preventing the release of more calcium. Thus, above certain threshold of N_{RyRs}, the total released calcium will be the same. Here we can see how calcium buffering smooths the temporal profiles due to the delay in the binding process between the free calcium and Rhod-2.

To have an idea of the local effects of the spatial heterogeneity of CaRUs sizes, three local regions of the cell with the distribution of RyR2s and the calcium dynamics averaged on that region are shown in Fig. 5.10. For the homogeneous distribution, the regions are almost equal with three CaRUs. On the other hand, for the heterogeneous distribution, the RyR2 distribution is different for each region and this variability is translated to the local calcium dynamics. For instance, in the second region the size of the sparks is much lower than for the other regions. For both distributions, the local calcium dynamics presents sparks with different sizes and shapes but all of them have a short time duration ($\leq$ 1s).

In order to quantify these results, the distribution of the main characteristics of sparks has been computed and it is shown in Fig. 5.11a. The mean values of these distributions are shown in Fig. 5.11b. Although the spark properties do not seem to qualitatively change between the homogeneous and the heterogeneous configurations, we observe a 6-fold increase in the macrospark frequency between

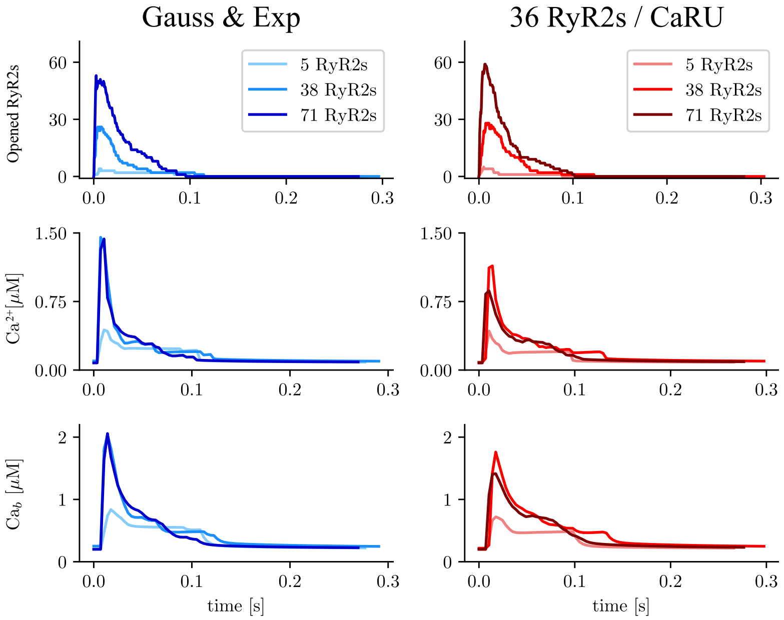

FIGURE 5.9: **Calcium sparks as function of the number of RyR2s.** Three calcium sparks as function of the number of RyR2s opened during the release event. From top to bottom, number of opened RyR2, local free calcium concentration and local calcium bound to Rhod-2 concentration. Concentrations are expressed in μM.

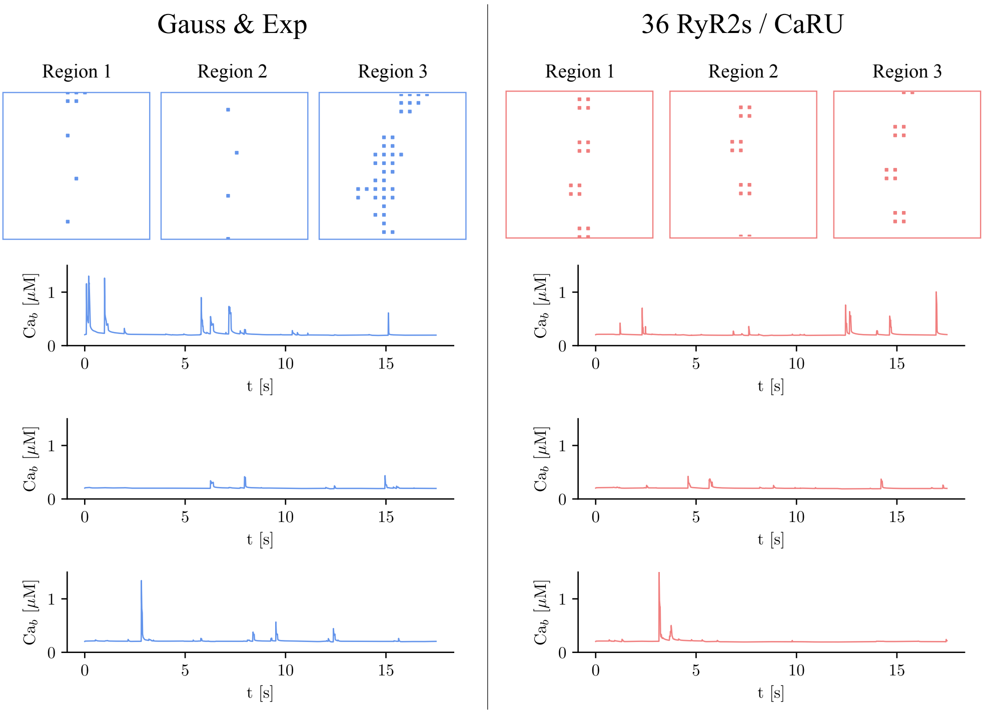

FIGURE 5.10: **Variability of the local traces.** Three representative regions of the cell with the RyR2s distribution and the local calcium dynamics averaged over the specific region.

the homogeneous and heterogeneous distributions. This suggests that the microstructure of the CaRU determines the appearance of macro-events that, in turn, would be able to promote delayed afterdepolarizations or arrhythmias during calcium overload [133, 125].

Next, we study how the properties of sparks depending on the number of open RyRs in each event. In Fig. 5.12a the number of events per unit of time has been plotted as function of the RyR2s that have been opened. Both configurations follow an exponential distribution while the heterogeneous one (blue bars) seems to have a long tail. However, the differences are not stronger enough to ensure that this variability is important. As can be observed in Fig. 5.12b, both FWHM and the relative amplitude increase with the number of RyR2s showing the strong correlation with the number of RyR2s. Above certain value of RyR2s (~ 25), the dispersion in the mean values hides the tendency of these curves due to the lack of statistics. On the other hand, FDHM and time to peak seem to decrease with the number of RyR2s.

Finally, we have studied the average calcium concentration in each pixel. To do so, the calcium concentration in each pixel of the grid has been averaged during all the simulations. This temporal averaging is shown in Fig. 5.13a, where the RyR2 distribution have been plotted. Visually, we can see that the levels of calcium are

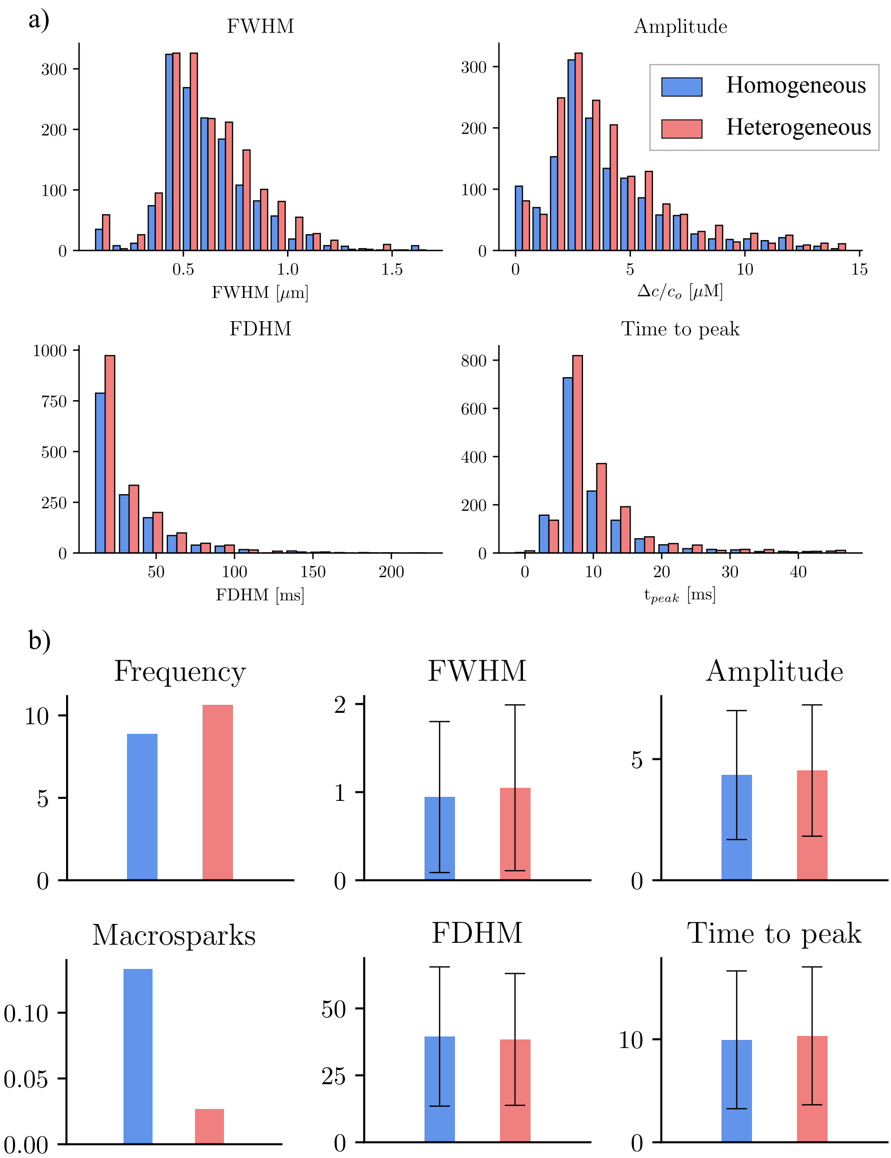

Figure 5.11: **Spark properties.** a) Spark frequency, amplitude, FDHM and time to peak for the homogeneous (red) and the heterogeneous (blue) distributions. b) Mean value of the distributions presented in subfigure a). Here I have included the frequency of sparks as well as the frequency of macrosparks. Macrosparks are those sparks with a FWHM ≥5 μm, following the definition from [175].

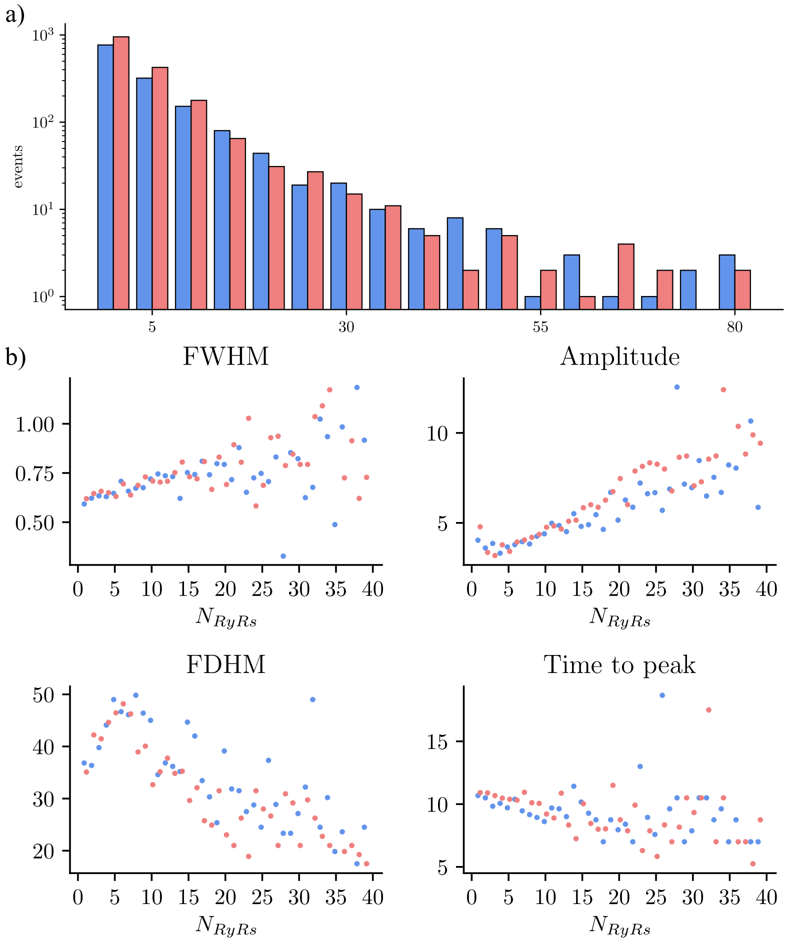

FIGURE 5.12: **Correlation between spark properties and the number of RyR2s.** a) Number of events as function of the activated RyR2s. b) Spark properties as function of the number of RyR2s. FWHM is measured in μm, FDHM and time to peak in ms and amplitude is a non-dimensional magnitude.

nonuniform in both the homogeneous and the heterogeneous distributions. Thus, one would infer that these differences are due to random fluctuations. However, the average calcium concentration in a pixel depends on the RyR2 distribution. In the heterogeneous distribution, pixels which are close to more RyR2s present larger levels of calcium. This effect is shown in Fig. 5.13b. While in the homogeneous distribution the basal level is independent on the number of surrounding RyR2s, in the heterogeneous distribution a 8% increase is observed between the pixels without surrounding RyR2s and the ones with 100 RyR2s. This result enhances the hypothesis that the structural properties of the CaRUs determines the stochastic local calcium release in terms of the spatial localization.

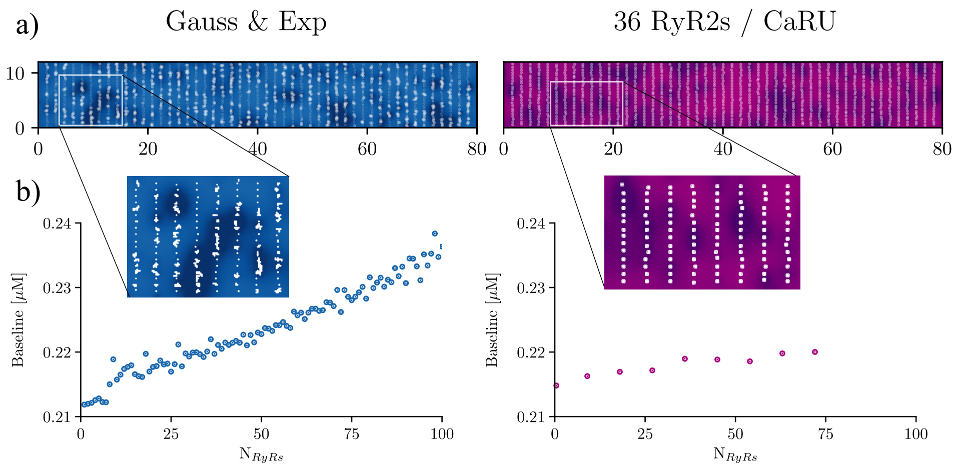

FIGURE 5.13: **Influence of CaRU structure on local calcium concentrations.** a) Sum of all frames from a single realization of the RyR2 distribution. The white dots represent the RyR2 distribution. b) Average Ca^{2+}-Rhod2 concentration per pixel as function of the number of RyR2s in the neighborhood. This number is defined as the number of RyR2s that are within a radius of 0.3μm of each pixel. Both scatter plots have been obtained by averaging over 13 realizations of 12.5s.

5.3 Discussion

Calcium release units are the fundamental structures that determine the morphology of calcium sparks. The high spatial resolution of our model allows us to study in detail the dynamics in the surroundings of the CaRUs, that is, the local calcium concentrations and, thus, the spark activity. In this chapter I have analyzed the effects of changes in the structure of CaRUs on calcium sparks.

Effects of cluster size and spatial distribution. In section 5.1, I have analyzed the effects of CaRUs on calcium sparks by simulating four different distributions. The first CaRU distribution that I have used is an homogeneous distribution with exactly 36 RyR2s in each CaRU and with low noise in the position with respect to the z-line ($\sigma = 0.4$). We have defined it as the reference distribution and it has been used in both sections of this chapter. Two more configurations are defined with the same number of RyR2s in each CaRU and with more dispersion the position of the CaRUs, $\sigma = 2$ and 3.6, respectively. In a fourth configuration, CaRUs are formed by 6 grid points, so that, each CaRU represents 54 RyR2s. These larger CaRUs are obtained increasing their size, but maintaining the density of RyR2s, similar to what is observed in atrial cells presenting AF [175]. We have defined three magnitudes to characterize the CaRU distributions: mean area occupied by a CaRU, nearest-neighbor distance among CaRUs and longitudinal dispersion with respect to the z-line.

We have calculated the spark frequency as well as the spark properties such as the FDHM, the amplitude or the time to peak. Simulations suggest a decrease in spark frequency with CaRU spatial dispersion (Fig. 5.3a). This is correlated with an increase in CaRU nearest-neighbor distance, suggesting that cooperativity among local release events at nearby CaRUs could play an important role in the generation of sparks. In fact, sparks encompassing several CaRUs have also been observed experimentally [144]. The time to peak and the amplitude follow the same trend, they decrease with the longitudinal dispersion (Fig. 5.3a). Finally, simulations suggest that the FDHM is almost constant for all configurations. When the same total number of RyR2s in the cell are distributed in larger CaRUs, we observe an increase in spark frequency (Fig. 5.3a). Both time to peak and amplitude increase with the larger assembly of RyR2s while the FDHM remains constant. Moreover, the number of opened RyR2s in each calcium spark has been recorded. This last calculation is an added value of all this study, since, at this moment, the experimental resolution is not able to record this information. Simulations suggest that the spatial assembly of RyR2s in larger CaRUs promotes the activation of more RyR2s (Fig. 5.3b) and, thus, the appearance of big sparks (or macrosparks).

Effects of a heterogeneous distribution of RyR2s per CaRU. The heterogeneity on CaRU distribution has been generalized in section 5.2. An algorithm to produce random configurations of irregular CaRUs that follow a bimodal distribution has been presented, where the bimodal distribution arises from the combination of an exponential and a Gaussian distributions. The algorithm has been fitted to experimental findings [175, 262]. This novel procedure generates CaRUs with different shapes and sizes, as it can be seen in Fig. 5.6. The total number of RyR2s is the same as in the previous section. With this new assembly, simulations have been approached to a more realistic situation including the spatial heterogeneity to the original model. The resulting spark properties have been compared with an homogeneous configuration with 36 RyR2s in each CaRU. Simulations suggest that the formation of macro-clusters promotes the appearance of hot spots, that is, large clusters that fire repeatedly (Fig. 5.8). The fine discretization of the model allows us to study the local calcium activity. In this sense, there is variability of the local calcium traces as a function of the number of RyR2s (Fig. 5.9). Although strong differences between configurations in terms of the spark properties are not observed, the model suggests that the appearance of macro-sparks is linked to the presence of macro-clusters, which are only possible in the heterogeneous distribution. These macro-sparks would be related to the presence of DADs and even arrhythmias during increased RyR2 open probability [234, 100] and calcium overload [42, 164]. In this respect, I have evaluated the correlation between the average local calcium concentration and the number of surrounding RyR2s. Simulations suggest that regions with more RyR2s in the heterogeneous distribution have a larger level of calcium concentration, while this effect is not shown in the homogeneous distribution (see Fig. 5.13). Finally, the distribution of events per number of RyR2s follows a decreasing exponential distribution. This result has also been observed in Macquaide et al. [175].

Chapter 6

RyR2 activity modulators during AF

AF has been associated with changes in the expression or activity at the subcellular level, as has been explained in chapter 1. Recent works have evidenced [158, 268] that modulations in CSQ concentration and in RyR2 phosphorylation cause an heterogeneous distribution of calcium sparks that could lead to ectopic activity and calcium waves. To asses these situations, we have modified the RyR2 Markov model in the subcellular model to include the dependence on (1) the free CSQ concentration and (2) a RyR2 phosphorylation spatial factor. These studies are explained in sections 6.1 and 6.2, respectively. Finally, I have included a general Discussion reviewing the effects of two RyR2-modulators above-mentioned.

6.1 Calsequestrin

CSQ is one of the major Ca^{2+}-binding proteins in the SR with high capacity and low affinity [192]. CSQ is preferentially anchored close to the RyR2 channels [132, 80]. Nowadays it is known that CSQ is the key element that controls the RyR2 gating [99, 143, 252] through the calcium bound to CSQ. In particular, it has been shown that the absence of CSQ enhances the RyR2 channel opening and, thus, promotes premature spontaneous SR Ca^{2+} macro events. In addition to simply storing Ca^{2+}, CSQ concentrates Ca^{2+} near the points of release consequently influencing the release process by controlling free Ca^{2+} dynamics near the luminal regulatory sites of the RyR2 complex [15, 14, 16].

Dysregulations in CSQ dynamics have been associated with heart diseases [63, 221]. The first experiments that studied the effects of CSQ in Ca^{2+} handling were done by Sato et al. [227] and Jones et al. [131], where it was shown that an overexpression (20-fold) of CSQ in mouse ventricular myocytes produces high SR load and leads to HF. At that time, other studies suggested that the activity of the RyR2s depends on the Ca^{2+} in the SR [243, 47] although both calcium transients and sparks were reduced in amplitude and frequency. It was not obvious to explain why an increase in the SR load produced a reduction of calcium handling in the cytosol. Recently, these changes have been attributed to: (1) an inhibition of RyR2s by high levels of CSQ [101] (2) an increase of the SR volume [143] as a compensatory mechanism to preserve the Ca^{2+} release. On the other hand, experiments with rat myocytes have shown an increase in the Ca^{2+} transient with a three to four-fold over-expression of CSQ and also an increase on the refractory period of the RyR2 channels [270]. In contrast, CSQ knockdown leads to shorter Ca^{2+} transients and fast restitution of the RyR2s yielding to global oscillations and DADs. The ablation of CSQ causes a form of tachycardia, namely, catecholaminergic polymorphic ventricular tachycardia (CPVT) [63, 48]. Exactly, there are 15 known mutations in CSQ which are known to cause CPVT [102]. Therefore, modulation of CICR properties is an important mode for treating cardiac diseases.

6.1.1 Methods

In recent years many attempts have been done to thoroughly understand all the causes and consequences of CSQ modulation. We will briefly describe the main contribution to the topic as well as the objectives of our work.

The relation between CSQ mutations and spontaneous calcium release has been studied in both guinea pig ventricular myocyte [72] and human cells [122]. Both models are able to reproduce the spontaneous calcium release and the enhancement of DADs when the expression of CSQ is altered. The most important limitation of these studies is that they are based on common-pool models and this is at odds with well-known experimental results: (1) the CICR process is produced by the coupling of unitary calcium release events (sparks) and (2) the pathological CICR occurs in the form of Ca^{2+} waves, that is, heterogeneous calcium patterns.

Although early models [246, 247, 152, 2] do not include an explicit regulation of CICR by CSQ through a modification of RyR2 gating, they already proposed an indirect relation between the SR luminal calcium and the activity of RyR2. Later, new mathematical models investigated novel mechanisms that include direct CSQ regulation of RyR2 gating [153]. These models can, for instance, explain the increase on spontaneous Ca^{2+} release with reduced CSQ.

CSQ has been demonstrated to have two main effects. On one hand, it works as a reservoir of Ca^{2+} in the SR that binds and unbinds to free calcium. This dynamics is represented by the reaction equation already presented in section 3.4.3. On the other hand, CSQ modulates the RyR2 gating. To take into account this effect, Lee et al. [153] proposed a four state model where transition rates depend on the calcium bound to CSQ (q). Initially, they worked with an eight state model that can be simplified to four states if one assumes the rapid buffer approximation of CSQ. The scheme of the RyR2 is equivalent to the one presented in Fig. 3.3. We have incorporated the CSQ dependence on two rates: k_{co} and k_{i2i1}, which now are defined as:

$$k_{co}(c_i, q) = k_a^*(q)\frac{c_i^3}{1+\left(\frac{c_i}{c_i^*}\right)^3} \qquad k_{i2i1}(c_i, q) = k_b^*(q)\frac{c_i^3}{1+\left(\frac{c_i}{c_i^*}\right)^3} \tag{6.1}$$

and k_a^* and k_b^* depends on CSQ following:

$$k_a^* = \frac{(k_2 K_1^d)^3 + (k_{11} q)^3}{(K_1^d)^3 + q^3} \tag{6.2}$$

$$k_b^* = \frac{(k_2 K_8^d)^3 + (k_{11} q)^3}{(K_8^d)^3 + q^3} \tag{6.3}$$

The modified four state RyR2 model is shown in Fig. 6.1a. The dependence of k_a^* and k_b^* on the unbound CSQ concentration is shown in Fig. 6.1b. We have followed the same notation as in [153]. k_{11} and k_2 are the rates of RyR2 opening when CSQ is attached or not to them, respectively; K_1^d and K_8^d are the dissociation constants of the model. q is the concentration of free CSQ. The total concentration of CSQ (B_{CSQ}) has been measured in patients with and without AF [158] where the CSQ concentration is larger in patients without AF. Moreover, it has been shown that B_{CSQ} varies through the cell [268]. In both conditions B_{CSQ} is higher near the membrane and then decreases throughout the cell. In our simulations, it has been considered that in the no AF condition, B_{CSQ} varies between 6mM and 2.25mM and, in case of AF, it varies between 3.38mM and 1.5mM. It has been assumed that it decreases linearly with the distance to the membrane. Then, the total amount of calsequestrin is given by:

$$B_{CSQ}(r) = B_0 + 2(B_1 - B_0)\frac{r}{L_y}, \tag{6.4}$$

where B_0 is the total concentration of CSQ in the membrane, B_1 is the total concentration of CSQ at the farthest points, which are in the center of the cell, and r is the distance from any point (x, y) to the center of the cell. The reduction of B_{CSQ} induces a reduction of free CSQ concentration q and, in turn, an increment of the open rate k_{co} (see Fig. 6.1b). The spatial distribution of $B_{SQ}(r)$ is shown in Fig. 6.1c.

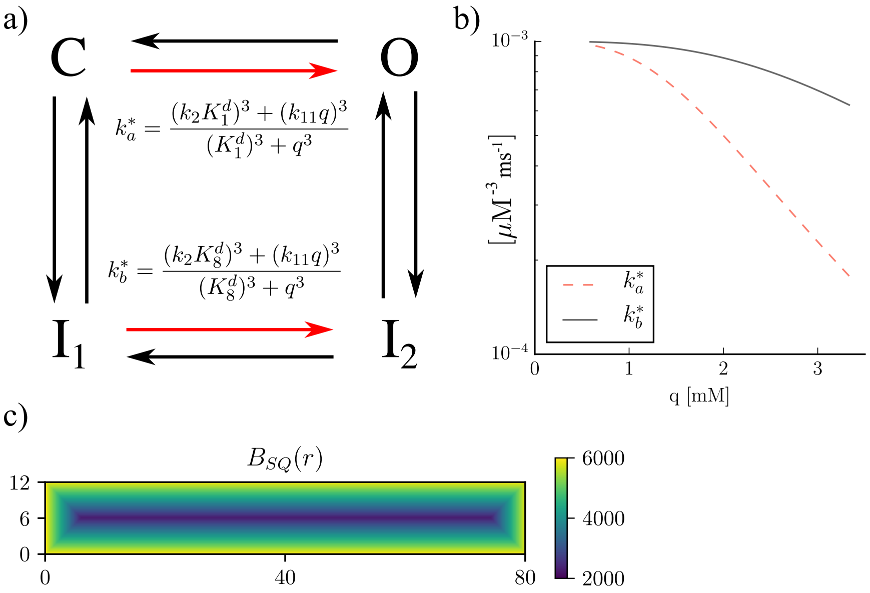
a)
C
O
$k_a^* = \frac{(k_2K_1^d)^3 + (k_{11}q)^3}{(K_1^d)^3 + q^3}$
$k_b^* = \frac{(k_2K_8^d)^3 + (k_{11}q)^3}{(K_8^d)^3 + q^3}$
I_1
I_2
b)
10^{-3}
10^{-4}
$[\mu M^{-3} ms^{-1}]$
k_a^*
k_b^*
0
1
2
3
q [mM]
c)
$B_{SQ}(r)$
12
6
0
0
40
80
6000
4000
2000

FIGURE 6.1: **Modeling of CSQ as a RyR2-modulator.** a) Diagram of four state model of the RyR2 with CSQ modulation on the red rates: k_{co} and k_{i2i1}. b) Dependence of k_a^* and k_b^* on the unbound CSQ concentration q. c) Spatial distribution of $B_{SQ}(r)$ for the no AF conditions. The colorbar is in μM.

6.1.2 Results

The influence of CSQ on the spark features has been evaluated assuming the description presented in the previous section. Thus, several spark properties have been recorded and are shown in Fig. 6.2. We have measured the full duration at half maximum (FDHM), the full width at half maximum (FWHM), the time to peak measured as the time between the first opened RyR2 and the time when the calcium peak is reached and the amplitude relative to the baseline. These properties do not show strong differences. Simulations suggest that the calcium sparks produced in both normal and AF conditions in terms of the CSQ concentration do not change despite minor differences.

However, the heterogeneous distribution of CSQ through the cell leads to a non-uniform spatial distribution of sparks. Thus, since the amount of CSQ decreases with the distance to the membrane, a high density of sparks is present in the interior of cell. To address this issue, I have calculated the spark frequency through concentric rings of 1 μm (Fig. 6.3). The spark distribution has a peak in the outer ring close to the membrane due to geometric effects, since the density of CaRUs on the cell membrane is twice the density on the rest of cell. The lack of CSQ in the center of cell produces an almost linear increase with the distance to center of the cell.

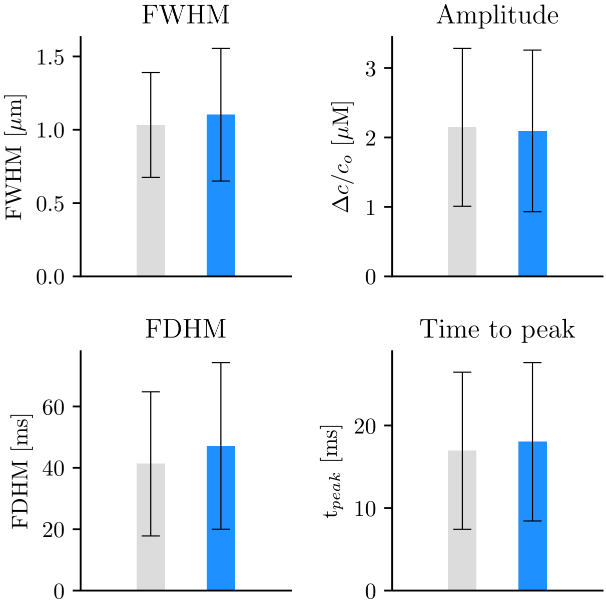

FIGURE 6.2: **Spark properties for no AF and AF conditions due to the lack of calsequestrin.** The effect of CSQ has been characterized in terms of the FWHM, amplitude, FDHM and time to peak for both cell conditions.

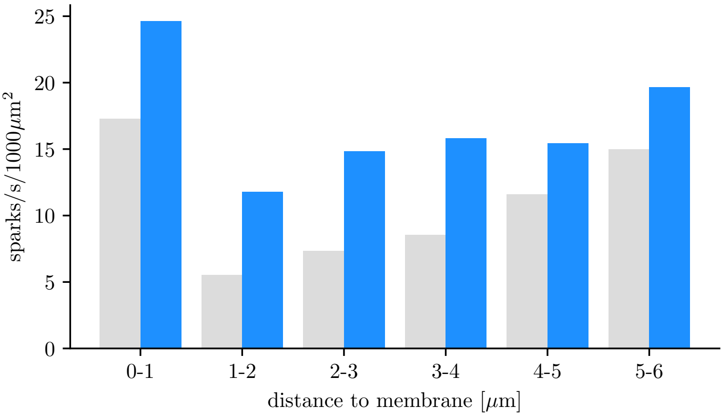

FIGURE 6.3: **Spark frequency as function of the distance to membrane.** The spark frequency has been normalized with the area of the corresponding layer.

6.2 Phosphorylation

Phosphorylation of RyR2 consists in the binding of many proteins to the different phosphorylation sites [264, 103]. These proteins, such as kinases and phosphatases, phosphorylate and dephosphorylate the RyR2s increasing and decreasing the open probability, respectively. The rate of phosphorylation of these sites depends on a dynamic balance between multiple protein kinases [105], allowing precise control of the channels activity [294]. Alterations in RyR2 phosphorylation play a critical role in many cardiac diseases, including HF as well as atrial and ventricular arrhythmias [171]. It is likely that phosphorylation, together with a reduction of SERCA and enhancement of NCX, contributes to the depletion of SR Ca^{2+} content in HF [182]. Moreover, RyR2 phosphorylation has been related to many CVDs. For instance, the development of diastolic Ca^{2+} leak has been suggested to be due to increased phosphorylation of the RyR2 [185].

The RyR2 complex has several sites where proteins can attach producing a modification of the structure and the functionality. The most studied regulatory proteins are Calmodulin protein kinase II (CaMKII) and Serine (S2808). Both have been suggested to be leading agents that promote RyR2 phosphorylation [185, 145, 183]. They have been shown to be important regulators that modify SR Ca^{2+} release. When over-expressed in diseased hearts, these proteins may cause an increase of RyR2 open probability, causing an excessive diastolic Ca^{2+} leak. This sudden increase in SR Ca^{2+} release activates the NCX current, which can cause DADs and, in turn, trigger lethal ventricular arrhythmias. HF, a frequent cause of AF, induces SR Ca^{2+} overload and DADs [306]. RyR2 over-activity has been also measured in AF, both in human and dog myocytes [182, 291]. The main protein that has been related to the RyR2 remodeling during AF is S2808. In recent studies, phosphorylation has been measured to be heterogeneous through the cell, decreasing with the distance to the membrane [268]. This behavior is 1.75-fold increased throughout the cell in myocytes with AF with respect to myocytes without AF.

Modeling analysis also support the idea that CaMKII enhances the phosphorylation of RyR2s, increasing the sensitivity of release to Ca^{2+} and thus increasing RyR2 open probability [237].

6.2.1 Methods

The RyR2 phosphorylation is modeled as a multiplicative factor (α) that increases the open rate (k_{co}). We have defined the RyR2 phosphorylation (P) following [268]. The value of P changes linearly across the cell with a different range of values for cells with and without AF. For cells with no AF it varies between 0.7 and 0.85, and for cells with AF it varies between 0.9 and 1.2. The multiplicative factor (α) of the k_{co} is defined as

$$\alpha(P) = 1 + 15\frac{P^{12}}{P^{12} + 1.1^{12}}. \tag{6.5}$$

This function is plotted in Fig. 6.4a, where the variability of α changes its order of magnitude for cells with AF while it is almost constant for the no AF condition. The dependence of α has been adjusted to fit with the experimental findings of [268]. The spatial distribution of α is plotted in Fig. 6.4b. Then, the open rate is redefined as

$$k_{co} = k_a^* \frac{c_i^3}{1 + (c_i/c_i^*)^3} = \alpha(P) k_a \frac{c_i^3}{1 + (c_i/c_i^*)^3}. \tag{6.6}$$

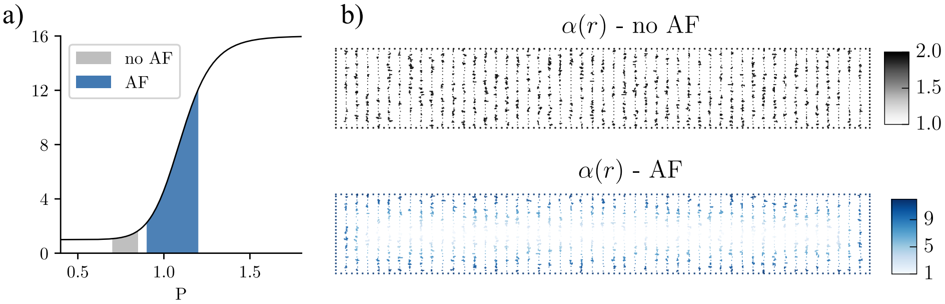

FIGURE 6.4: **Modeling of phosphorylation as a RyR2-modulator.** a) Plot of $\alpha(P)$ following Eq. 6.5. The variability ranges of P and α are shown for simulated cells with and without AF. b) Spatial distribution of the RyR2-phosphorylation factor $\alpha(r)$ for no AF (gray) and AF (blue).

6.2.2 Results

The over-expression of the RyR2-phosphorylation produces larger calcium sparks. This effect is seen in Fig. 6.5, where the mean value of the main spark properties are plotted. RyR2-phosphorylation produces larger sparks in terms of FWHM and amplitude.

Moreover, the heterogeneous distribution of RyR2-phosphorylation produces an heterogeneous distribution of sparks. In particular, the number of events decreases with the distance to the cell membrane. This result is shown in Fig. 6.6, where we can see that close to the membrane the number of events is much higher due to the geometrical distribution of RyR2s at that zone. It is important to note that the RyR2-phosphorylation increases the absolute spark frequency by a factor 4.

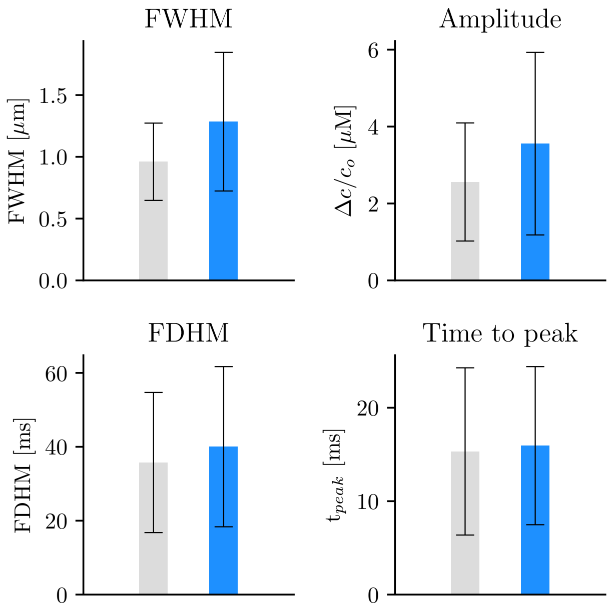

FIGURE 6.5: **Spark properties for no AF and AF conditions due to RyR2-phosphorylation.** The effect of the RyR2-phosphorylation has been characterized in terms of the FWHM, amplitude, FDHM and time to peak for both cell conditions.

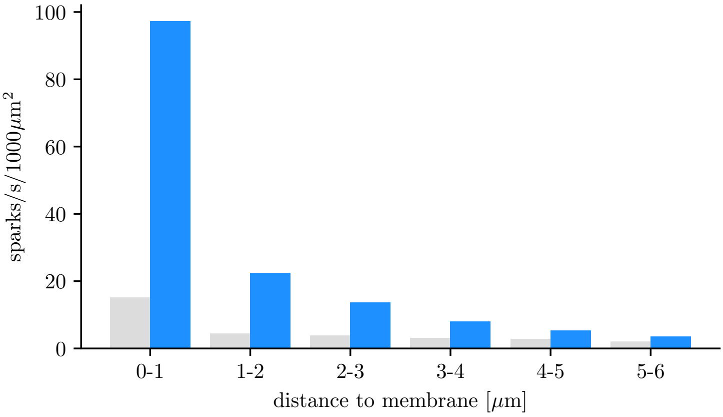

FIGURE 6.6: **Spark frequency as function of the distance to membrane.** The spark frequency has been normalized with the area of the corresponding layer.

6.3 Effects of pathological conditions during AF

It has been observed that, in cells with AF, both effects (reduction of CSQ and increment of RyR2-phosphorylation) are present. In sections 6.1 and 6.2, the partial results of each of these modulations have been presented in order to explain the methodology employed and quantify their contribution to the spark characteristics. Now, the chapter is concluded with the combination of both effects and a more detailed analysis of the results.

The pathological conditions in AF produces a 10-fold increase in the spark frequency as have been observed in [268]. In AF conditions, due to the higher sensitivity of the RyR2s, the number of opened RyR2s per event also increases. This result is shown in Fig. 6.7. As we can see, while in the case with no AF conditions, the maximum number of opened RyR2s is 15, in the case with AF conditions it is 55 and the total number of events is also larger in cells with AF. Moreover, the decay of the events with number of RyR2s is exponential on both conditions although slower in AF conditions.

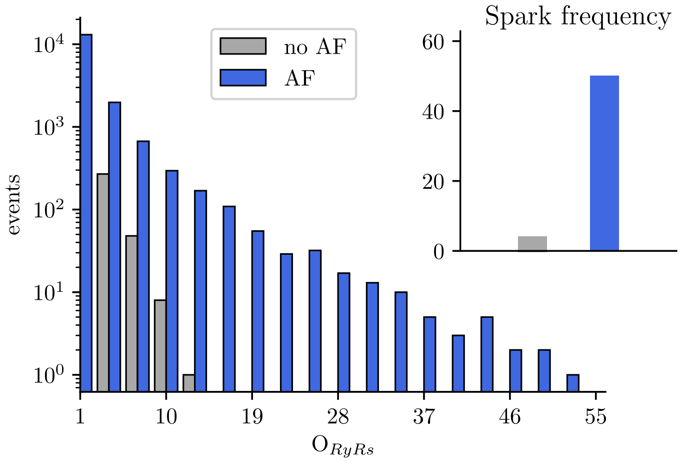

FIGURE 6.7: **Number of sparks as function of the opened RyR2s.** Distribution of events as function of the number of opened RyR2s. Inner figure: spark frequency in s^{-1}.

Thus, the increase in the RyR2 sensitivity due to the lack of CSQ and the RyR2-phosphorylation produces larger events in terms of activated RyR2s. This issue is translated in the spark properties, where the calcium sparks in AF conditions are larger in terms of amplitude, duration and spatial size (see Fig. 6.8), a issue already observed experimentally [158].

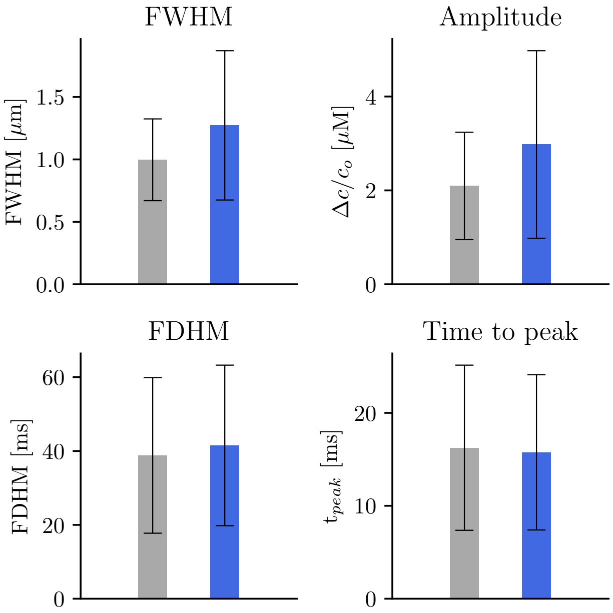

FIGURE 6.8: **Spark properties for no AF and AF conditions.** FWHM, amplitude, FDHM and time to peak for both cell conditions.

To go deeper into the effect of opened RyR2s, in Fig. 6.9 I show the same spark properties as before classifying the events in terms of the number of opened RyR2s. A strong correlation is observed between FWHM, amplitude and FDHM with the number of RyR2s, while the time to peak does not show relevant changes.

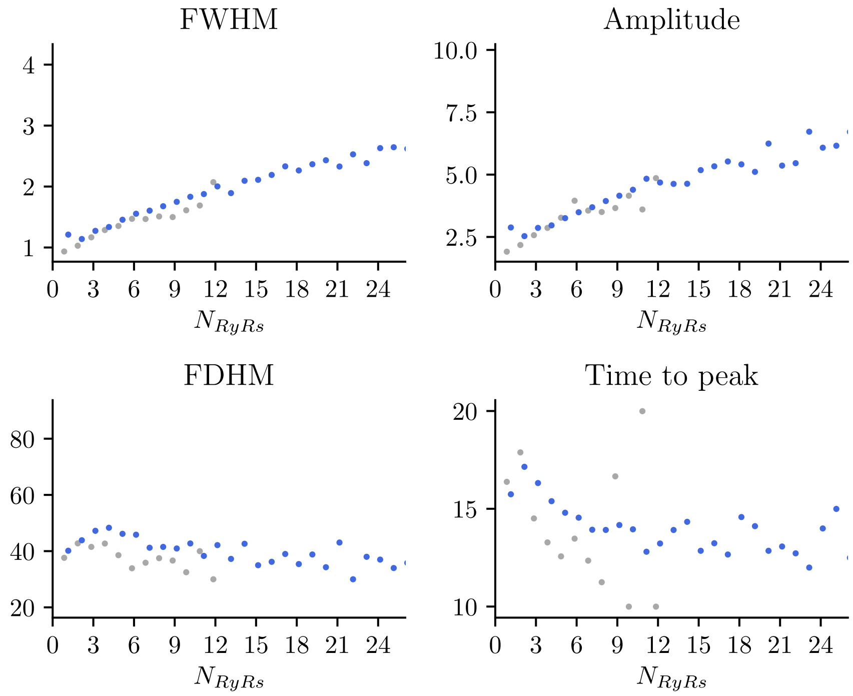

FIGURE 6.9: **Correlation between the spark properties and the RyR2s.** Spark characteristics as function of the opened RyR2s. The same color code is used as in previous figures: no AF (gray) and AF (blue). Due to the lack of statistics, the events with more than 26 RyR2s have been discarded.

Finally, the spatial heterogeneity produced by CSQ and RyR2-phosphorylation is translated to the spark distribution. While CSQ promotes the appearance of calcium sparks in the center of the cell (see Fig. 6.3), RyR2-phosphorylation produces a higher activity of the peripheral RyR2. Experimentally, it has been shown that these two effects compete and the latter prevails leading to a spark distribution with more events at the cell membrane [268]. The incorporation of these RyR2-modulators to the model produces an heterogeneous distribution that follows the same trend observed experimentally for both conditions, as it can be seen in Fig. 6.10. However, simulations show a prominent peak near the membrane for both conditions due to the 2-fold increase in the CaRU density at subsarcolemmal. Although this structural property is well-known experimentally, it is unclear if those clusters in the periphery have the same morphology that the ones in the center of the cell, in terms of the number of RyR2s. Recent studies suggest that the CaRUs in the membrane contain fewer RyR2s [239], which may explain this discrepancy in the spark frequency close to the membrane.

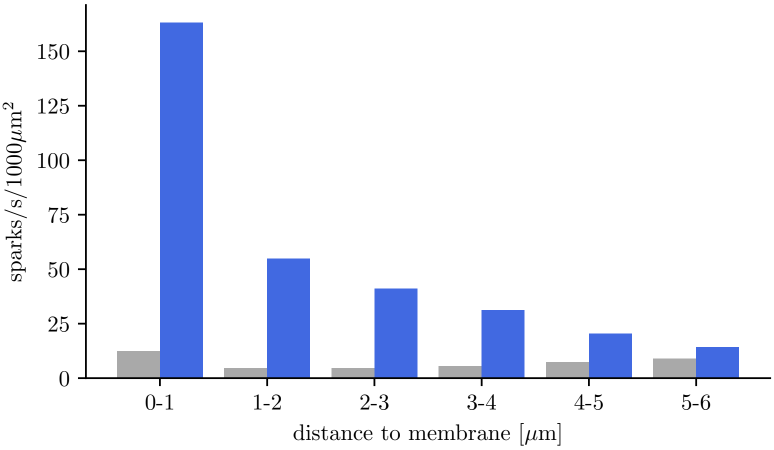

FIGURE 6.10: **Spatial distribution of sparks for no AF and AF conditions.** Concentric rings of 1μm width have been considered.

6.3.1 Discussion

AF has been associated with many structural and biochemical changes at the single cell level [115, 285, 291]. Spontaneous Ca^{2+} release due to RyR2 dysfunctions is the almost an ever-present finding [115, 290, 306] which, in turn, may promote the appearance of DADs [291, 290, 306]. Moreover, other CVD are also related to SR calcium overload. For instance, HF promotes the SR Ca^{2+} leak leading to an increase in Ca^{2+} spark frequency and, in advanced stages, the emergence of waves, serving as the molecular trigger for arrhythmia [295]. In this chapter, two fundamental mechanisms have been studied by means of the subcellular model.

Calsequestrin as a RyR2 modulator. The dynamics of CSQ has been recognized as a fundamental key to understand the calcium handling in the cell [99, 143, 252]. CSQ plays two relevant roles in calcium handling. It is not just a calcium store in the SR, but it also modifies the open probability of the RyR2 channels [15, 14, 16]. The lack of CSQ enhances the RyR2 opening promoting premature SR Ca^{2+} and, eventually, the appearance of macro-events. Moreover, the lack of CSQ has been related not only to AF, but also to HF (overview in [25]). In this chapter, the effect of CSQ in terms of the calcium sparks has been characterized. The influence of CSQ on the RyR2 rates has been modeled considering that the amount of free calsequestrin (q) modifies the open rate of the RyR2 Markov model. A decrease on q will increase the open rate (k_{co}). The redefinition of this rate has been done following previous works [153]. Moreover, we have considered an heterogeneous distribution of the total amount of CSQ (B_{CSQ}), which linearly decreases between the cell membrane and the cell center.

Calcium sparks due to the modulation of CSQ do not show relevant differences in their properties. The lack of CSQ produces a higher spark frequency and, in both conditions, the spark frequency increases with the distance to the cell membrane. Simulations suggest that this heterogeneity on B_{CSQ} produces a nonuniform spark distribution through the cell where more sparks in the center of the cell than in the periphery are present (see Fig. 6.3).

An over-expression of the RyR2-phosphorylation. The rate of phosphorylation plays a crucial role in many cardiac diseases [171]. It has been associated with HF and AF [182], among other CVDs. In this chapter, the effect of RyR2-phosphorylation has been modeled empirically by means of a sigmoid function that depends on the rate of phosphorylation ($\alpha(P)$) and that has been adjusted to fit with experiments. This function $\alpha(P)$ multiplies the open probability of the RyR2s producing and heterogeneous distribution of RyR2- phosphorylation across the cell (see Fig. 6.4b).

Due to the increment on the open probability, the calcium sparks are larger in time and space, where an increment of 30% on FWHM and amplitude is observed in Fig. 6.5. Moreover, this modulator produces nonuniform distribution sparks with a high frequency near the membrane.

Pathological conditions during AF. The real situation in fibrillated atrial cells is produced by a combination of the two effects reported in this chapter. Both modulators produce an over-activity of the RyR2s, which is modeled with an increase of the open rate probability. However, the spatial distribution of the sparks in terms of the distance to the membrane goes in opposite directions. While the lack of CSQ enhances the appearance of sparks in the center of the cell, the RyR2-phosphorylation promotes the calcium events close to the cell membrane. During AF conditions, the latter modulator is dominant producing a nonuniform distribution of sparks with a higher density of them close to the cell membrane, as it is shown in Fig. 6.10. The high frequency of sparks near the cell membrane would induce DADs and even arrythmias in advanced stages of AF. The simulation of atrial cells during pathological conditions produces larger sparks in terms of spatial size and temporal duration (see Fig. 6.8). Finally, due to the fine discretization of the model, the correlation between the spark properties and the number of opened RyR2s has been established.

Chapter 7

Detubulation

Note: the results obtained in this section have been presented in [181] and the text has been extracted from the aforementioned paper.

In ventricular cells, the cell membrane has prominent penetrations into the cytosolic space called transversal tubules (t-tubules). The presence of t-tubules implies, directly, a presence of L-type calcium channels (LCCs) in the internal space of the cell and, thus, a simultaneous calcium release when whole cell electrical activation takes place.

The role and presence of t-tubules in atrial myocytes is still not completely understood. Originally, t-tubules were assumed to be a property of ventricular cells, with a very minor presence in atrial myocytes. For instance, confocal microscopy in cat atrial myocytes revealed non-homogeneous spatial calcium profiles caused by the absence of t-tubules [117]. T-tubules were also assumed to be absent in rat atrial myocytes [109], although, nowadays, it has been proven that they present a minor lattice of transversal and axial tubules (TATS) [141]. These TATS are the leading structure that determines the calcium transients. In particular, calcium transients are activated through subsarcolemmal CaRUs, leading initially to peripheral elevation of Ca^{2+}, which travels through the center of the cell within approximately 100 ms [33]. In these experiments it was observed that spontaneous Ca^{2+} sparks do not appear uniformly in the cell, but they occur around the RyR2s close to the membrane. In addition, it was shown that TATS are more relevant in the left atrium, generating higher pressures than in the right atrium. Lately, important improvements in the techniques to analyze t-tubules have been developed [97, 208], allowing a better determination of the tubular structure.

Although both ventricular and atrial mycoytes may present t-tubules, comparison between them [244] suggests strong differences. In the former, the presence of a highly ordered t-tubule lattice enhances the whole synchronization. In the latter, it is suggested that some myocytes have membrane intubation which accelerate the centripetal wave propagation. Moreover, depending on the mammal, the density of t-tubules varies. In general, the larger the mammal is, the more t-tubules it has [244]. In this respect, it has been shown the prominent presence of t-tubules in cow, horse and sheep, as well as in human cells [220]. For instance, sheep atrial myocytes posses an extensive t-tubule network that synchronizes the Ca^{2+} profile [62], showing a small the peak to peak time delay between the membrane and interior. There exist also differences between right and left atrial myocytes. For example, [9] observed that, in the case of dogs, t-tutubles are more prominent in the left atria than in the right atria. There is also present an inter-cellular variability in the amount of t-tubules from single subjects, probably related to the functional roles of different cell populations [83]. Besides the density of t-tubules, the conformation of these intubations changes during depolarization to produce the heart contraction, with an increase in both volume and length of t-tubules during contraction [186].

In addition, it has been showed that the t-tubule density and structure change during atrial fibrillation (AF) and heart failure (HF). During HF the number of t-tubules is highly reduced. T-tubule remodeling leads the transition between hypertrophy and HF [296]. Differential t-tubule remodeling processes were observed between left ventricle and right ventricle myocytes. Persistent AF has also been related to structural remodeling: uncoupling between t-tubules and RyR2s channels, changes in the extracellular matrix [154]. Recent studies highlight a possible role for t-tubule remodeling (disorganization) in desynchronization of SR Ca^{2+} release sites in HF [162, 168]. In particular, submicron changes are induced due to the transition to HF: [92] proposed that the gap between LCCs and faced RyR2s enlarges during remodeling (resulting in "orphaned" RyR2s [253]). This has been supported by [187], who observe that Ca^{2+} sparks are not uniformly distributed within HF cells and disappear from areas devoid of t-tubules, leading to a loss of local control and Ca^{2+} instability in HF. T-tubules also affect the current carried by the NCX, which is activated by the release from the RyR2s, mostly placed on the t-tubules [274]. T-tubules also modulate the activity of NCX since it is mediated by the RyR2s which are preferentially placed on the t-tubules [274]. Also sparks are likely to take place near the t-tubules since RyR2s are placed near them. Modeling studies have shown a relation between the density and spatial organization of t-tubules and the occurrence of alternans and triggered activity [199, 254, 52].

To simulate the effect of TATS we include points in the interior of the cell that present both the NaCa exchanger pump and LCC channels. For t-tubules, we consider intubations of a given length, where we assume that this length (inward penetration) follows an exponential distribution

$$P(x;\mu) = \frac{1}{\mu} e^{-x/\mu} \tag{7.1}$$

where μ is the mean penetration length of the t-tubules. To generate a random configuration, we follow three steps: 1) pick an exponential random number: P_μ, 2) scale this value with the spatial length: $L_\mu = L_y P_\mu$. This random number L_μ is the inward penetration for the first t-tubule. 3) Repeat the process for all t-tubules. These steps are summarized in Fig. 7.1A.

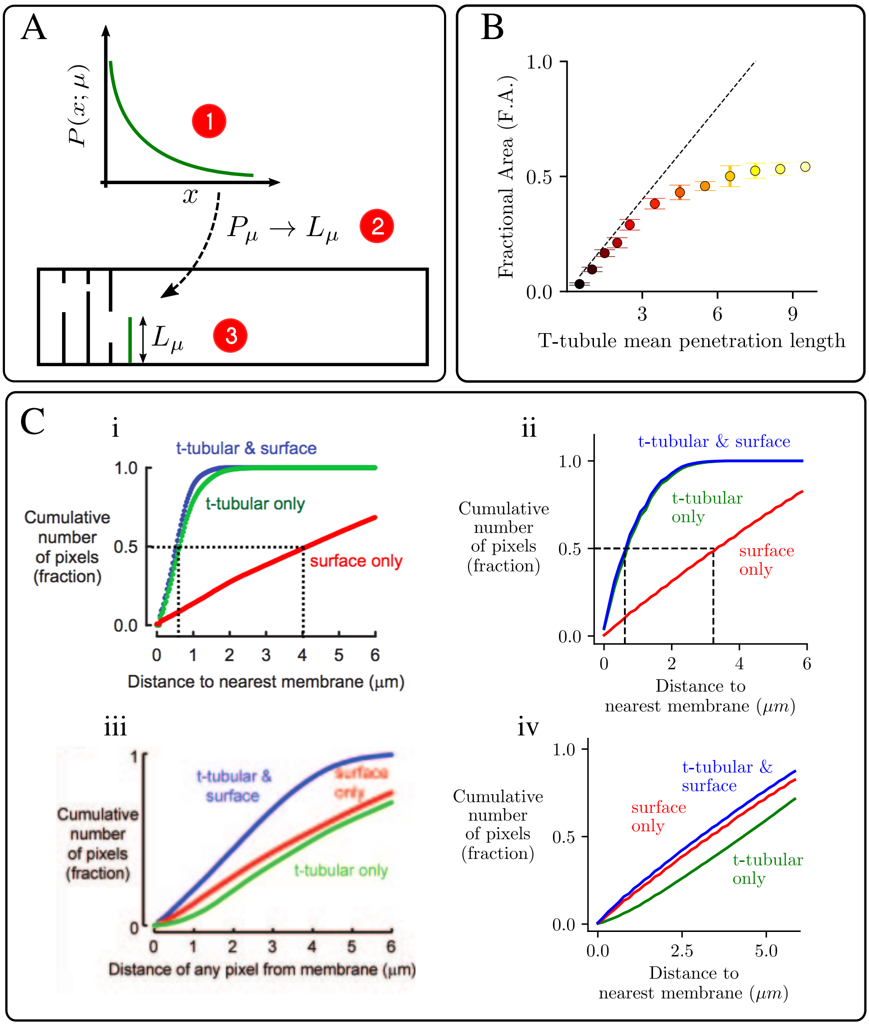

FIGURE 7.1: **Characteristics of the t-tubule network.** A: Schematics of the protocol used for the creation of the t-tubular network in the model. B: Fractional area occupied by the LCCs as a function of μ. For each value of μ ten different configurations of the t-tubular network have been averaged. The dashed line is the linear function $2\mu/L_y$. C: Cumulative number of pixels at a distance from any membrane smaller than a given one, showing contributions of t-tubule and surface membrane. i) Figure extracted from [62]. ii) Result from the current model for F.A. = 0.466. iii) Figure extracted from [62] corresponding to an atrial cell with HF (loss of t-tubules). iv) Result from the current model for F.A. = 0.033.

Moreover, we have investigated the axial tubules contribution to the calcium handling. In a similar fashion to the transversal tubules case, we have simulated the existence of these axial tubules by including longitudinal chains that present the NaCa exchanger pump and LCC channels. We assume that the axial tubules length follows a Gaussian distribution, with average length of 1.7μm and standard deviation of 1μm.

7.1 Analysis

Once the t-tubule distribution is set, the internal space of the cell is partially occupied by the LCCs of the t-tubules and associated NCX pump. We can calculate the fractional area (F.A.) occupied by the t-tubules in comparison with the case of fully occupation, i.e., the t-tubules cross through all the transversal section of the cell. To analyze the dependence of the F.A. with μ we have simulated ten random configurations for the same value of μ following the probability distribution of Eq. (7.1). The mean F.A. is shown in 7.1B. For low values of μ the relation between the F.A. and μ follows the theoretical straight dashed line $2\mu/L_y$. As μ increases, the length of the t-tubules could be greater than $L_y/2$, producing a possible overlap between opposite t-tubules. To avoid this situation, the algorithm limits the length of the t-tubules to $L_y/2$. For that reason, the mean F.A. is smaller than $2\mu/L_y$ for large values of μ. In the following, we will use F.A. as a measure of t-tubules penetration.

A common measure of t-tubule density is given by how close a given point in the cell is to the nearest t-tubule compared with the cell membrane [62, 220, 61, 84]. This calculation provides us with a quantitative idea of the importance of t-tubules.

As an example, we show in Fig. 7.1C data in a control case with the presence of t-tubules (i), and the corresponding data for a cell with a decreased t-tubule density, as for instance, in HF (ii). One can compare those figures with the experimental ones obtained, for instance, in [62], where Fig. 7.1Ci would correspond to the t-tubular network of a sheep ventricular myocyte (Fig. 3B in [62]), and Fig. 7.1Cii to that of a sheep atrial myocyte in an animal presenting heart failure (Fig. 6B in [62]). The corresponding values of the F.A. (F.A.$=$ 0.466 and F.A. $=$ 0.033, respectively) would be consistent with values measured experimentally, of ~ 0.3 for ventricular myocytes and up to ~ 0.1 for sheep atrial myocytes [37]. Typical branch length in atrial myocytes varies from 1.5-2μm in small mammals (rat, mouse, rabbit) to $\sim 2\mu$m in humans [32]. In our model this again would correspond to a F.A. of about 0.1-0.2 (Fig. 7.1), that we can take as our typical value for an atrial myocyte.

7.2 Results

7.2.1 Calcium transients

We first start analyzing properties of the global Ca^{2+} transient. As expected, the average value of the Ca^{2+} concentration is very dependent on the amount of t-tubules (Fig. 7.2). Besides, we observe that, for a given penetration length μ, the cytosolic Ca^{2+} peak depends on the specific realization considered (see gray area in Fig. 7.2A). This effect is more visible in the case of a larger t-tubule density. In order to quantify this behavior, we have averaged both peak and diastolic cytosolic calcium values for ten configurations with the same value of μ but different values of the F.A. The equivalent calculation has also been done for the SR content. The results are shown in Figs. 7.2B (i and ii). In the cytosol (Fig. 7.2Bi) the diastolic value does not depend on the F.A. However, the peak value highly increases with the amount of t-tubules, with a more than 2-fold increase. A similar trend is observed in the case of the SR content (Fig. 7.2Bii), where the minimum value decreases with the F.A., while the diastolic value remains almost constant. Thus, the increase in fractional release is not related to a higher SR load. We will later study in more detail this effect.

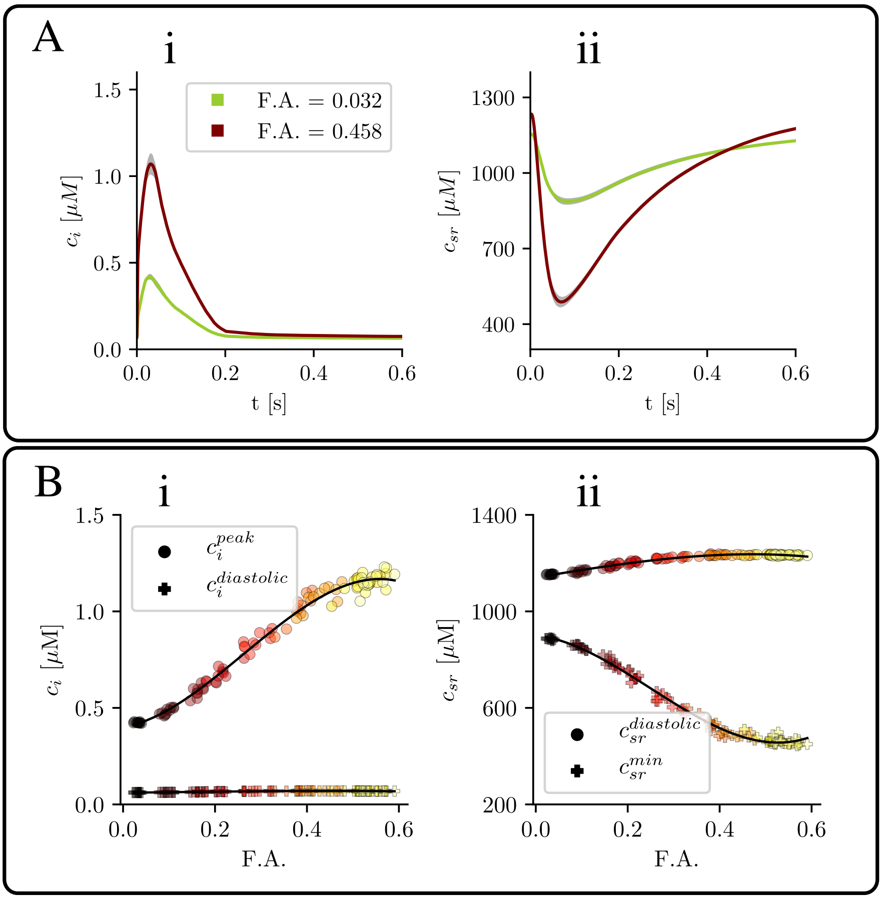

FIGURE 7.2: **Ca^{2+} transient characteristics as a function of F.A.**. A: Mean value of calcium concentration (i) in the cytosol and (ii) in the SR, for two different values of the F.A. The dispersion is calculated with ten different configurations of the t-tubular network. B: calcium peak and baseline as function of the F.A. in the cytosol (i) and the SR (ii). Each point represents the mean value over the last 24 beats and one configuration of the t-tubular network. Points with the same color come from the same value of μ, the parameter in the length distribution of t-tubules. The solid line is an eye guide to follow the behavior. In all the figures the pacing period is 800 ms.

The disruption of the t-tubular system may have a considerable impact in the regulation of atrial contraction [62]. It is, for instance, possible that the cell has a different response to fast pacing frequencies. In Fig. 7.3 (top) we show the calcium peak and SR load dependence with the pacing period for the cases of a small and large t-tubule density. In both cases, the diastolic value of SR load and the cytosolic Ca^{2+} peak increase slightly first with pacing frequency, and then decrease at frequencies larger than about 2Hz. There is also a continuous decrease of the release flux with frequency, that becomes more abrupt at larger frequencies, and it is probably due to refractoriness of release [242, 5]. Both the release flux and the calcium influx through the LCC is smaller in the case of disrupted t-tubules, although the decrease in the former is not as pronounced as in the latter, due to a larger EC gain in detubulated cells, thus partly avoiding the effects of the reduced calcium influx. From this, it arises the idea that the dynamics is robust enough to maintain always physiological values.

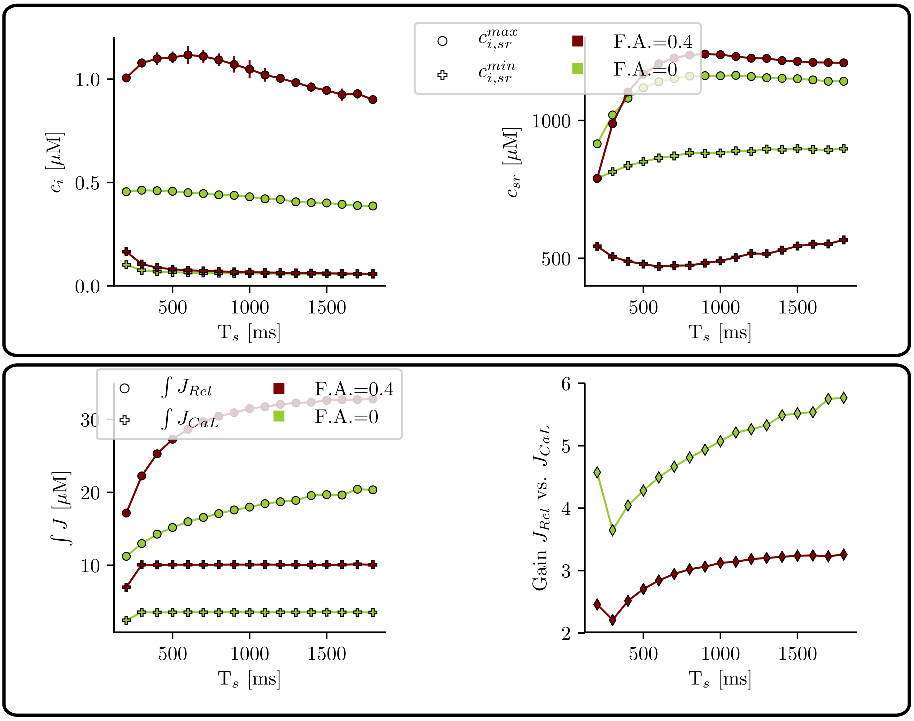

FIGURE 7.3: **Dependence on the pacing period.** Top: calcium peak for different values of the pacing period (T$_s$) for two scenarios: the loss of t-tubules due to HF (green) and the control situation with t-tubules (red). Bottom: average Ca^{2+} release and influx (in μM), obtained integrating the fluxes J_{rel} and J_{CaL} over a period and averaging over 20 stimulations (same color coding).

Often, t-tubule disruption is accompanied by a decrease in SERCA strength, as, for instance, during HF [79, 87]. We have checked the effect of this dysfunction by modifying two parameters of the SERCA pump: the strength of SERCA, g_{up}, has been decreased 30%, while its cytosolic calcium dissociation constant, K_i, has been increased by 30%.

This results in a slower SERCA, with lower affinity for cytosolic calcium, producing a reduction of about a 17-18% in the calcium transient and SR Ca^{2+} load (Fig. 7.4), in the case of tubulated cells (F.A.=0.466), and a slightly lower reduction of a 9-13% for detubulated cells (F.A.=0.033). As also happened in the control case (see Fig. 7.2), for the modified SERCA function, SR Ca^{2+} load does not change much with the amount of t-tubules, while both the fractional release and the amplitude of the calcium transient are reduced in about a factor 2 when the fractional area is reduced from F.A=0.466 to F.A.=0.033.

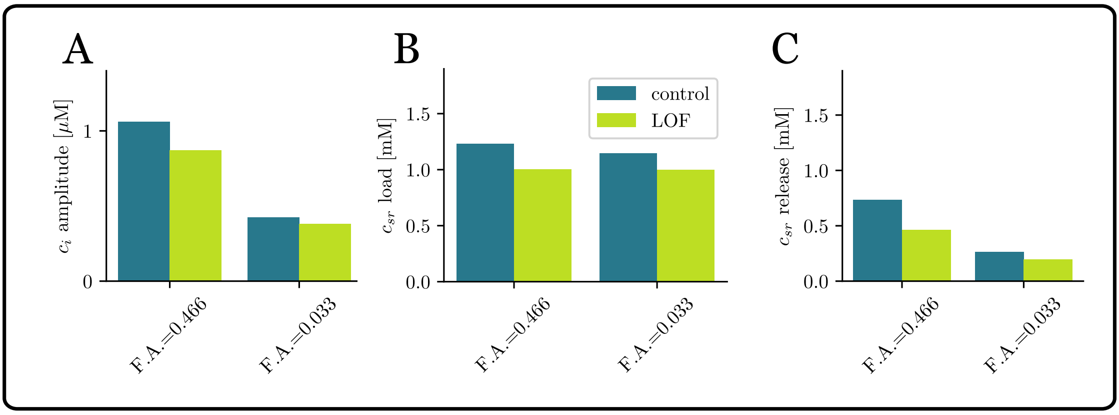

FIGURE 7.4: **Effect of a dysfunctional SERCA pump.** Values of A: cytosolic Ca^{2+} peak; B: SR Ca^{2+} load; C: SR fractional release, for the control case and reduced activity of SERCA. The pacing period is 800 ms.

7.2.2 Inward propagation

The presence of t-tubules in atrial cells enhances the homogenization of calcium profiles, i.e. the synchronization between the center of the cell and peripheral region. Inward calcium propagation is highly dependent on the t-tubules distribution. This can be observed plotting the averaged calcium content in two regions: close to the membrane (red line in Fig. 7.5) and in the central region (black line in Fig. 7.5). The average line scan is calculated using:

$$\langle c(x,y)\rangle_x = \int_0^{L_x} c(x,y)dx, \tag{7.2}$$

where $c(x,y)$ is the calcium concentration at (x,y). For low values of F.A. the peak in the center is practically nonexistent (Fig. 7.5Bi). This contrasts with the prominent peak in the internal region for high values of F.A. This increment on the calcium content in the cytosol is produced by the increase of the fractional release in the SR, as we have already pointed in Fig. 7.2D. Thus, there is a strong correlation between the t-tubular geometry (shown in Fig. 7.5C) and the calcium dynamics.

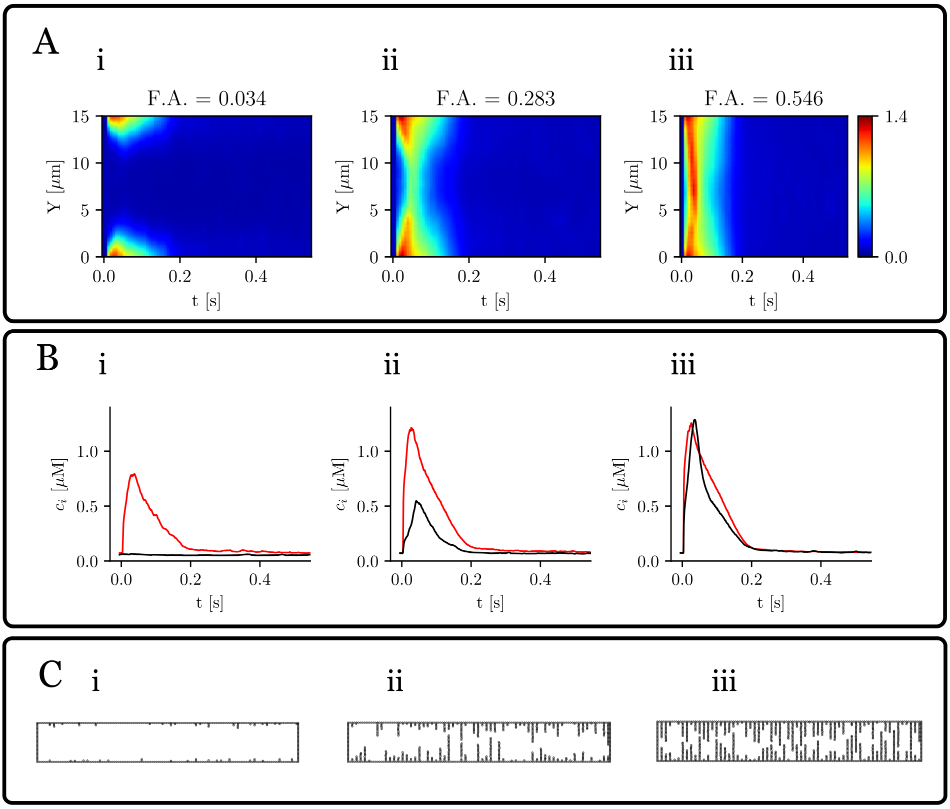

FIGURE 7.5: **Spatial Ca^{2+} profiles.** A: line scans averaged over the longitudinal direction for three values of the F.A. The color bar corresponds to calcium concentration in μM. B: mean value of calcium close to the membrane (red) and in the center of the cell (black). C: the three t-tubular network configurations. Pacing period of 800 ms.

Related to this, we have calculated the cytosolic calcium peak (Fig. 7.6Ai) and SR fractional release (Fig. 7.6Aii) close to the membrane and in the central region for several values of the F.A. Figs. 7.6A show that full inward propagation is only achieved for the highest value of the F.A. In addition, we show the delay time between subsarcolemmal and internal peaks in Fig. 7.6B. For low values of the F.A., the central peak is small and, in many cases, almost nonexistent, so that the delay time, if present, is high. As the F.A. increases both peaks become more synchronized meaning that the internal space is triggered simultaneously with the submembrane. This synchronization is also observed in the ratio between subsarcolemmal and central peaks. Fig. 7.6C shows that for low values of the F.A., this ratio tends to zero, given that the peak in the internal region tends to vanish. On the other limit, for high values of the F.A., both peaks become synchronized and this ratio tends to 1.

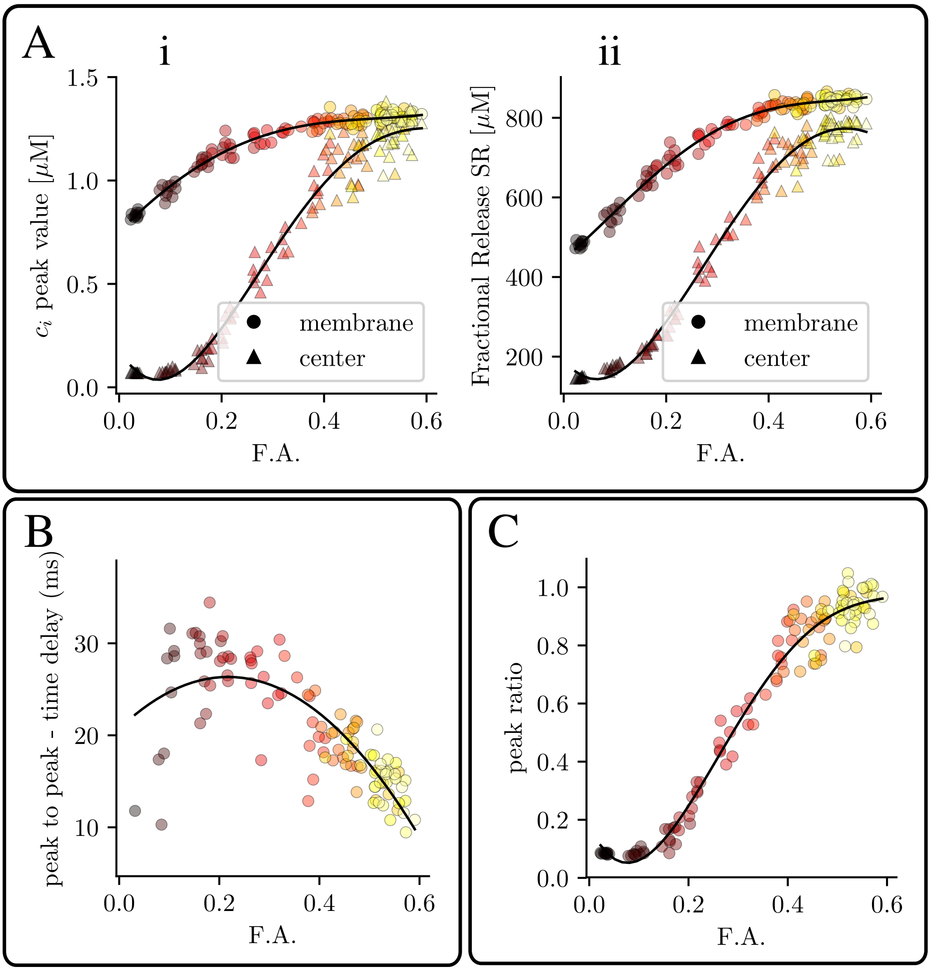

FIGURE 7.6: **Inhomogeneity in release as a function of t-tubule density.** Ai: cytosolic calcium peak close to the membrane and in the center of the cell as function of the F.A. Aii: fractional release from the SR close to the membrane and in the center as function of the F.A. B: delay time between peripheral and central regions as function of the F.A. C: Peak ratio between peripheral and central region ($Ca^{2+}_{ct}/Ca^{2+}_{ss}$) as function of the F.A. Pacing period of 800 ms.

Effect of axial tubules in calcium propagation

To study how dependent calcium inward propagation is on the amount, not only of t-tubules, but also of axial tubules, we have redone some of the simulations, including a varying density of axial tubules. In Fig. 7.7 we show the results, for a given value of the F.A. of t-tubules that in the absence of axial tubules results in failure of inward propagation. We observe that, increasing the density of axial tubules, a peak in cytoslic calcium in the central region is obtained, with a delay with respect to the peak at the subsarcolemmal region. In the linescans, this results in a V shape, that has been often described experimentally [61] (Fig. 7.7).

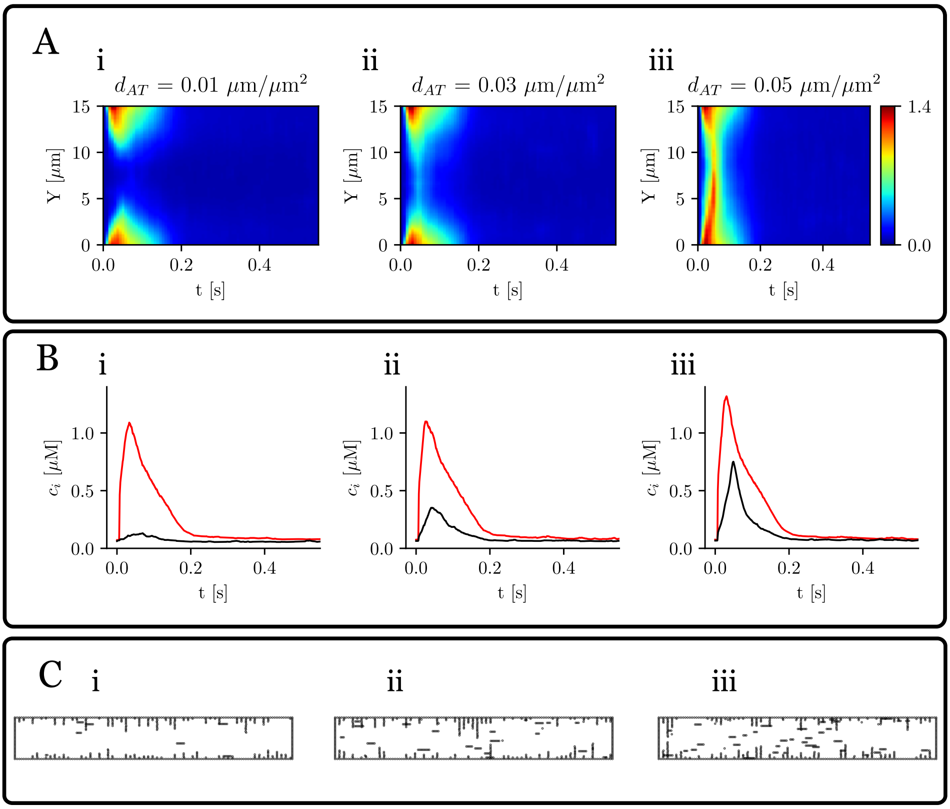

FIGURE 7.7: **Effect of axial tubules.** Calcium traces as a function of axial tubule density d_T, defined as the ratio of axial tubules total length and cell surface. A: line scans averaged over the longitudinal direction for three values of $d_T = 0.01, 0.03$, and $0.05\ \mu m/\mu m^2$, for a fractional area of t-tubules of F.A.=0.16. The colorbar corresponds to calcium concentration in μM. B: mean value of calcium close to the membrane (red) and in the center of the cell (black). C: the three tubular network configurations. Pacing period of 800 ms.

7.2.3 Local dynamics

In the previous sections we have observed that, as the amount of t-tubules decreases, there is a delay between the rise of calcium close to the membrane and in the interior of the cell. This spatial desynchronization can be studied in more detail computing the release characteristics of individual RyR2s in the cell. In this analysis, we have recorded the open time for all the RyR2s during 19 beats and different values of the F.A.

The time to release (t_{tr}) is defined as the time passed between the beginning of the stimulation and the first release of a RyR2. This time depends on many factors: diffusion coefficient, SR load, opening rate in the RyR2 stochastic model, etc. In particular, simulations show that t_{tr} heavily depends on the t-tubule density. In Fig. 7.8Ai the probability distribution of t_{tr} is shown for different values of the F.A. The bigger the F.A., the higher and narrower the peak becomes. Also the mean value of t_{tr} decreases with the F.A. (Fig. 7.8Aii). Once a given RyR2 has opened, it typically does not open again during the same stimulation, i.e, the number of times each individual RyR2 opens (Fig. 7.8Biii) is approximately always one and it does not change with F.A.

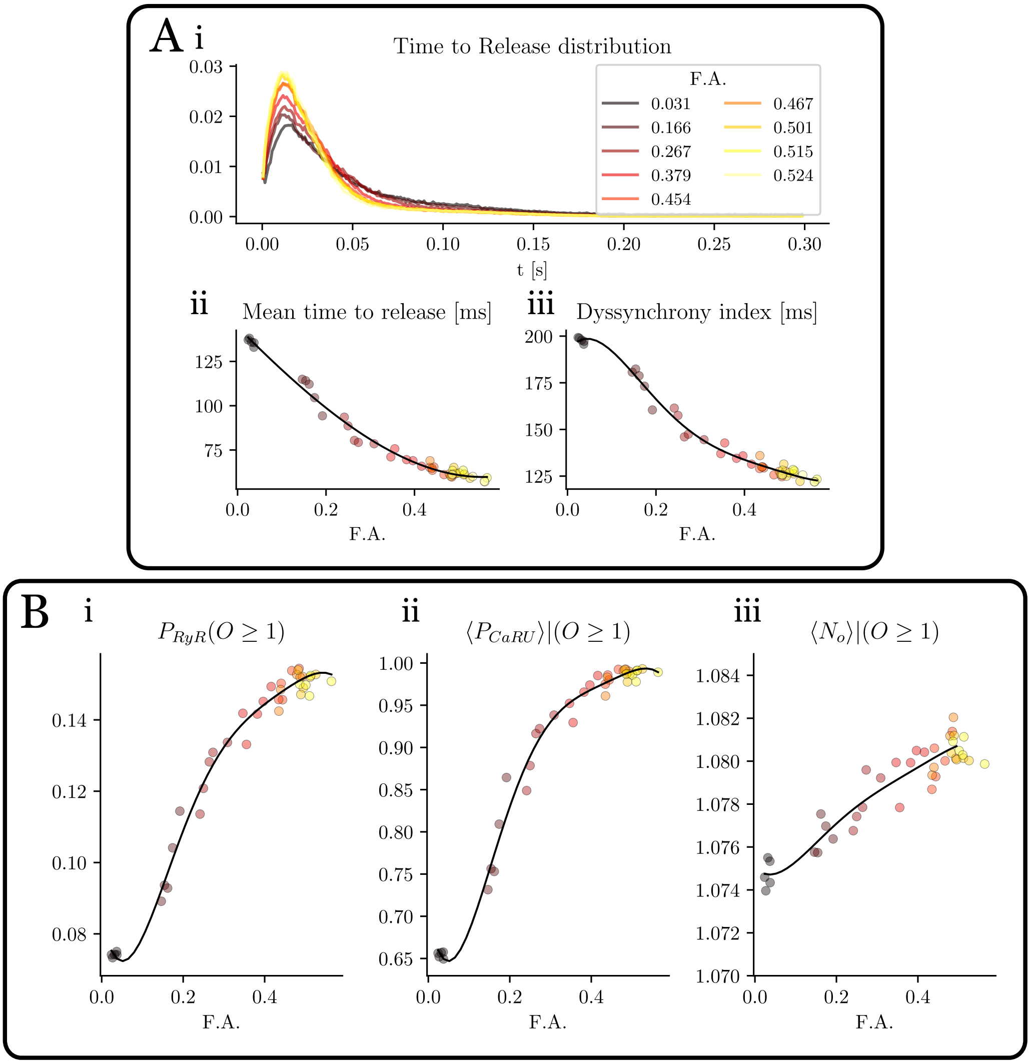

FIGURE 7.8: **Statistical measures of RyR2 activity.** A: time to release distribution (i), average time to release (ii) and dyssynchrony index (iii) as function of the F.A. B: Dependence on the F.A. of (i) fraction of RyR2 that open, (ii) fraction of CaRU with at least one RyR2 that opens and (iii) average number of times a given RyR2 opens in a given beat. Pacing period of 800 ms.

An usual characterization of RyR2 release synchronization is obtained with the Dyssynchrony Index (DI), defined as the standard deviation of the t_{tr} distribution. This clearly shows that an increase of t-tubule density enhances RyR2s synchronization (Fig. 7.8Aiii). It is not just that RyR2 release is more synchronized, but, as the t-tubule density increases, the ratio of RyR2s that open also increases. We have defined the opening probability (P_o) of the RyR2s as the number of RyR2s that have opened at least once ($N_{RyR}(O \geq 1)$) in a given beat, divided by the total number of RyR2s N_{RyR}. It increases almost linearly with t-tubule density, up to a point where it saturates. Interestingly, if we compute, not the individual RyR2s, but the fraction of CaRUs where, at least one RyR2 opens, we see that it reaches almost the value one, for a F.A. of 0.5. Thus, at this point, all CaRUs fire, some by direct stimulation from the LCCs at the t-tubules, others, due to recruitment from adjacent CaRUs.

7.3 Discussion

The TAT network has long been recognized as an essential ingredient to ensure excitation-contraction coupling and subcellular synchronized Ca^{2+} release. Contrary to ventricular cells, that present a well organized t-tubular network, the amount of t-tubules in atrial cells depends on the animal species [220, 244] and within a given species, on the location of the cell in the atria [83, 9]. When present, t-tubules help to synchronize the rise of the systolic Ca^{2+} transient also in atrial cells [62, 154]. Probably linked to this, the central calcium transient has been found of similar amplitude than the initial subsarcolemmal transient in some species [117], while in others it is significantly reduced [169]. T-tubules are often disrupted in diseased conditions, such as heart failure in the ventricles [98, 168, 253, 296] or atrial fibrillation [154]. In both cases, the loss of t-tubule structure results in a decreased calcium transient and loss of synchrony in release.

Previous modeling studies have addressed the relation between t-tubule density and spatial organization, and the appearance of alternans and triggered arrhythmias. Song et al [254], in a model of a ventricular myocyte, found that alternans were promoted at intermediate values of the t-tubule density, when the fraction of orphaned RyR2s was in an intermediate range. In this regime, the LCC clusters and NCX are properly matched so that the CaRUs can be sufficiently synchronized by the LCC clusters and spontaneous Ca^{2+} releases are not suppressed by NCX, potentiating triggered arrhythmias. T-tubule disruption was also found to give rise to a steeper SR Ca release-load relationship, predisposing for the appearance of alternans. For atrial myocytes, on the contrary, Colman et al [52] found that alternans appeared at low values of t-tubule density, since this resulted in alternating behavior of success and failure of inward calcium wave propagation. Spontaneous Ca^{2+} waves originate from regions with no T-tubules, probably because the lack of NCX allows a local spontaneous release to trigger neighboring RyR2 clusters.

In this chapter we have studied the effect of modifying the amount of t-tubules in a subcellular model of a cardiac cell. The t-tubular structure is reproduced considering transverse t-tubules of variable penetration length, taken from an exponential distribution (Fig. 7.1A), that results in a given t-tubular structure. We have then considered averages over different realizations with the same mean penetration length. Since different realizations could give rise to a different value of the F.A. occupied by t-tubules, we found more useful to use this last variable to characterize the t-tubular network. Interestingly, the network so constructed gives a good agreement with statistical measures of distances to the membrane, obtained experimentally [62, 220, 61].

Detubulation reduces the Ca^{2+} transient but does not affect SR load In detubulated ventricular cells, the amplitude of the systolic Ca^{2+} transient and its rate of rise have been observed to be reduced [34, 136], while the rate of decay remains largely unchanged. This is consistent with our results (Fig. 7.2), where the calcium transient increases almost three-fold from purely detubulated cells to cells with a dense t-tubular network. The SR Ca^{2+} load, however, remains almost constant. This agrees with results obtained in detubulated myocytes [136], as well as in during AF, where a decrease in release was observed despite similar SR content [154].

In our simulations, a reduction in the length of t-tubules results in an effective reduction of ICaL and NCX currents (Fig. 7.3). However, both are modified equally so, if they are in equilibrium for a cell with a dense t-tubular network, they are expected to be in equilibrium in a detubulated cell. In terms of Ca^{2+} homeostasis, this means that one expects diastolic values of cytosolic and SR Ca^{2+} to remain almost unchanged. One would expect a similar results if in a tubulated cell one decreases the strength of both ICaL and NCX. This analogy is true except for spatial effects, that may become important at fast pacing rates, where diffusion is not fast enough to equilibrate concentrations, and diastolic values in both cases start to diverge (Fig. 7.3).

Detubulation and SERCA dysfunction impair release in different manners In HF, a reduction in the t-tubular network is accompanied by a decrease in SERCA functionality [79, 87]. Although both result in decreased Ca^{2+} transients (Fig. 7.4), their effect is very different. Detubulation reduces release by reducing the amount of CaRUs that fire (Fig. 7.6), thus modifying systolic values of Ca^{2+} (cytosolic Ca^{2+} peak, SR fractional release), but with little effect on diastolic values. It thus directly affects SR release. A reduction in SERCA, on the other hand, results in a change in diastolic Ca^{2+} levels, i.e., a reduction of SR Ca^{2+} load, that produces a reduction of SR release.

Detubulation produces desynchronization in release Contrary to normal ventricular cells, in atrial and ventricular detubulated cells, a delay is observed between the Ca^{2+} rise close to the membrane and at the cell center [83, 244, 117, 157, 35]. In line scans, this gives rise to a specific U-shaped pattern [83, 244, 35]. This effect is clearly observed in the simulations as the t-tubular F.A. is varied (Fig. 7.4). When the F.A. is reduced, the amplitude of the interior Ca^{2+} transient is much reduced with respect to that close to the cell membrane (Fig. 7.5), while the time delay between both peaks increases.

This dyssynchrony in release can be observed in the statistics of release events at individual RyR2s (Fig. 7.6). A computation of the time at which each individual RyR2 opens for the first time shows that RyR2s start to open upon the entrance of

Ca^{2+} into the cell, with a mean time to release that increases in detubulated cells. In this case, the distribution is also broader, as orphaned RyR2s start to open. Defining a dyssynchrony index as the standard deviation of that distribution, one can observe that it increases in detubulated cells. This had already been shown in a computational study [206], using a simpler model for release that accounted for CaRU recruitment, but with instantaneous opening of a fraction of the RyR2s.

Interestingly, the number of CaRUs that open at least once increases with F.A. in an almost linear fashion (Fig. 7.6), but is always larger than the fractional area, meaning that many orphaned RyR2s open. Even in the total absence of t-tubules, about half of the CaRUs open (Fig. 7.6).

Axial tubules enhance inward calcium propagation Besides transverse tubules, axial tubules have been observed in several animal species [33, 32] and, in fact, in some species they can represent the main component of the TAT network [32]. We find that axial tubules have a profound impact for centripetal wave propagation. In situations where the t-tubular network alone does not produce inward propagation in our simulations, a small amount of axial tubules is enough to produce release in the central region (Fig. 7.7). In the absence of axial tubules, for a typical F.A.=0.1-0.2 of an atrial myocyte our results do not show inward propagation, less alone if it is detubulated, contrary to some experimental observations [34, 30], where detubulation results in a smaller global transient and a delay between the subsarcolemmal and central calcium peaks, but with still an appreciable central calcium transient. This would agree with the presence of axial t-tubules, that reproduce the typical V shape in the linescans obtained in experiments. Interestingly, the density of axial tubules measured in experiments [32] ($d_T \sim 0.04 - 0.08 \mu\text{m}/\mu\text{m}^2$, for small mammals) agrees well with our results that show that the central peak is recovered for that density of axial tubules (Fig. 7.7).

Orphaned RyR2s increase LCC-release gain in detubulated cells In detubulated cells there is a decrease in calcium entrance through the LCC. This is partly compensated by an increase in the excitation contraction (ECC) gain function, measured as $\Delta[Ca^{2+}]_{rel}/\Delta[Ca^{2+}]_{influx}$, i.e., total calcium released from the SR compared to total Ca^{2+} entry through the LCC channels (Fig. 7.3). So detubulation results in a reduction of the SR release and cytosolic transient in a less pronounced manner than that of LCC total current. The reason is linked to recruitment of orphaned RyR2s, so the increase in cytosolic Ca^{2+} due to the opening of CaRUs where LCCs are present produces secondary openings of orphaned RyR2s. Thus, release in this case is a mixture of coupled and propagated Ca^{2+} release. This may serve as an adaptive mechanism when t-tubule remodeling occurs [106]. However, it seems to be in contradiction to what has been observed in cardiomyocytes in post myocardial infarction (PMI) animals [93], suggesting that probably other mechanisms beyond detubulation are in play during PMI, i.e., a mismatch or an increased gap between LCCs and RyR2s.

Above a certain value of the t-tubular density, complete coupling is obtained The different measures of the Ca^{2+} transient (Ca^{2+} release and peak systolic Ca^{2+}, ratio of peripheral to interior Ca^{2+} peak, etc) saturate above a certain density of t-tubules. So, for a F.A. above 50%, the addition of t-tubules does not have any effect on the transients. As we already discussed, this is due to the recruitment of orphaned RyR2, so, for F.A. above around 50%, all CaRUs open (Fig. 7.6B). Interestingly, a value of F.A. close to 50% was measured experimentally in rat ventricular cells [120], that was reduced 2-fold in case of HF.

Chapter 8

Calcium oscillations

Note: the results obtained in this section have been presented in [179] and the text has been extracted from the aforementioned paper.

Calcium oscillations and waves are often behind instances of extradepolarizations in cardiac cells, eventually giving rise to life-threatening arrhythmias. Often, mortality is related to the appearance of rapid cardiac rhythms, such as tachycardia and fibrillation, that result in contractability loss, reducing cardiac output and eventually leading to sudden cardiac death [116]. Although the onset of rapid arrhythmias can be due to a large variety of factors [216], including changes in the properties of cardiac tissue [4], often arrhythmias are triggered by spontaneous intracellular calcium releases [255, 50]. In cardiac cells, calcium is responsible for regulating cell contraction, but it also modulates several currents that affect the action potential. Thus, spontaneous calcium release in the interbeat interval, during diastole, may elicit extra action potential depolarizations and excitation waves, potentially disrupting normal wave propagation. This sometimes leads to the formation of rotors (functional reentry) and eventually a disordered electrical state characteristic of fibrillation [113, 212, 309].

Often, this focal activity is due to the presence of periodic calcium waves, that result in calcium oscillations [204, 147, 42, 178, 279, 66]. In paced cardiac cells, oscillations necessarily compete with the external pacing frequency and they may be behind occurrences of spontaneous calcium release events during diastole [210]. Calcium oscillations arise typically due to a malfunction of the RyR2 [134, 214, 160, 210], a ligand-gated calcium channel [280] that controls the amplitude of the intracellular calcium transient, by regulating the release of calcium stored at the SR. Since calcium dynamics in cardiac cells is regulated by the release of calcium at several tens of thousands of CaRUs, global oscillations must appear as a result of an oscillatory regime at the local cluster level that can later be coordinated by diffusion of free calcium. Alternatively, when synchronization is not complete, oscillations at the local level can give rise to periodic calcium waves, providing a pro-arrhythmic substrate [305, 241]. Calcium oscillations have been observed to appear in ventricular myocytes under elevated values of cytosolic calcium [260], due to periodic opening and closing of the RyR2s. An increase in cytosolic calcium concentration results in a higher frequency of the oscillations until, at larger values, the SR is depleted because the RyR2 becomes permanently open [260]. A similar transition has also been studied in models under conditions of SR calcium overload [283, 303, 19].

A key element in the regulation of intracellular calcium dynamics is CSQ. As we have already explained in section 6.1, this is one of the major Ca^{2+}-binding proteins in the SR, with high capacity and low affinity [192]. CSQ is preferentially anchored close to the RyR2 channels [132, 80]. Nowadays it is known that CSQ is an important regulator of RyR2 gating [99, 143, 252] through the calcium bound to CSQ. Therefore, CSQ plays two roles in cardiac cells: it can be considered a Ca^{2+} reservoir for release from the luminal space, but it is also thought to act as a modulator of RyR channel gating. So that, in addition to simply storing Ca^{2+}, CSQ influences the release process by controlling free Ca^{2+} dynamics near the luminal regulatory sites of the RyR2 complex [15, 14, 16]. Dysregulations in CSQ dynamics have been associated with heart diseases [63, 221]. In particular, it has been shown that the absence of CSQ enhances the RyR2 channel opening and, thus, promotes premature spontaneous SR Ca^{2+} macro events. The ablation of CSQ causes a form of tachycardia, namely, catecholaminergic polymorphic ventricular tachycardia (CPVT) [63].

In this chapter, we use the subcellular model widely used in this Thesis to show the appearance of periodic calcium waves and then analyze this phenomenon using a deterministic model of calcium in a cardiac cell (or in a CaRU). We study the existence and stability of different solutions and their dependence on CSQ levels and function. We show that oscillations typically appear at high global calcium concentration and/or high RyR2 open probability. Their appearance depends on a delicate balance between the total calcium level in the cell and the level of buffering of calcium available. For instance, at high values of CSQ, the system presents a transition from a low concentration, excitable state, to a high concentration state. Such a transition has been proposed to be the basis of complex states, such as long-lasting sparks [256]. At low concentrations of CSQ, in between these two stable states, oscillations appear. We study this transition using a minimal model, that includes the concentration of dyadic and SR calcium and the open probability of the RyR2 and show that it suffices to explain the appearance of oscillations. A further reduction to a minimal two-dimensional model allows us to explain the transition to the oscillatory regime in terms of the nullcline structure of the system.

8.1 Materials and methods

The methods used in this chapter have two clear different natures. First, we use the fully detailed subcellular stochastic model of calcium handling presented in part II to report numerical results showing calcium oscillations. We analyze under which conditions oscillations appear in a controlled scenario where no external pacing is present, and there are no calcium fluxes with the extracellular medium. Later, in order to gain insight regarding the origin of the oscillations that we observe in the full model, we construct a minimal deterministic model for the local dynamics of calcium at the level of the CaRU. The numerical and mathematical analysis of this model allows us to analyze the underlying mechanism of Ca^{2+} oscillations disregarding the coordination effects of the full model.

8.1.1 Detailed subcellular calcium model

Under physiological conditions, the total amount of calcium in the cell at steady state is fixed by calcium homeostasis, i.e. the complex interaction of LCC, exchanger and pumps, which affect the steady state level at which the calcium entering the cell balances the calcium extruding. In this chapter, we are interested in studying instabilities in calcium cycling, under constant cell calcium content. This allows us to focus the analysis on the conditions for appearance of calcium oscillations under different possible calcium homeostatic levels. Thus, we neglect calcium exchange with the extracellular medium, setting the conductances of the L-type calcium channels and the NCX equal to zero. Then, the total amount of calcium in the cell, Q_T, is given by:

$$Q_T = v_i(c_i + c_{b,TnC} + c_{b,SR} + c_{b,CaM}) + v_{sr}(c_{sr} + c_{bSQ}). \tag{8.1}$$

For a better comparison with the results from a reduced calcium model, described later, we will consider as our control parameter the average calcium content of the cell $\bar{c}_T = Q_T/(v_i + v_{sr})$. Thus, in our simulations, $\bar{c}_T$ is a constant value that is determined by the initial conditions for cytosolic and luminal calcium (free and bound to buffers). Moreover, we have not considered the effect of the luminal calcium as a mechanism to shut down RyR2s. We will discuss later why we do this consideration.

8.1.2 Reduced calcium model

The minimal model for the local dynamics of calcium is based on the schematics shown in Fig. 8.1. We consider a simplified description of the system, with dynamics of the total calcium concentration in the SR, c_{SR}^{tot}, and in the cytosolic space close to the RyR2, or dyadic space, c_d, and of the open probability of the RyR2, P_o,

$$\frac{dc_d}{dt} = J_{rel} - J_d \tag{8.2}$$

$$\frac{dc_{sr}^{tot}}{dt} = \frac{v_i}{v_{sr}} J_{up} - \frac{v_d}{v_{sr}} J_{rel} \tag{8.3}$$

$$\frac{dP_o}{dt} = k_p c_d^2 (1 - P_o) - k_m P_o \tag{8.4}$$

with the currents given by

$$J_{rel} = gP_o(c_{sr} - c_d), \quad J_d = \frac{c_d - c_i}{\tau_i}, \quad J_{up} = g_{up}\frac{c_i^2}{K_s^2 + c_i^2} \tag{8.5}$$

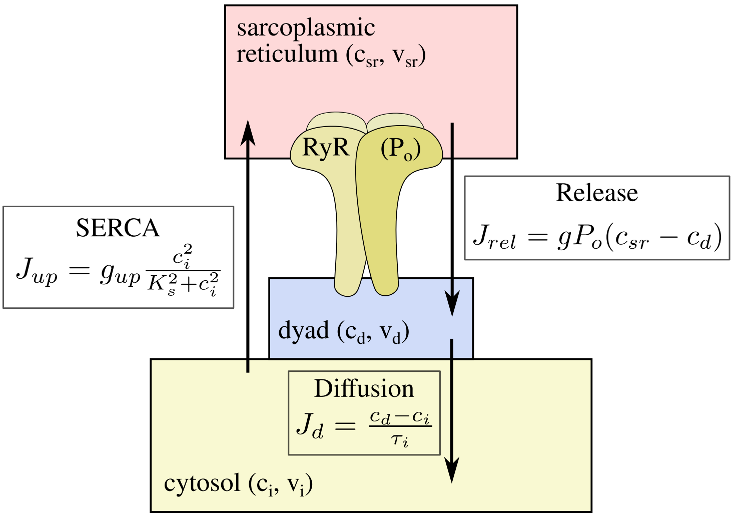
sarcoplasmic reticulum (c_{sr}, v_{sr})
RyR
(P_o)
Release
$J_{rel} = gP_o(c_{sr} - c_d)$
SERCA
$J_{up} = g_{up}\frac{c_i^2}{K_s^2+c_i^2}$
dyad (c_d, v_d)
Diffusion
$J_d = \frac{c_d - c_i}{\tau_i}$
cytosol (c_i, v_i)

FIGURE 8.1: **Structure of the simplified model.** Sketch of the different compartments considered in the simplified model, with the internal variables and the equations of the respective calcium fluxes.

A detailed derivation of these equations and their range of validity can be found in Appendix B. Notice that, as in the full model, we consider a situation where no external pacing is imposed. In this sense, neither external intake from the LCC is considered, nor any extrusion via the sodium calcium exchanger.

For simplicity we consider a SERCA pump without an equilibrium condition, that always pumps calcium from the cytosol to the SR. This gives a basal solution at $c_i = c_d = 0$, instead of the physiological value of $\sim$ 100nM. However, given that, at basal conditions, $c_{sr} \sim$ 1mM, this is a reasonable simplification. As in the detailed subcellular model, we assume the approximation of rapid CSQ buffer, so we can compute the amount of free luminal calcium c_{sr} from the total luminal calcium c_{sr}^{tot} from Eq. (3.30).

To close the system we should introduce an extra equation for calcium concentration in the cytosol c_i. However, as we assume that the total calcium content in the cell is constant, then we have a conservation equation. Therefore, we can compute c_i solving the following quadratic equation for the conservation of $\bar{c}_T$

$$\bar{c}_T = \frac{v_i}{v_{cell}}\left(c_i + \frac{B_b c_i}{K_b + c_i}\right) + \frac{v_d}{v_{cell}}c_d + \frac{v_{sr}}{v_{cell}}c_{sr}^{tot}, \tag{8.6}$$

where v_{cell} is the unit volume defined as $v_{cell} \equiv v_i + v_{sr} + v_d$, and B_b is the concentration of a generic buffer in the cytosol.

To simplify the analysis, we proceed to work with the assumption that the dynamics of opening of the RyR2s is faster than that of calcium concentration ($\dot{P}_o \simeq 0$), obtaining then a minimal two-variable model. This will be our baseline minimal model. However, we will later also consider an alternative model with fast dynamics for the dyadic calcium concentration ($\dot{c}_d \simeq 0$). Clearly, under the assumption that both processes are fast, as considered often in the literature [111], in the model oscillations would disappear. A third possibility, with fast dynamics of luminal calcium, although theoretically possible, does not have much physiological sense, as SERCA is typically slow compared to release or diffusion from the dyadic space.

Fast RyR2 dynamics In this case, we assume that the open and close dynamics of the RyR2 are fast, so we can assume that it is in quasi-steady state ($\dot{P}_o \simeq 0$). Then, from Eq. (8.4), we obtain:

$$P_o = \frac{c_d^2}{K_o^2 + c_d^2} \tag{8.7}$$

where the parameter $K_o^2 = k_m/k_p$ is the ratio of the open and close rates of the RyR2. Then, with these assumptions, the simplified model becomes

$$\begin{aligned} \frac{dc_d}{dt} &= g\frac{c_d^2}{K_o^2 + c_d^2}(c_{sr} - c_d) - \frac{c_d - c_i}{\tau_i} && (8.8) \\ \frac{dc_{sr}^{tot}}{dt} &= \frac{v_i}{v_{sr}} g_{up} \frac{c_i^2}{K_s^2 + c_i^2} - \frac{v_d}{v_{sr}} g \frac{c_d^2}{K_o^2 + c_d^2}(c_{sr} - c_d) && (8.9) \end{aligned}$$

Fast dyadic calcium dynamics In order to test the robustness of the analysis, we will also consider a simplified model given by Eqs. (8.2)-(8.4), and consider the limit of fast dynamics in the dyadic space and take $\dot{c}_d \simeq 0$. Then, from Eq. (8.2):

$$c_d = \frac{\tau_i g P_o c_{sr} + c_i}{1 + \tau_i g P_o} \tag{8.10}$$

Substituting this expression in Eqs. (8.3) and (8.4), we obtain another minimal model, given by

$$\begin{aligned} \frac{dc_{sr}^{tot}}{dt} &= \frac{v_i}{v_{sr}} g_{up} \frac{c_i^2}{K_s^2 + c_i^2} - \frac{v_d}{v_{sr}} g P_o (c_{sr} - c_d) && (8.11) \\ \frac{dP_o}{dt} &= -k_m P_o + k_p c_d^2 (1 - P_o) && (8.12) \end{aligned}$$

where again, c_i must be computed solving the quadratic equation for the conservation of mass $\bar{c}_T$ [Eq. (8.6)]. For simplicity we will consider the case where no CSQ is present $B_{SQ} = 0$.

8.2 Results

We first present the results of the numerical simulations of both the full detailed model and the minimal model of calcium cycling. Both produce the same basic scenarios for intracellular calcium dynamics, with three different dynamical behaviors, which we then proceed to analyze. The goal of the development of the minimal model is, precisely, to be able to perform this analytical treatment and check how the behavior depends on total calcium and buffering levels.

8.2.1 Results from the subcellular model

The full detailed model allows us to investigate the different behaviors present in cardiomyocyte calcium cycling when there is no external pacing. We should point out that, under these conditions, the average calcium concentration in the cell $\bar{c}_T$ is conserved since the total amount of calcium Q_T in the cell is constant. We produce simulations with different levels of average calcium concentration and observe very different behaviors (Fig. 8.2a). For the lowest value of $\bar{c}_T$, the RyR2s remain almost closed, and most of the calcium content is stored in the SR. Despite the stochasticity of the system, the average values obtained are reproduced reliably with only the presence of local sparks as fluctuations of this global state. This state corresponds to an excitable state, which is the expected behavior of the cell if it has to react properly to external excitation. We call this general state a global shut down state.

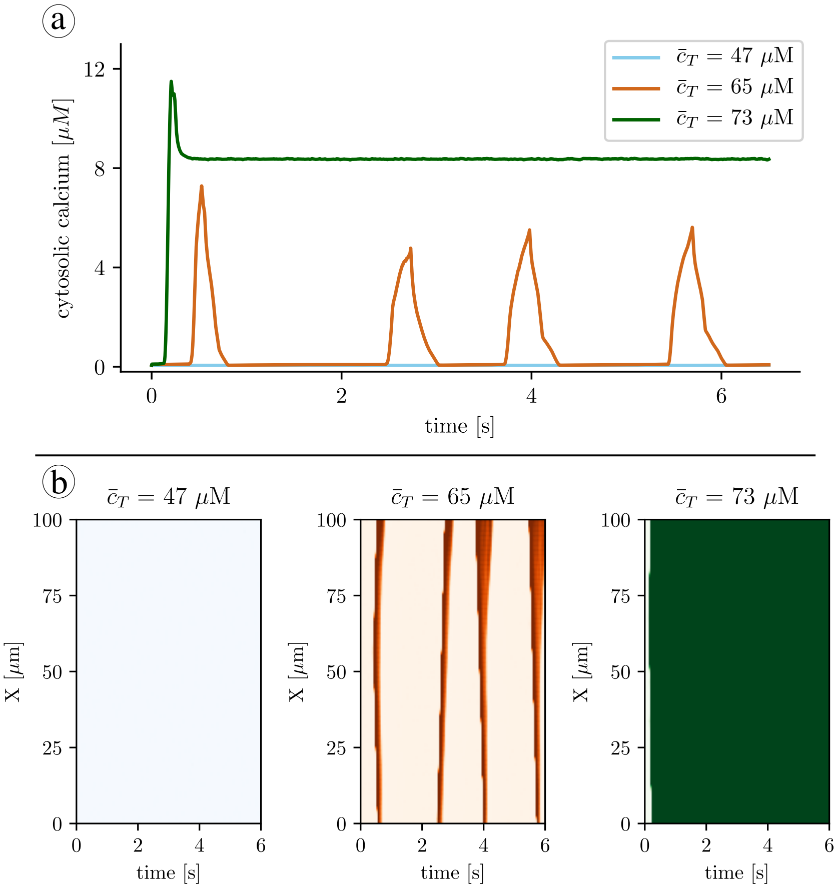

FIGURE 8.2: **Calcium profiles obtained with the subcellular model.** a) Calcium traces obtained with the full subcellular model and three different values of the average calcium concentration, $\bar{c}_T$. b) Line-scans at different values of the load. Increasing the load, the system undergoes a transition from a low cytosolic calcium state (at $\bar{c}_T = 47\mu$M), where RyR2s remain in the close state, to spontaneous oscillations, giving rise to calcium waves ($\bar{c}_T = 65\mu$M). Finally, at high calcium loads ($\bar{c}_T = 73\mu$M) oscillations give rise to a high cytosolic calcium state, where the RyR2s remain open, resulting in SR calcium depletion.

When the calcium load increases, the system starts to spontaneously show calcium waves. These waves persist in time with different shapes and durations, giving rise to a nearly periodic oscillation in the global calcium signal. Roughly, we observe one calcium wave per second (Fig. 8.4). Waves are normally initiated at different sites each time but they appear systematically indicating a strong oscillation at the substrate level that we will address in the discussion.

Finally, at large values of $\bar{c}_T$ oscillations disappear, giving place to a stable state with a high level of calcium in the cytosolic space and a depleted SR. In this state, the RyR2s are generally open allowing for the depletion of the SR and the increase of cytosolic calcium. Except for local fluctuations this state is globally stable and we can call it the open state. This state would not to respond to external pacing, however it would produce the activation of the NCX exchanger which would slowly decrease the average concentration model. As we pointed out previously, the elimination of the calcium intake and extrusion in the model allows us to focus in the general behavior of the cell under different homeostatic scenarios. Numerical simulation indicate that as the calcium level is increased, the cell goes from a shut-down and ready-to-respond state to an oscillatory regime to a global open state where the cell does not respond.

Including RyR2 regulation by SR, Ca^{2+} does not change this scenario, but rather, it actually increases the region where oscillations appear. Increasing the load (see Fig. 8.3), the system undergoes a transition from a low cytosolic calcium state, where RyR2s remain in the close state, to spontaneous oscillations, giving rise to calcium waves. This transition happens at the a similar value of $\bar{c}_T$ as in the case without SR luminal dependence. However, the transition to the high cytosolic calcium state, where the RyR2s remain open, occurs at larger values of the total calcium content. Thus, these simulations suggest that the range of oscillations is broader when the SR dependence is included to the model. Then, we have considered the subcellular model without the luminal dependence on the RyR2 in order to be more similar to the minimal models presented above.

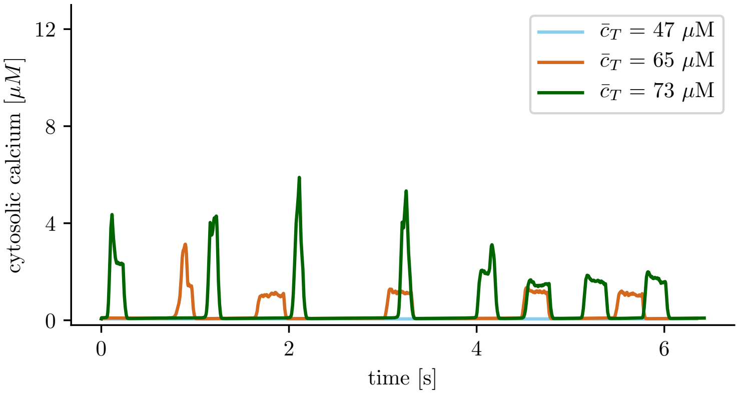

FIGURE 8.3: **Subcellular model with SR luminal dependence on the RyR2.** Calcium traces obtained with the full subcellular model and three different values of the average calcium concentration, c_T. The open rate between the open and the closed state has been modified to include a dependence on the luminal calcium following Eq. 3.13, with $H = 10$, $EC_{50} = 500\mu$M, and $\alpha = 15$.

A similar trend has been observed experimentally by Stevens et al. [260], even if in the experimental preparation the control parameter was the amount of cytosolic calcium, and not total calcium, as in our simulations. Oscillations appear as the amount of calcium in the cell increases, giving rise to a state with depleted SR calcium (and RyR2s in the open state), at high calcium concentrations. Furthermore, experimentally it has been shown that changes in buffering levels can have also important effects on this transition. More specifically, Stevens et al. [260] have shown that the reduction of CSQ in the SR bulk enhances the appearance of oscillations. We have checked if this situation is also present in our simulation and found this to be the case. As shown in Fig. 8.4, when we reduce the CSQ concentration, the oscillations appear at lower values of $\bar{c}_T$, they have a higher frequency and the range of oscillations in terms of $\bar{c}_T$ becomes broader.

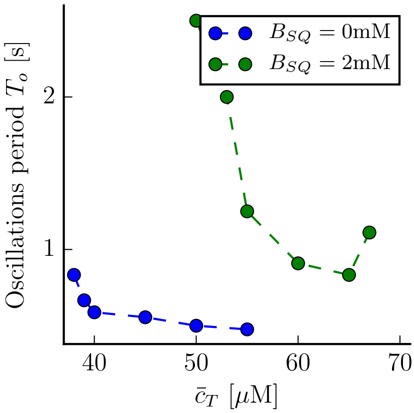

FIGURE 8.4: **Oscillations in the subcellular model.** Average period of oscillations at different values of the average calcium concentration $\bar{c}_T$, for a concentration of CSQ of $B_{SQ} = 2$mM (green dots), and in the absence of CSQ (blue dots).

8.2.2 Minimal model without calsequestrin

We proceed to explain the results obtained in the minimal model where we find the same qualitative behavior as in the results obtained with the full subcellular stochastic model. We have performed simulations in the approximation of fast RyR2 opening dynamics at different values of the cell average calcium concentration $\bar{c}_T$. We consider first the case where no calsequestrin is present, $B_{SQ} = 0$. As we observed in the full subcellular model, at low values of $\bar{c}_T$ the system remains in a low concentration steady state (Fig. 8.5). In this state the system is excitable, so the fixed point is locally stable, but a large enough perturbation produces an increase in calcium concentration, resulting in a calcium transient typical from CICR. On the other hand, at high calcium loads there is a new fixed point with high cytosolic calcium concentration, that has been related to the appearance of long-lasting sparks [256]. As in the subcellular model, in between the low concentration fixed point and the permanently open state, the system presents oscillations (Fig. 8.5), that are stable for a quite broad range of loads.

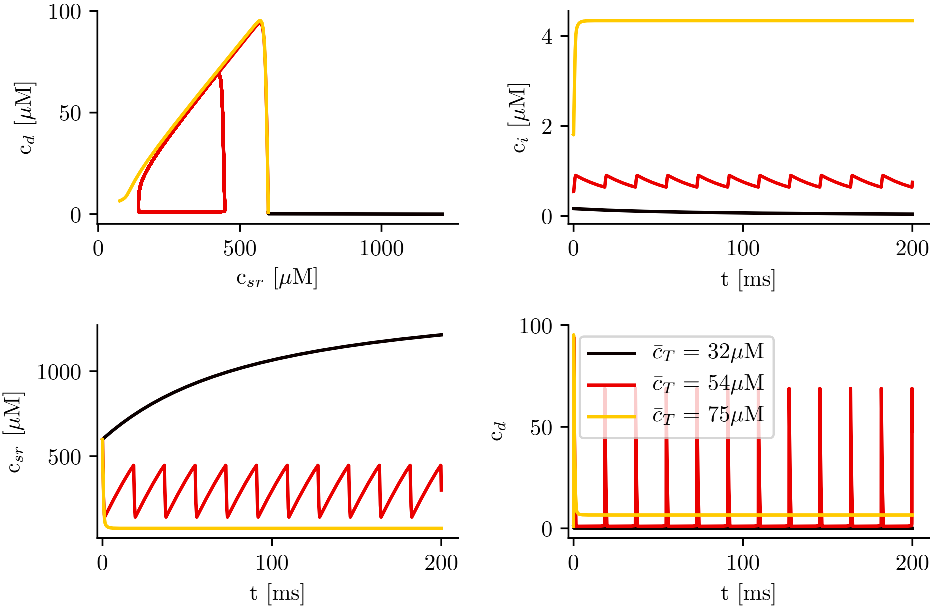

FIGURE 8.5: **Time traces of the different calcium concentrations for different values of total calcium concentration, $\bar{c}_T$, and calsequestrin concentration set to zero ($B_{SQ} = 0$).** After a transient, the system ends up in either a steady state which is excitatory at low levels of total calcium in the cell with observed low levels of calcium in the cytosol, in an oscillatory state with intermediate levels of total calcium in the cell, or in a state of high total levels of calcium in the cell with observed high cytosolic calcium levels.

Indeed, the number of stationary solutions changes with the calcium concentration $\bar{c}_T$. The fixed points of the system can be found from:

$$0 = g\frac{c_d^2}{K_o^2 + c_d^2}(c_{sr} - c_d) - \frac{c_d - c_i}{\tau_i} \tag{8.13}$$

$$0 = -\frac{v_d}{v_{sr}}g\frac{c_d^2}{K_o^2 + c_d^2}(c_{sr} - c_d) + \frac{v_i}{v_{sr}}g_{up}\frac{c_i^2}{K_s^2 + c_i^2} \tag{8.14}$$

together with:

$$c_i + \frac{B_b c_i}{K_b + c_i} = \frac{1}{v_i}\left(v\bar{c}_T - v_d c_d - v_{sr} c_{sr}^{tot}\right) \tag{8.15}$$

Eqs. (8.13)-(8.15) represent three algebraic equations that give the concentrations c_i, c_d and c_{sr} as a function of total calcium concentration in the cell $\bar{c}_T$. When no calsequestrin is present $B_{SQ}=0$, it is easy to obtain that

$$c_d = c_i + \frac{v_i}{v_d}\tau_i g_{up}\frac{c_i^2}{K_s^2+c_i^2} \tag{8.16}$$

$$c_{sr}^{tot} = \frac{1}{v_{sr}}\left[v\bar{c}_T - v_d c_d - v_i\left(c_i + \frac{B_b c_i}{K_b + c_i}\right)\right] \tag{8.17}$$

Introducing these expressions into Eq. (8.13) we obtain an equation of the form $f(c_i;\bar{c}_T)=0$. For each value of $\bar{c}_T$ we can obtain the values of c_i that solve the equation. For instance, for a global average calcium concentration of $\bar{c}_T=32$ μM we have only one solution, as shown in Fig. 8.6a. This solution, given by $c_d=c_i=0$ and $c_{sr}^{tot}=v/v_{sr}\bar{c}_T$, exists for all values of $\bar{c}_T$. At high values of the average concentration, $\bar{c}_T=54$ and 75 μM, another two solutions appear, as depicted in Figs. 8.6b and c.

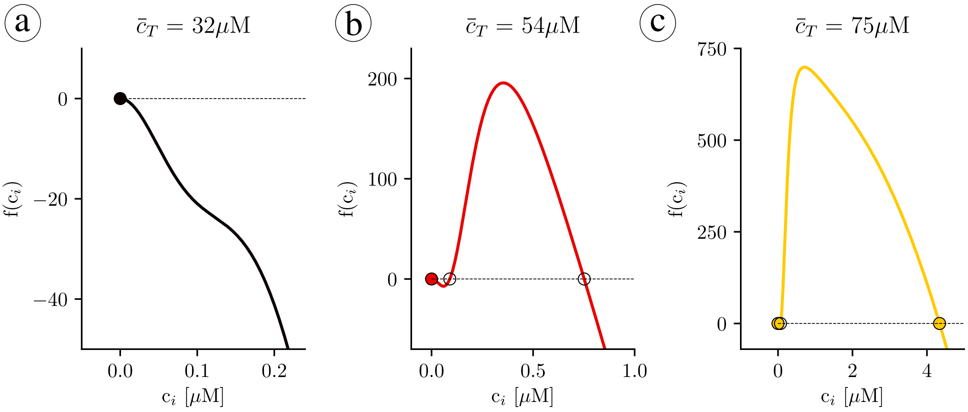

FIGURE 8.6: **Plot of the function $f(c_i)$ for different values of the $\bar{c}_T$ concentration.** a) At low concentrations there is a single fixed point. b) At higher concentrations two extra unstable fixed points appear. c) At high concentrations the upper fixed point becomes stable.

To calculate the stability of the stationary solutions, we have computed the value of the eigenvalues of the Jacobian matrix, corresponding to Eqs. (8.8)-(8.9). We find that, while the lower branch is always stable, the other branch of solutions is unstable for a large range of parameters (Fig. 8.7), due to the appearance of oscillations. The stability of the corresponding periodic orbit has been calculated using XPPAUT [69] (Fig. 8.7). We obtain that, as $\bar{c}_T$ is increased, a limit cycle appears in a global homoclinic bifurcation, with zero frequency (Fig. 8.8c). Increasing $\bar{c}_T$, this limit cycle finally disappears in a Hopf bifurcation, at which the upper fixed point becomes stable (Fig. 8.8b).

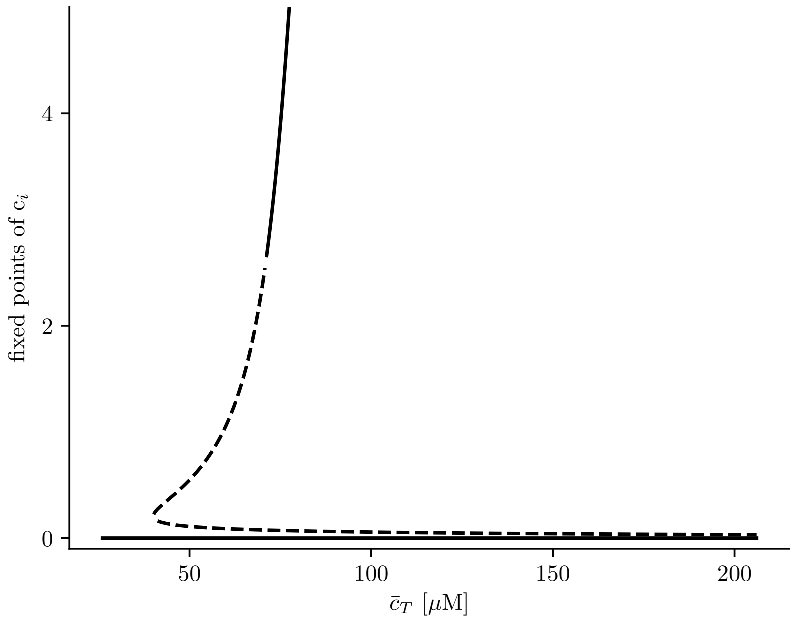

FIGURE 8.7: **Solutions for cytosolic calcium concentration, c_i, as a function of total calcium concentration, $\bar{c}_T$.** Discontinuous lines represent unstable solutions while continuous lines stable ones.

8.2.3 Minimal model with calsequestrin

We present now the main results of the simulation in the fast RyR2 minimal model when calsequestrin is present. We use Eqs. (8.8)-(8.9), with Eq. (3.30) that relates free with CSQ-bound SR calcium concentrations. Typically $K_{SQ} = 650\mu M$ and B_{SQ} somewhere between zero and 20 mM. We have then calculated the different fixed points as a function of the total concentration $\bar{c}_T$ for different values of B_{SQ} (Fig. 8.9). When $B_{SQ} \neq 0$, increasing $\bar{c}_T$, the appearance of two extra solutions occurs at larger values of $\bar{c}_T$, meaning that the close state solution is stable for a wider range of $\bar{c}_T$. Besides, the oscillatory range becomes narrower when B_{SQ} increases, until at certain point oscillations disappear. The disappearance of oscillations is due to the transformation of the bifurcation at which the upper fixed value gains stability, from a Hopf bifurcation into a saddle-node bifurcation.

In addition, at this point, the system presents five fixed points where only the lowest and uppermost are stable. It is important to note that this shows that CSQ enhances the elimination of oscillations. Finally, for high values of $\bar{c}_T$, the system has again three fixed points.

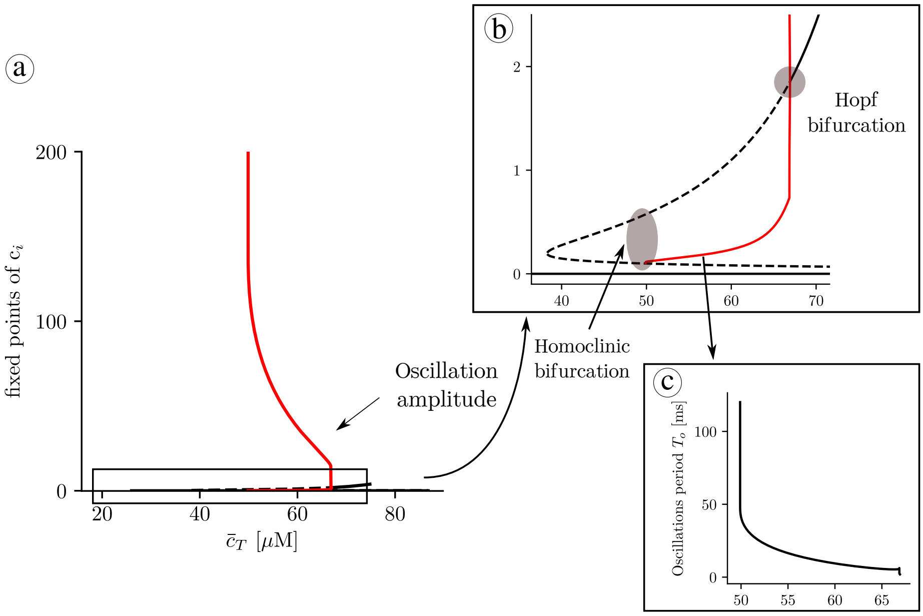

FIGURE 8.8: **Stability of the fixed points and the oscillations.** a) Solutions for cytosolic calcium concentration, c_i, as a function of total calcium concentration, $\bar{c}_T$. Discontinuous lines represent unstable solutions while continuous lines stable ones. When reducing the total concentration, at $\bar{c}_T \approx 66$ μM, a limit cycles emerges in a Hopf bifurcation, from the upper state, that then becomes unstable. The red lines represent the lower and upper values of the limit cycle. At $\bar{c}_T \approx 50$ μM, the intermediate unstable fixed point collides with the limit cycle, that disappears in a homoclinic bifurcation. Below $\bar{c}_T \approx 39$ μM, the RyR2 close state is the only solution. c) Oscillation periods as a function of $\bar{c}_T$.

Analytical results

The mathematical tractability of the minimal model allows us to get a better understanding of the transition to the upper state via oscillations. A first insight can be obtained by plotting the nullclines of the system (Fig. 8.10), which can help us understand the main mechanisms behind the transition to the oscillatory state. In particular, we obtain the critical average calcium concentration for the onset of oscillations, that depends on buffering levels, and the conditions for the appearance of the upper state.

Nullclines and stability of solutions. Besides the transition from one to three solutions (Figs. 8.10a and b), nullclines present a clear restructuring of their branches well before the upper state becomes stable. Increasing the total concentration, there is a sudden pinch-off in the c_d-nullcline (Figs. 8.10b and c). Before this change in nullcline topology, the lower state (with all the calcium in the luminal

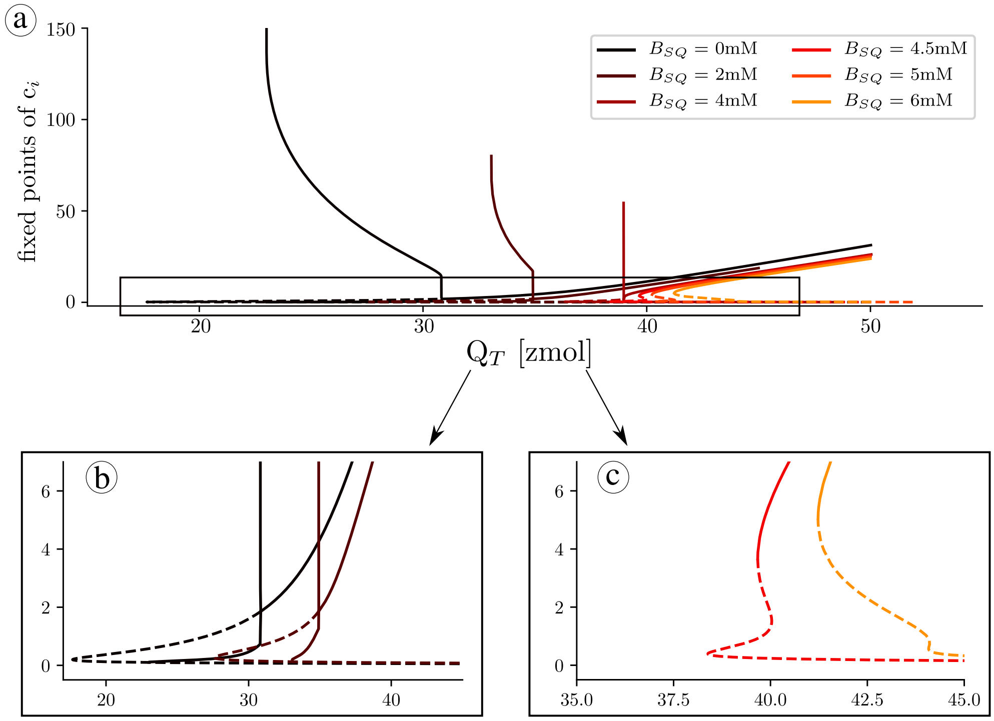

FIGURE 8.9: **Fixed points as function of CSQ.** Number of fixed points and stability of those fixed points as a function of total calcium in the unit, for different values of calsequestrin concentration.

space and none in the cytosol) is the only stable attractor. Once the c_d-nullclines split, oscillations may appear around the upper unstable fixed point.

We can understand the effect of the pinch-off by plotting the trajectories for values of $\bar{c}_T$ close to the transition. Below the pinch-off, the trajectory follows the fast dynamics of the c_d-nullcline (the black line in Figs. 8.10 and 8.11), until it reaches the fixed point. As the load is increased, the branches of the c_d-nullclines come closer until at a certain point the break-up occurs (Fig. 8.11c). Due to the emergence of the pinch-off, the dynamics follows the lower nullcline up to the tip, at the largest value of c_{sr}, where, due to the fast dynamics in the c_d direction, it jumps to flow again the nullcline, at larger values of c_i. Since there is no stable point, the trajectory starts a persistent oscillation around the unstable fixed point. We can state that, for this problem, the nullcline break-up is the necessary and sufficient condition to obtain oscillations.

Onset of oscillations. Using this observation, we can calculate analytically the critical value of $\bar{c}_T$ beyond which the system oscillates. At the pinch-off of the nullclines, the cubic solution of $\dot{c}_d = 0$ (black nullcline) loses two of the three solutions at a given c_{sr}. To calculate this point analytically, first we observe that the pinch-off occurs at values of $c_d < K_o$ ($K_o = 15\mu$M). To simplify the calculations,

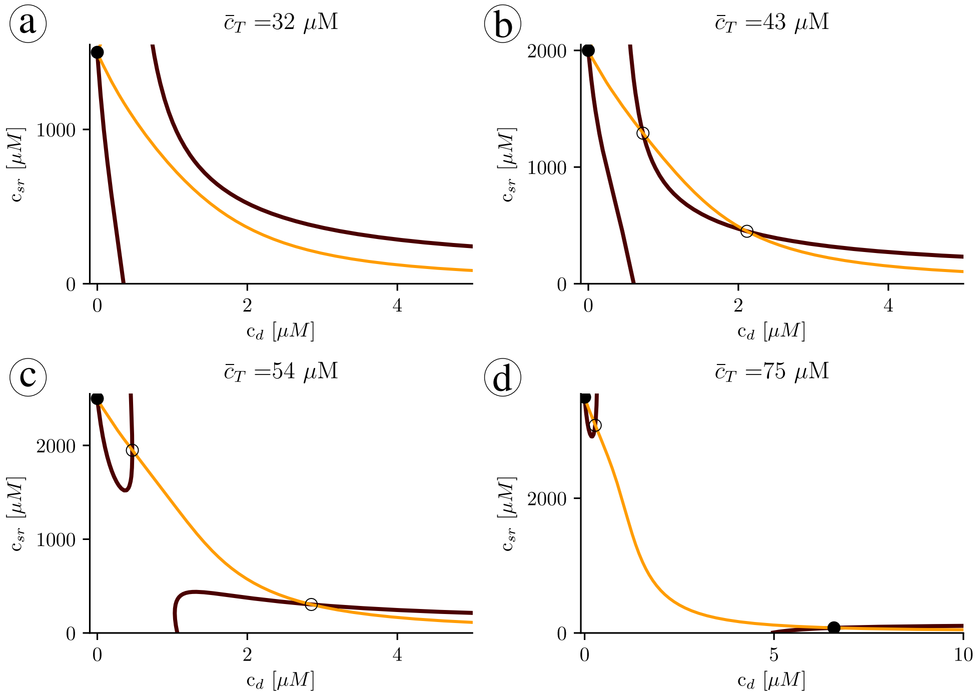

FIGURE 8.10: **Structure of the nullclines at different values of $\bar{c}_T$ indicated in the title of each panel.** The black line indicates the first nullcline $\dot{c}_d = 0$, while the orange lines corresponds to $\dot{c}_{sr} = 0$. Dots indicate the fixed points. Filled dot: stable fixed point and unfilled dot: unstable fixed point.

let us make the approximations that, at the pinch-off, the c_d satisfies $c_d \ll K_o$ and $c_d \ll c_{sr}$. Being this the case, then Eq. (8.8) reduces to

$$\frac{dc_d}{dt} = 0 = g\frac{c_d^2}{K_o^2}c_{sr} - \frac{c_d - c_i}{\tau_i} \tag{8.18}$$

Furthermore, from Eq. (8.15), we can write c_i in terms of c_{sr} (assuming $B_{SQ} = 0$, $c_d \ll c_{sr}$)

$$c_i + \frac{B_b c_i}{K_b + c_i} = \frac{v\bar{c}_T - v_{sr}c_{sr}}{v_i} \tag{8.19}$$

Assuming that the concentration of bound cytosolic calcium is much larger than that of free cytosolic calcium, we obtain

$$c_i = \frac{K_b(v\bar{c}_T - v_{sr}c_{sr})}{v_i B_b - (v\bar{c}_T - v_{sr}c_{sr})} \tag{8.20}$$

From the polynomial equation for c_d, Eq. (8.18), solutions of c_d are lost at values of c_{sr} given by $1 - 4\tilde{g}c_i c_{sr} \leq 0$, with $\tilde{g} = g\tau_i/K_o^2$. Expanding, this gives the critical

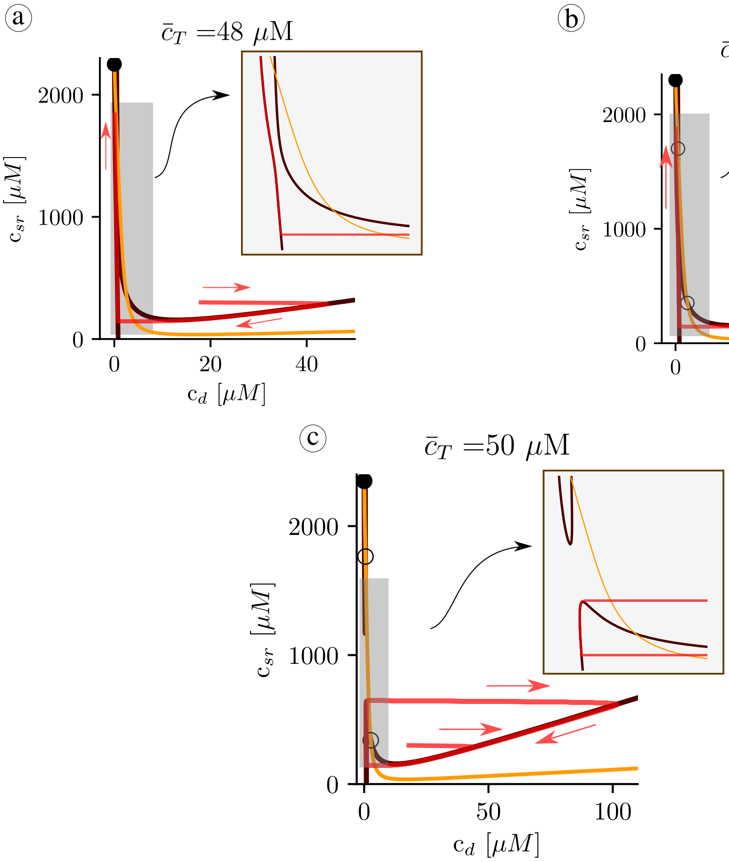

FIGURE 8.11: **Structure of the nullclines at different values of $\bar{c}_T$ indicated in the title of each panel.** The black line indicates the nullcline $\dot{c}_d = 0$, while the orange line corresponds to $\dot{c}_{sr} = 0$. The red curve is a trajectory with a direction indicated by the red arrows.

value of c^*_{sr} as:

$$v_i B_b - v\bar{c}_T + v_{sr}c^*_{sr} - 4\tilde{g}c^*_{sr}K_b(v\bar{c}_T - v_{sr}c^*_{sr}) = 0 \tag{8.21}$$

The same equation can be written as

$$(c^*_{sr})^2 + c^*_{sr}\frac{v_{sr} - 4\tilde{g}K_b v\bar{c}_T}{4\tilde{g}K_b v_{sr}} + \frac{v_i B_b - v\bar{c}_T}{4\tilde{g}K_b v_{sr}} = 0 \tag{8.22}$$

Once the pinch-off has been produced (Fig. 8.10c), there are two values of c^*_{sr}, corresponding to the lowest and highest values of the upper and lower nullclines, respectively. Just at the pinch-off these two points merge. This allows to establish the critical value at which the oscillation appears as the one that makes zero the discriminant of the second order polynomial of c^*_{sr}. After some algebra, the condition for the critical $\bar{c}_T^*$ becomes

$$(v_{sr} - 4\tilde{g}K_b v\bar{c}_T^*)^2 - 16K_b\tilde{g}v_{sr}(v_iB_b - v\bar{c}_T^*) = 0 \tag{8.23}$$

which can be written as

$$(\bar{c}_T^*)^2 + \frac{v_{sr}}{2\tilde{g}K_b v}\bar{c}_T^* + \frac{v_{sr}^2}{16\tilde{g}^2K_b^2v^2} - \frac{v_{sr}v_iB_b}{\tilde{g}K_bv^2} = 0 \tag{8.24}$$

This gives

$$\bar{c}_T^* = \sqrt{\frac{v_{sr}v_iB_b}{v^2\tilde{g}K_b}} - \frac{v_{sr}}{4\tilde{g}K_bv} \tag{8.25}$$

Using the parameters in Table B.1, this expression gives a critical value for the onset of oscillations at around $\bar{c}_T^* = 50\ \mu$M, that given the approximations considered, agrees quite well with the value obtain from the simulations of $\bar{c}_T^* \approx 51\ \mu$M. Thus, when the total calcium content exceeds this critical value $\bar{c}_T^*$, corresponding to a calcium concentration in the SR of $c_{sr} = v/v_{sr}\bar{c}_T^* = 2.28$mM (in the lower state), the system starts to oscillate, at a value of diastolic SR calcium load, given by:

$$c_{sr}^* = \frac{v\bar{c}_T^*}{2v_{sr}} - \frac{1}{8\tilde{g}K_b} = \frac{1}{2}\sqrt{\frac{v_iB_b}{v_{sr}\tilde{g}K_b}} - \frac{1}{4\tilde{g}K_b} \tag{8.26}$$

which gives a value of $c_{sr}^* = 0.86$ mM. At the onset of oscillations, there is thus a sudden decrease in basal SR calcium concentration, to less than half its previous value before the oscillations.

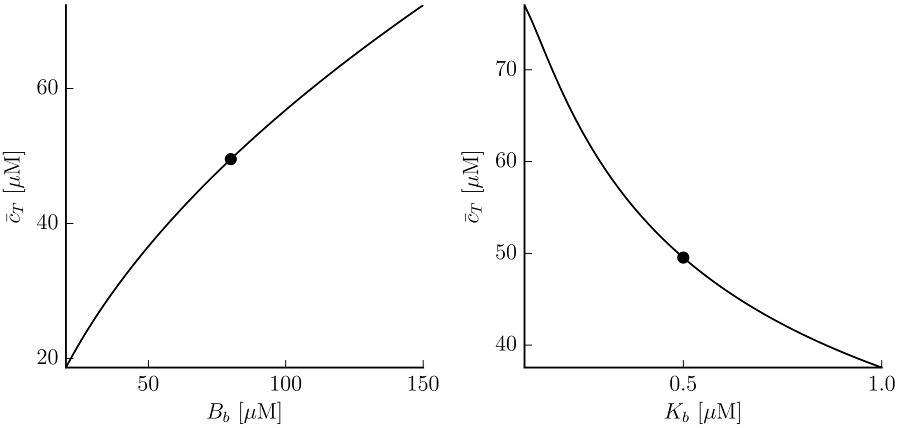

FIGURE 8.12: **Dependency of the onset of oscillations with buffer parameters.** The filled dots represent the control values $B_b = 80\mu$M, $K_b = 0.5\mu$M, given in Table B.1.

An increase in the quantity of cytosolic buffers (higher B_b) results in a delay

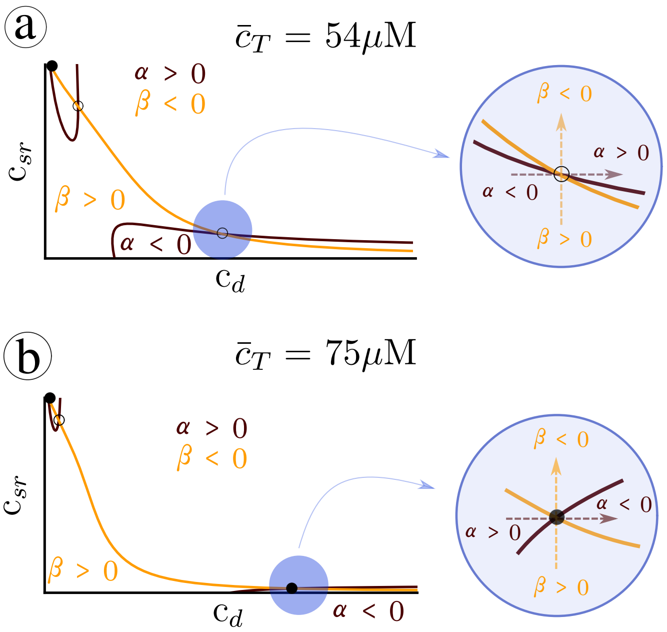

FIGURE 8.13: **Structure of the nullclines.** Structure of the nullclines at two different values of a) $\bar{c}_T = 54$ μM, b) $\bar{c}_T = 75$ μM. A black line corresponds to the nullcline $\dot{c}_d = 0$, while the orange line indicates $\dot{c}_{sr} = 0$. The functions f_1 and g_2 are the elements of the diagonal of the Jacobian matrix defined as $f_1 = \partial_{c_d}\dot{c}_d$ and $g_2 = \partial_{c_{sr}}\dot{c}_{sr}$.

in the onset of oscillations, that would occur at higher calcium load (Fig. 8.12a). A higher calcium affinity (lower K_b) on the contrary, would result in oscillations at lower loads (Fig. 8.12b). It is interesting to notice, too, that the strength of SERCA does not affect the onset of oscillations.

Transition to the upper state. The oscillations disappear at a Hopf bifurcation when the upper state becomes stable. It is possible to relate this transition to the structure of the nullclines in Fig. 8.10. For that, let us recover the definition of the Jacobian matrix **J**:

$$\mathbf{J} = \begin{bmatrix} \frac{\partial \dot{c}_d}{\partial c_d} & \frac{\partial \dot{c}_d}{\partial c_{sr}} \\ \frac{\partial \dot{c}_{sr}}{\partial c_d} & \frac{\partial \dot{c}_{sr}}{\partial c_{sr}} \end{bmatrix} \equiv \begin{bmatrix} f_1 & f_2 \\ g_1 & g_2 \end{bmatrix} \tag{8.27}$$

A fixed point will be stable provided $f_1 + g_2 < 0$. When $f_1 g_2 - f_2 g_1 > 0$ the stable fixed point corresponds to a node and if $f_1 g_2 - f_2 g_1 < 0$ to a stable spiral. We can use this to relate the slope of the nullclines to the stability of the upper fixed point. Let us denote $\alpha \equiv \dot{c}_d$ and $\beta \equiv \dot{c}_{sr}$ the time derivatives of the independent variables.

At large values of the total concentration (see Fig. 8.13a, with $\bar{c}_T = 75$ μM), the slope of the black nullcline ($\alpha = 0$) at the fixed point is positive, while the slope of the orange nullcline ($\beta = 0$) is negative. Then, increasing c_d at constant c_{sr}, α goes from being positive to negative. This means that $f_1 \equiv \partial\alpha/\partial c_d < 0$. Using the same argument, it is easy to check that also $g_2 \equiv \partial\beta/\partial c_{sr} < 0$, and therefore the fixed point is stable. At lower values of the total concentration (see, for instance, Fig. 8.13a, for $\bar{c}_T = 54$ μM) the slope of the black nullcline becomes negative. Thus, in this case, while g_2 is still negative, f_1 becomes positive, and it is not possible to determine the stability of the fixed point. It will actually depend on the speed of rate of c_d and c_{sr} close to the fixed point. If the dynamics of c_d is faster, then one expects this point to be unstable, if it is c_{sr} that varies fast, then stable. One would then expect that buffers that change the dynamics either in the cytosol or in the SR would have an effect on the stability of the fixed point and, therefore, in the range of existence of the limit cycle.

8.2.4 Robustness of the results

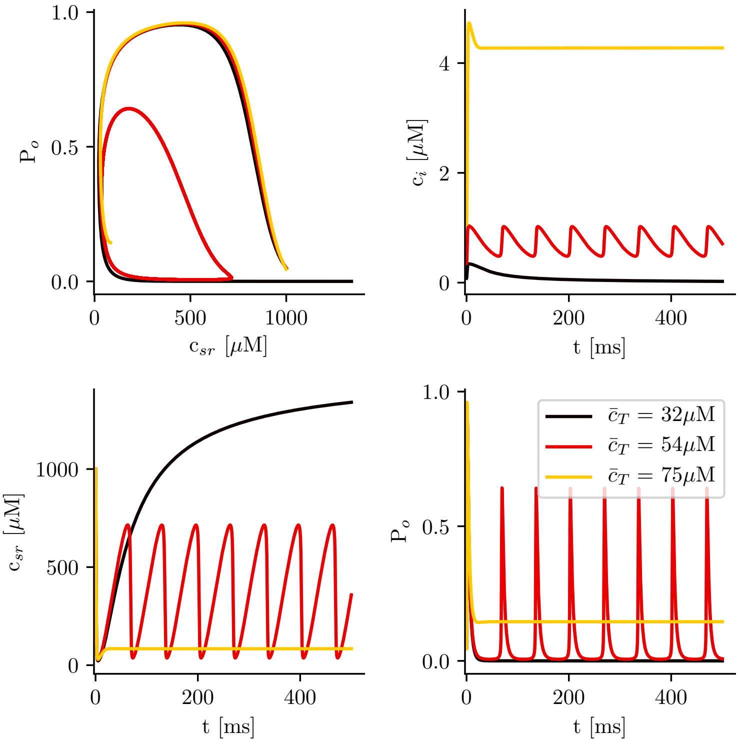

FIGURE 8.14: **Solutions as a function of total calcium concentration $\bar{c}_T$, with calsequestrin concentration set to zero when the fast dyadic approximation is used.** We obtain the same type of structure as expected.The system can be in a monostable state, which is excitatory (low load), in an oscillatory state (intermediate load), or in a bistable state (high loads), where it usually ends in a state of open RyR2 and depleted SR calcium concentration.

Fast dyadic calcium dynamics. It is useful to check that the basic points of our discussion hold when different possible approximations are applied to the minimal model. Namely, if the time scale of RyR2 opening is not as fast as the time scale of calcium diffusion near the dyadic space we should analyze the fast dyadic calcium approximation and not the fast RyR2 opening approximation in order to obtain information from the nullcline analysis. To this end, we have performed simulations of Eqs (8.11)-(8.12) at different values of the total calcium concentration $\bar{c}_T$ (Fig. 8.14) and test that we find the same basic behavior: at low values of $\bar{c}_T$ the system remains in a low concentration steady state (Fig. 8.15), but oscillations appear for a range of $\bar{c}_T$, up to a limit where an upper state becomes stable.

More importantly, the basic structure of the nullclines determines the possible solutions and again, oscillations appear when pinch-off is produced (Fig. 8.14). The fixed points in this case are the same as in Fig. 8.7, since they correspond to fixed points of Eqs. (8.2)-(8.4). However, different slaving conditions may change the stability of the fixed points, that now are analyzed in the plane (c_{sr}, P_o). Similarly to what we found in the previous analysis, calculating the stability, we find that the intermediate state is always unstable while the upper branch is stable above certain value of $\bar{c}_T$. Both states appear at around $\bar{c}_T \approx 54\mu$M, indicating the robustness of our analysis.

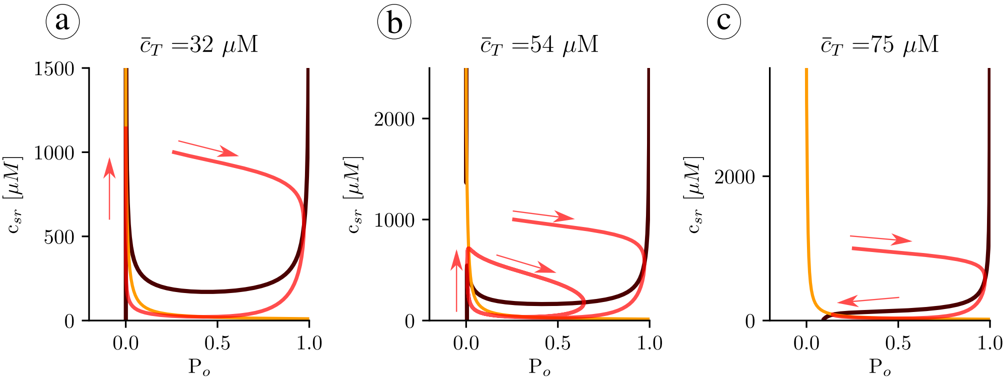

FIGURE 8.15: **Structure of the nullclines at different values of $\bar{c}_T$ indicated in the title of each panel.** The black line indicates the nullcline $\dot{P}_o = 0$, while the orange line corresponds to $\dot{c}_{sr} = 0$. The red curve is a trajectory with a direction indicated with the red arrows.

Stochastic effects. In real systems, the opening and closing of the RyR2 channels presents intrinsic stochastic dynamics. This is also the case in the full subcellular model. When considering average variables overall the cell, most of this stochasticity is averaged out. However, even if small, stochastic effects may play an important role [7] and, in particular, affect the properties of oscillations [149, 65]. We have thus studied these effects by including stochasticity in the minimal model

(8.8)-(8.9), adding to the open probability (P_o) a small random fluctuation, such that:

$$P_o = \frac{c_d^2}{K_o^2 + c_d^2} + \sigma(U - 0.5) \tag{8.28}$$

where σ is the strength of the noise and U is a random number between 0 and 1. The magnitude of σ has been adjusted to be much smaller than P_o when the system is in the open state or oscillates but large enough to be able to affect the dynamics close to the homoclinic bifurcation. In Fig. 8.16a the calcium traces for both domain (cytosol and SR) are plotted. For high values of the load, the system oscillates in the same way as in the deterministic limit ($\bar{c}_T = 54\mu M$). In the deterministic model, the homoclinic bifurcation appears at $\bar{c}_T \simeq 50\mu M$, so it is reasonable to expect the same behavior for loads above this threshold. Below it, the oscillations in the stochastic system persist and the period increases as the load is decreased, as is typical for homoclinic bifurcations in the presence of noise [225]. For low values of $\bar{c}_T$ ($\bar{c}_T = 35\mu M$) the period has changed an order of magnitude ($\sim$ 1s) and now the calcium traces resemble closer those observed in the subcellular model, or in experiments [260]. The dependence of the period on the total load is shown in Fig. 8.16b.

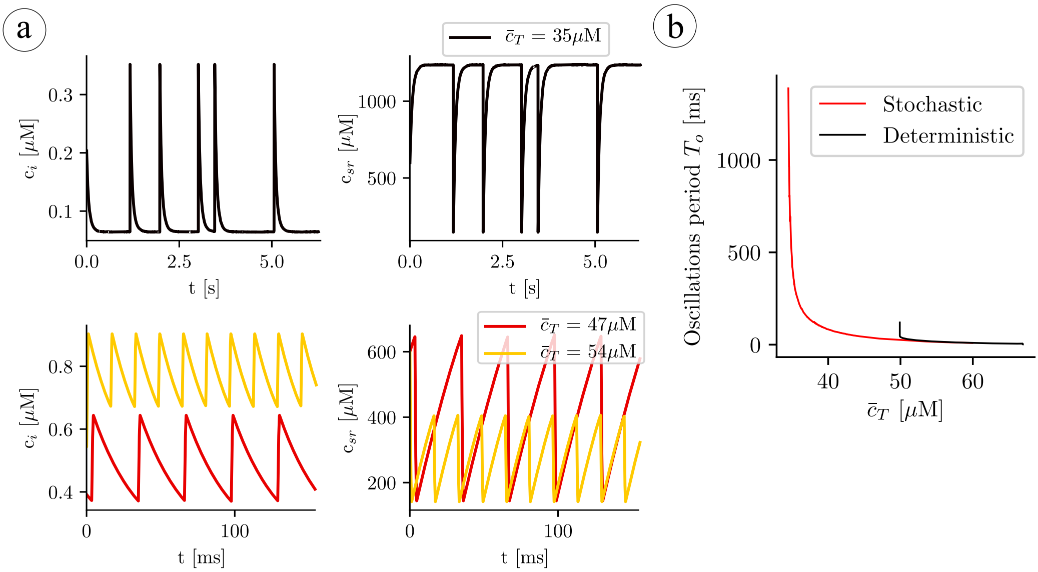

FIGURE 8.16: **Stochastic effects on the minimal model.** a) Traces of the cytosol and SR calcium concentrations for three different values of total calcium concentration $\bar{c}_T$. b) Oscillation periods as a function of $\bar{c}_T$. The strength of the noise is $\sigma = 2 \cdot 10^{-3}$.

8.3 Discussion

Calcium oscillations play an important role in cardiac cells, from the regulation of growth in human cardiac progenitor cells [77], to the control of the pacemaker rhythm in both early embryonic heart cells [286, 226] and in sinoatrial nodal pacemaker cells (SANCs) [151, 289, 288]. Calcium oscillations have been observed under conditions of high cytosolic calcium concentration [260] or SR calcium overload. High levels of cytosolic calcium affect the opening probability of the RyR2, which may result in oscillations or in a permanently open state [260, 223]. Calcium overload can be obtained, for instance, by inhibition of the Na^+-K^+ pump current I_{NaK}, that results in $[Na^+]_i$ overload. The consequent build-up of $[Na^+]_i$ reduces the effectiveness of the Na^+-Ca^{2+} exchanger at removing calcium from the cell and intracellular calcium concentrations become elevated. A similar effect is observed in models of hypercalcemia [6]. The effect of elevated $[Na^+]_i$ has been studied in computational models, finding calcium oscillations [282], that, depending on the model, appear via a supercritical Hopf [283] or a homoclinic bifurcation [303, 19].

The instability of the diastolic resting state is thus well-known [278, 108, 240] and it plays an important role in the initiation of various cardiac arrhythmias [241]. However, the precise mechanistic relationship between Ca^{2+} and dangerous AP repolarization is still not well understood. One possibility that has been suggested in previous studies is that Ca cycling induces voltage deflections during the AP which can induce a substrate for wave break and reentry [297]. These voltage deflections are referred to as early-after-depolarizations (EADs), which can be caused by a variety of mechanisms, such as reactivation of the L-type Ca current during AP repolarization. Our results in this chapter suggest an alternative possibility that EADs may be caused by Ca^{2+} oscillations that are regulated by Ca^{2+} buffers such as CSQ. In this picture, oscillations of the RyR2-CSQ can perturb the AP via voltage sensitive currents such as the L-type Ca^{2+} current and sodium-calcium exchange. This suggests that crucial properties of EADs such as their amplitude and oscillation frequency may be determined by the Ca^{2+} cycling system. This picture is consistent with several studies in the literature showing that mutations in CSQ cause abnormal Ca^{2+} cycling rhythms that are directly linked to sudden cardiac death [287, 269]. Our study raises the possibility that Ca^{2+} cycling oscillations may be a crucial component to understand these arrhythmias. This viewpoint has not been explored in the literature and may be crucial to future therapeutic approaches to control or eliminate the presence of EADs.

We have shown, using a full subcellular model, that under global calcium overload, SR oscillations appear, leading finally to a state with permanently open RyR2 and depleted SR. In these simulations, oscillations give rise to periodic calcium waves, that propagate along the myocyte. To obtain a better understanding on the origin and parameter dependence of these transitions, we have studied them in a simplified model of the calcium dynamics. Despite not including all the physiological details (or because of that), minimal models are often useful to gain a better understanding of the origin of complex calcium rhythms [39], as oscillations [245].

We have thus analyzed the different transitions within a minimal model, that takes into account the RyR2 dynamics, as well as fluxes among different compartments. This allows us to explain the origin of oscillations using a nullcline analysis, as well as to give analytic expressions for the different transitions. A key conclusion is that all buffers can affect heavily the dynamics. One interesting conclusion is that buffers affect heavily the dynamics. The effect of buffers on oscillations has been studied previously [292], and experimentally a change in CSQ levels has been observed to alter the range of values of cytosolic calcium at which oscillations are observed [260]. Here we find that an increase in the levels of CSQ prevents altogether the oscillations, obtaining a direct transition to an open state, that also occurs at larger values of total calcium content. We have shown that this picture is robust and independent on which is faster, whether the opening of the RyR2 or the diffusion of calcium near it. Although in this paper we have focused on the effect of CSQ, an interesting extension of this work would be to study in more detail the effect of changes in cytosolic buffer dynamics, allowing, for instance, for mobile buffers. This would require to modify the minimal model to account for diffusion of the buffer to nearby calcium release units, and we defer it for future work.

The fact that oscillations appear both in a fully detailed stochastic model and in a simple deterministic model seems another proof of the robustness of the behavior. Our results with noise added to the minimal model seem to suggest that allowing the RyR2s to behave stochastically could actually increase the parameter region where oscillations appear. This effect has been observed previously, where some amount of noise coming from the stochasticity of the ion channels may sustain oscillations by the process of coherence resonance [230, 156]. Thus, contrary to the results from the deterministic minimal model, where there is a sudden decrease in basal SR calcium load at the onset of oscillation, the addition of noise provides a gradual transition from the resting state to the oscillatory regime. This would agree with the results obtained by Stevens et al [260], where oscillations appeared gradually as cytosolic calcium content was increased, together with a continuous decrease in the level of basal SR. The addition of noise also gives a longer oscillation period, as observed in the subcellular model or in experiments. Even with this limitation, the analysis of the deterministic minimal model is still useful since it determines the minimal period of oscillation and the possibility of having periodic calcium waves. In a cell, when each calcium release unit presents or is very close to the onset of oscillations, periodic calcium waves appear. Under these circumstances, all units have a tendency to fire periodically, with noise making some units have a slightly early release. Diffusion of calcium to neighbors triggers the release of other units that were already close to open again. Waves are thus the coordinating mechanism of the oscillatory substrate of each unit.

Contrary to other scenarios studied for the onset of calcium waves [278], in our case, the rest state is not unstable, but rather it coexists with the oscillatory state, although, as discussed above, small fluctuations may favor the latter. Oscillations appear when the SR Ca^{2+} flux through the RyR2s becomes large, either because of a large luminal calcium load or to sensitization of the RyR2 due to an increase in diastolic calcium. These conditions can be met from a lack of CSQ, under an increase in global cell calcium content, or upon phosphorylation of the RyR2, for instance. Under these circumstances, there is a strong release flux from the SR that results in SR depletion. As the SR is refilled, the SR release flux again increases, resulting in periodic oscillations. Although RyR2 inactivation is present in the subcellular model, in our simulations release refractoriness is due mostly to SR depletion, and its recovery is dictated by the slow refilling of the SR since this time scale is slower than the RyR2s recovery from inactivation. Thus, the latter modulates the conditions of oscillations but does not determine them. We cannot discard, however, that under conditions of fast SR refilling, RyR2 refractoriness could not become the determining factor of the oscillations. This is reminiscent of the situation observed in calcium alternans, where both a slow refilling of the SR and RyR2 inactivation have been deemed as possible mechanisms for the onset of that rhythm [67, 5].

Finally, in this chapter, we consider a cell which has achieved calcium balance where intrusion and extrusion match, and have neglected calcium fluxes across the cell membrane to focus on the internal calcium dynamics in order to decouple both processes. Under normal pacing, extracellular calcium fluxes typically represent about 10-20% of the total calcium fluxes, so it is not unreasonable to consider that the total calcium content remains constant once at a steady state. Under these conditions, cytosolic and SR calcium concentrations are not independent but linked, and a clear control parameter is the total calcium concentration. Here we show that it uniquely determines the state of the system. Of course, in the presence of transmembrane fluxes, calcium oscillations or waves, or a permanently open RyR2, would result in an extrusion of calcium out of the cell and an eventual decrease in the total calcium load of the cell, that would transition back to the quiescent state (in the absence of external pacing). It seems interesting to study in the future the effect of oscillations and waves in the action potential, as well as a paced cell at different periods and the interaction with the pacing period. Observing how the time scale related to oscillations interacts with the time scale needed to extrude the calcium in the cytosol if the open (upper state) is reached may lead to new interesting phenomena.

Part IV

Conclusions

Chapter 9

General conclusions

The heart is a complex multi-scale dynamical system crucial for the life. A synchronized behavior at all the spatio-temporal scales is needed to properly pump blood throughout the body. Although contraction is the main action carried out by this organ, some of its properties (and dysfunctions) can be already studied at rest conditions. With regard to calcium handling, this would be the case of spark morphology. In this Thesis I have explored a variety of calcium phenomena, all of them arising from the collective activation of the RyR2s, by means of a detailed subcellular model at the submicron scale. I have studied the effect of size and distribution of CaRUs regarding the local calcium activity. In this sense, I have developed a methodology to generate realistic CaRUs distribution based on experimental data. We have also examined the effects of CSQ and phosphorylation on the RyR2 dynamics. Their role as RyR2-modulators is essential to understand the physiology of AF. Furthermore, I have studied the consequences of detubulation in atrial cells, a structural change observed during AF and HF. Finally, we have mathematically explored the onset of calcium oscillations in atrial cells using both the full subcellular model and a toy model that allows us to do nullcline analysis of the problem.

The development of this Thesis has been a lengthy (and sometimes bumpy) road, that has allowed me to comprehend the stochastic nature of the subcellular calcium dynamics. In the beginnings, I started simulating paced cells to validate the model. We obtained physiological global calcium traces and we were able to reproduce the local heterogeneities due to the lack of t-tubules in atrial cells [117, 109]. The publication of the model in a scientific peer reviewed journal was done in the second year of the PhD after several months of thoroughly checks and testings [180]. This initial phase of the Thesis where we developed the model was the most laborious given the technical complexity of the model which, moreover, has a high computational cost. For that reason, I needed to optimize all the processes and subroutines. Simultaneously, during those months, I had tones of papers about cardiac dynamics to read and understand. The next question that naturally arose was: what happens if we include t-tubules in the simulations? Actually it was an interesting issue since many scientific studies claimed that t-tubules are not only present in ventricle cells but they may also be present in atrial cells, with a lower density [62, 244, 220]. In this respect, we modified the atrial model to include a variable density of t-tubules. Our results showed the significance of the t-tubular structure regarding the synchronization of the calcium signal. Besides, we studied the SERCA reduction during detubulation and the effects of axial tubules in paced cells. Both effects have been experimentally observed [79, 87, 61]. We proved that axial tubules are crucial during centripal wave propagation in paced cells. The synchronization between LCCs and RyR2s during stimulation is needed to achieve the cellular contraction. The high resolution of the model have allowed us to quantify this synchronization by means of opening times of the RyR2s [181]. With this second paper we published the first series of results regarding the structure of t-tubules. The application of the model to understand real situations was a motivating feeling to continue exploring the subcellular world of the cardiac dynamics. Based on the results about RyR2 synchronization, we felt the need to gain knowledge about interaction among RyR2s. It was at that time when we had long meetings to study the local dynamics of the RyR2s.

The existence of spontaneous global calcium oscillations under resting conditions is one of the main behaviors observed experimentally. In order to investigate the onset of these oscillations we developed a minimal model of CaRU where only the main calcium currents are present. The characterization of the calcium oscillations based on the nullclines and fixed points analysis allowed us to understand the role of the calcium load and, specifically, how the lack of calsequestrin enhances the appearance of these oscillations. Moreover, the addition of stochasticity to the minimal model allows the system to oscillate at physiological frequencies, a fact that underlies the relevance of the stochastic behavior of the RyR2s. The results found in the simplified model were also observed in the full subcellular model.

To follow the investigations on the local RyR2 dynamics, we studied the spatial organization of the RyR2s. Certainly, the scientific knowledge about the RyR2 distribution was unclear and contradictory, as it is shown in Fig. 5.4. However, we wanted to quantify the subcellular dynamics for several RyR2 distributions. In this regard, we developed a novel methodology to generate heterogeneous assemblies of RyR2s. In particular, we followed [175, 262] to assume a bimodal (Gaussian & Exponential) distribution. This extension of the model allowed us to generate more realistic RyR2 assemblies. The comparison between the homogeneous and the heterogeneous configuration shows us that, under normal conditions, not relevant differences are observed regarding the spark features. However, there exists a 6-fold increase in the probability of macrosparks in the heterogeneous distribution. Given the role played by macrosparks in the generation of abnormal cardiac rhythms, the natural continuation of this work would be in the line of simulating both configurations under pathophysiological conditions (increase of the SR load and increase of the open probability of the RyR2). Beyond the quantitative results, the spark characterization in terms of the number of opened RyR2s has allowed us to correlate this magnitude with the main characteristics of the sparks. Up to now, this analysis has never been done in real cells. This section about heterogeneous distributions of CaRUs has been finished in the final stage of the PhD and because of that it has not yet been published. However, in the near future we have in mind to write a paper explaining the work done in this line.

The study on RyR2-modulators led us to collaborate with Dr. Leif Hove-Madsen, from the Biomedical Research Institute Barcelona IIBB-CSIC, ar Hospital de Sant Pau, in order to go in depth in our analysis on the local RyR2 dynamics. Based on our meetings, we developed together the main findings of chapter 6 that will be partially published on [268]. In this work at Dr. Leif Hove-Madsen group, they analyzed the spatial distribution of CSQ and the degree of the RyR2 phosphorylation in real cells. It was proven that the heterogeneous distribution of both magnitudes utterly determines the frequency and distribution of calcium sparks in patients with and without AF. We included the dynamics of these magnitudes in our model following previous results [153]. With this, we simulated two type of cells depending on the levels of CSQ and RyR2-phosphorylation, which represented cells with and without AF, corresponding to the experimental findings. With our work, we proposed the mechanisms underlying the RyR2 over-activity during episodes of AF. Moreover, we have been able to quantify the spark features, reproducing the experimental results. The development of this part was laborious given that we had to adjust the model not to the general knowledge about sparks but to the specific experiment that we have referred to. In spite of that, we were able to reproduce the experimental findings by adding to the model another dimension of analysis. It was therefore worth the effort.

Chapter 10

Perspectives

In this Thesis I have analyzed different spatio-temporal patterns arising from several calcium pathways. In this way, I have studied the calcium patterns due to fire and diffusion mechanism, the leading process when a cell is paced. I have also shown the local calcium dynamics in the cell at rest conditions and how the cooperativity between clusters promotes the appearance of calcium sparks. These results provide the basis for further research work.

We have learned that the RyR2 assembly is an important structural property that determines the local calcium dynamics. In chapter 5 I have characterized different properties of the CaRU distributions such as the longitudinal dispersion through the z-lines or the assembly of RyR2s in bigger CaRUs (from 36 to 54 RyR2s). Moreover, we have studied the spark characteristics of a heterogeneous distribution of RyR2s. Futures studies will be devoted to understand the effect of other distributions that have already been observed experimentally and we have outlined in Fig. 5.4. Furthermore, the appearance of intracellular calcium waves is a widely effect studied both experimentally [204, 193, 261, 263] and computationally [40, 123, 140]. Thus, a future line of work that will follow the current Thesis would be the characterization of spontaneous calcium waves in terms of the subcellular assembly of RyR2s. We should include in that work the analysis of the different pathophysiological conditions such as the calcium overload or the increase on the open probability of the RyR2s.

In collaboration with the authors who first revealed the spatial distribution of calcium sparks during AF (Hove-Madsen et al.) [268], we have developed a mathematical description to simulate the experimental results. This description is based around two principles: the heterogeneous distribution of CSQ and RyR2-phosphorylation through the cell. In the coming years, the experimental findings will broaden the knowledge on the subcellular cell properties and our model will be a suitable tool for analyzing and predicting. Moreover, other chemical compounds have been reported to modulate RyR2 activity and, in turn, the appearance of pro-arrhythmic situations. These species are peroxides (H_2O_2), superoxides (O_2^-) or hydroxil radicals ($^{\cdot}OH$) among others, and are often referred together as reactive oxygen species (ROS) and they are mainly generated by mitochondria [195]. ROS are known to tune cardiac functioning under healthy conditions, but under pathophysiological conditions their effects may divert and promote the rise of arrhythmogenic behavior. In particular, ROS and other reactive nitrogen species react with cysteine residues on RyR2 to rapidly and reversibly modulate RyR2 Ca^{2+} sensitivity. As a result, an increase of SR Ca^{2+} leak is produced leading to alterations of the cytosolic Ca^{2+}.

The measurement of calcium sparks during experiments is subject to the resolution of the confocal microscopy. Although great enhancements have been done in this field, up to now, the noise produced by the photomultiplier hides many small calcium events. It is thought that these short sparks produce a passive calcium leak through the RyR2 [235], however the magnitude of this current is still unclear. To address this issue, the model can be used to give a quantification of this passive calcium leak in terms of the SR load.

Finally, the model can be used to test the effect of new drugs and gene mutations or genetic variants. The high resolution of the model would allow us to properly incorporate the dynamics of new chemical compounds. In silico experiments are the fastest and cheapest way to make the first approach to the testing of new drugs.

Bibliography

[1] II Abubakar, T Tillmann, and A Banerjee. “Global, regional, and national age-sex specific all-cause and cause-specific mortality for 240 causes of death, 1990-2013: a systematic analysis for the Global Burden of Disease Study 2013”. In: *Lancet* 385.9963 (2015), pp. 117–171.

[2] Amanda M Alexander et al. “Spontaneous calcium release in cardiac myocytes: Store overload and electrical dynamics”. In: *Spora: A Journal of Biomathematics* 1.1 (2015), p. 6.

[3] Maurits A Allessie, Felix IM Bonke, and Francien JG Schopman. “Circus movement in rabbit atrial muscle as a mechanism of tachycardia”. In: *Circulation research* 33.1 (1973), pp. 54–62.

[4] Sergio Alonso, Markus Bär, and Blas Echebarria. “Nonlinear physics of electrical wave propagation in the heart: a review”. In: *Reports on Progress in Physics* 79.9 (2016), p. 096601.

[5] Enric Alvarez-Lacalle et al. “Dependency of calcium alternans on ryanodine receptor refractoriness”. In: *PloS one* 8.2 (2013), e55042.

[6] Enric Alvarez-Lacalle et al. “Effect of RyR2 refractoriness and hypercalcemia on calcium overload, spontaneous release, and calcium alternans”. In: *Computing in Cardiology 2013*. IEEE. 2013, pp. 683–686.

[7] Enrique Alvarez-Lacalle et al. “Calcium alternans is due to an order-disorder phase transition in cardiac cells”. In: *Physical review letters* 114.10 (2015), p. 108101.

[8] Doron Aronson et al. “Risk score for prediction of 10-year atrial fibrillation: a community-based study”. In: *Thrombosis and haemostasis* 118.09 (2018), pp. 1556–1563.

[9] Rishi Arora et al. “Regional distribution of T-tubule density in left and right atria in dogs”. In: *Heart Rhythm* 14.2 (2017), pp. 273–281.

[10] Johann Auer et al. “Subclinical hyperthyroidism as a risk factor for atrial fibrillation”. In: *American heart journal* 142.5 (2001), pp. 838–842.

[11] David Baddeley et al. “Optical single-channel resolution imaging of the ryanodine receptor distribution in rat cardiac myocytes”. In: *Proceedings of the National Academy of Sciences* 106.52 (2009), pp. 22275–22280.

[12] Hilmar Bading, David D Ginty, and Michael E Greenberg. “Regulation of gene expression in hippocampal neurons by distinct calcium signaling pathways”. In: *SCIENCE-NEW YORK THEN WASHINGTON-* 260 (1993), pp. 181–181.

[13] Laura Barcenas-Ruiz and W Gil Wier. “Voltage dependence of intracellular [Ca2+] i transients in guinea pig ventricular myocytes.” In: *Circulation research* 61.1 (1987), pp. 148–154.

[14] NA Beard, Derek Rowland Laver, and Angela F Dulhunty. “Calsequestrin and the calcium release channel of skeletal and cardiac muscle”. In: *Progress in biophysics and molecular biology* 85.1 (2004), pp. 33–69.

[15] Nicole A Beard et al. “Calsequestrin is an inhibitor of skeletal muscle ryanodine receptor calcium release channels”. In: *Biophysical journal* 82.1 (2002), pp. 310–320.

[16] Nicole A Beard et al. “Regulation of ryanodine receptors by calsequestrin: effect of high luminal Ca2+ and phosphorylation”. In: *Biophysical journal* 88.5 (2005), pp. 3444–3454.

[17] Go W Beeler and H Reuter. “Reconstruction of the action potential of ventricular myocardial fibres”. In: *The Journal of physiology* 268.1 (1977), pp. 177–210.

[18] Raul Benítez, Enrique Álvarez, and Leif Hove-Madsen. “Method for detecting local events of intracellular calcium release”. In: (2010).

[19] Alan P Benson and Arun V Holden. “Calcium oscillations and ectopic beats in virtual ventricular myocytes and tissues: bifurcations, autorhythmicity and propagation”. In: *International Workshop on Functional Imaging and Modeling of the Heart*. Springer. 2005, pp. 304–313.

[20] JOSHUA R Berlin. “Spatiotemporal changes of Ca2+ during electrically evoked contractions in atrial and ventricular cells”. In: *American Journal of Physiology-Heart and Circulatory Physiology* 269.3 (1995), H1165–H1170.

[21] Joshua R Berlin, JW Bassani, and Donald M Bers. “Intrinsic cytosolic calcium buffering properties of single rat cardiac myocytes”. In: *Biophysical journal* 67.4 (1994), pp. 1775–1787.

[22] M J Berridge. “Inositol triphosphate and calcium signalling”. In: *Cell* 361.2 (1993), pp. 315–325.

[23] Michael J Berridge. “Elementary and global aspects of calcium signalling.” In: *The Journal of physiology* 499.2 (1997), pp. 291–306.

[24] MJ Berridge. *Cardiac calcium signalling.* 2003.

[25] Donald M Bers. “Calcium cycling and signaling in cardiac myocytes”. In: *Annu. Rev. Physiol.* 70 (2008), pp. 23–49.

[26] Donald M Bers. “Cardiac excitation–contraction coupling”. In: *Nature* 415.6868 (2002), p. 198.

[27] Donald M Bers and Thomas R Shannon. “Calcium movements inside the sarcoplasmic reticulum of cardiac myocytes”. In: *Journal of molecular and cellular cardiology* 58 (2013), pp. 59–66.

[28] John L Bixby and William A Harris. “Molecular mechanisms of axon growth and guidance”. In: *Annual review of cell biology* 7.1 (1991), pp. 117–159.

[29] Vladimir E Bondarenko, Glenna CL Bett, and Randall L Rasmusson. “A model of graded calcium release and L-type Ca2+ channel inactivation in cardiac muscle”. In: *American Journal of Physiology-Heart and Circulatory Physiology* 286.3 (2004), H1154–H1169.

[30] Martin D Bootman et al. “Atrial cardiomyocyte calcium signalling”. In: *Biochimica et Biophysica Acta (BBA)-Molecular Cell Research* 1813.5 (2011), pp. 922–934.

[31] Martin D Bootman et al. “Calcium signalling during excitation-contraction coupling in mammalian atrial myocytes”. In: *Journal of cell science* 119.19 (2006), pp. 3915–3925.

[32] Sören Brandenburg et al. “Axial tubule junctions activate atrial Ca2+ release across species”. In: *Frontiers in Physiology* 9 (2018), p. 1227.

[33] Sören Brandenburg et al. “Axial tubule junctions control rapid calcium signaling in atria”. In: *The Journal of clinical investigation* 126.10 (2016), p. 3999.

[34] Fabien Brette, Kimiaki Komukai, and Clive H Orchard. “Validation of formamide as a detubulation agent in isolated rat cardiac cells”. In: *American Journal of Physiology-Heart and Circulatory Physiology* 283.4 (2002), H1720–H1728.

[35] Fabien Brette et al. “Spatiotemporal characteristics of SR Ca2+ uptake and release in detubulated rat ventricular myocytes”. In: *Journal of molecular and cellular cardiology* 39.5 (2005), pp. 804–812.

[36] Didier XP Brochet et al. “Quarky calcium release in the heart”. In: *Circulation research* 108.2 (2011), pp. 210–218.

[37] Jessica L Caldwell et al. “Dependence of cardiac transverse tubules on the BAR domain protein amphiphysin II (BIN-1)”. In: *Circulation research* 115.12 (2014), pp. 986–996.

[38] MB Cannell and DG Allen. “Model of calcium movements during activation in the sarcomere of frog skeletal muscle”. In: *Biophysical Journal* 45.5 (1984), pp. 913–925.

[39] Inma R Cantalapiedra et al. “Minimal model for calcium alternans due to SR release refractoriness”. In: *Chaos: An Interdisciplinary Journal of Nonlinear Science* 27.9 (2017), p. 093928.

[40] Wei Chen et al. “A mathematical model of spontaneous calcium release in cardiac myocytes”. In: *American Journal of Physiology-Heart and Circulatory Physiology* 300.5 (2011), H1794–H1805.

[41] Ye Chen-Izu et al. “Three-dimensional distribution of ryanodine receptor clusters in cardiac myocytes”. In: *Biophysical journal* 91.1 (2006), pp. 1–13.

[42] H Cheng et al. “Calcium sparks and [Ca2+] i waves in cardiac myocytes”. In: *American Journal of Physiology-Cell Physiology* 270.1 (1996), pp. C148–C159.

[43] Heping Cheng, WJ Lederer, and Mark B Cannell. “Calcium sparks: elementary events underlying excitation-contraction coupling in heart muscle”. In: *Science* 262.5134 (1993), pp. 740–744.

[44] Heping Cheng, WJ Lederer, and Mark B Cannell. “Calcium sparks: elementary events underlying excitation-contraction coupling in heart muscle”. PhD thesis. University of Maryland, 1994.

[45] Elizabeth M Cherry and Steven J Evans. “Properties of two human atrial cell models in tissue: restitution, memory, propagation, and reentry”. In: *Journal of theoretical biology* 254.3 (2008), pp. 674–690.

[46] Elizabeth M Cherry, Harold M Hastings, and Steven J Evans. “Dynamics of human atrial cell models: restitution, memory, and intracellular calcium dynamics in single cells”. In: *Progress in biophysics and molecular biology* 98.1 (2008), pp. 24–37.

[47] Li Lien Ching, Alan J Williams, and Rebecca Sitsapesan. “Evidence for Ca2+ activation and inactivation sites on the luminal side of the cardiac ryanodine receptor complex”. In: *Circulation research* 87.3 (2000), pp. 201–206.

[48] Nagesh Chopra et al. “Modest reductions of cardiac calsequestrin increase sarcoplasmic reticulum Ca2+ leak independent of luminal Ca2+ and trigger ventricular arrhythmias in mice”. In: *Circulation research* 101.6 (2007), pp. 617–626.

[49] David E Clapham. “Calcium signalling”. In: *Cell* 80.2 (1995), pp. 259–268.

[50] Michael A Colman. “Arrhythmia mechanisms and spontaneous calcium release: Bi-directional coupling between re-entrant and focal excitation”. In: *PLoS computational biology* 15.8 (2019).

[51] Michael A Colman et al. “A computational model of spatio-temporal cardiac intracellular calcium handling with realistic structure and spatial flux distribution from sarcoplasmic reticulum and t-tubule reconstructions”. In: *PLoS computational biology* 13.8 (2017), e1005714.

[52] Michael A Colman et al. “A new model of the human atrial myocyte with variable T-tubule organization for the study of atrial fibrillation”. In: *2016 Computing in Cardiology Conference (CinC)*. IEEE. 2016, pp. 221–224.

[53] David Colquhoun and FJ Sigworth. "Single-channel recording". In: (1995).

[54] Marc Courtemanche, Rafael J Ramirez, and Stanley Nattel. "Ionic mechanisms underlying human atrial action potential properties: insights from a mathematical model". In: *American Journal of Physiology-Heart and Circulatory Physiology* 275.1 (1998), H301–H321.

[55] Tapaswini Das and Masahiko Hoshijima. "Adding a new dimension to cardiac nano-architecture using electron microscopy: coupling membrane excitation to calcium signaling". In: *Journal of molecular and cellular cardiology* 58 (2013), pp. 5–12.

[56] Jorge M Davidenko et al. "Stationary and drifting spiral waves of excitation in isolated cardiac muscle". In: *Nature* 355.6358 (1992), p. 349.

[57] Semahat S Demir et al. "A mathematical model of a rabbit sinoatrial node cell". In: *American Journal of Physiology-Cell Physiology* 266.3 (1994), pp. C832–C852.

[58] Dario Di Francesco and Denis Noble. "A model of cardiac electrical activity incorporating ionic pumps and concentration changes". In: *Philosophical Transactions of the Royal Society of London. B, Biological Sciences* 307.1133 (1985), pp. 353–398.

[59] Mary E Díaz, Stephen C O'neill, and David A Eisner. "Sarcoplasmic reticulum calcium content fluctuation is the key to cardiac alternans". In: *Circulation research* 94.5 (2004), pp. 650–656.

[60] ME Diaz, AW Trafford, and DA Eisner. "The role of intracellular Ca buffers in determining the shape of the systolic Ca transient in cardiac ventricular myocytes". In: *Pflügers Archiv* 442.1 (2001), pp. 96–100.

[61] Katharine M Dibb et al. "A functional role for transverse (t-) tubules in the atria". In: *Journal of molecular and cellular cardiology* 58 (2013), pp. 84–91.

[62] Katharine M Dibb et al. "Characterization of an extensive transverse tubular network in sheep atrial myocytes and its depletion in heart failure". In: *Circulation: Heart Failure* 2.5 (2009), pp. 482–489.

[63] Wessel P Dirksen et al. "A mutation in calsequestrin, CASQ2D307H, impairs Sarcoplasmic Reticulum Ca2+ handling and causes complex ventricular arrhythmias in mice". In: *Cardiovascular research* 75.1 (2007), pp. 69–78.

[64] Paulina Donoso, Humberto Prieto, and Cecilia Hidalgo. "Luminal calcium regulates calcium release in triads isolated from frog and rabbit skeletal muscle". In: *Biophysical journal* 68.2 (1995), pp. 507–515.

[65] Geneviève Dupont and Huguette Croisier. "Spatiotemporal organization of Ca2+ dynamics: A modeling-based approach". In: *HFSP journal* 4.2 (2010), pp. 43–51.

[66] Geneviève Dupont et al. "Calcium oscillations". In: *Cold Spring Harbor perspectives in biology* 3.3 (2011), a004226.

[67] Blas Echebarria et al. “Mechanisms Underlying Electro-Mechanical Cardiac Alternans”. In: *Nonlinear Dynamics in Biological Systems.* Springer, 2016, pp. 113–128.

[68] David W Ehrhardt, Rebecca Wais, and Sharon R Long. “Calcium spiking in plant root hairs responding to Rhizobium nodulation signals”. In: *Cell* 85.5 (1996), pp. 673–681.

[69] B Ermentrout. “Simulating, analyzing, and animating dynamical systems: a guide to XPPAUT for researchers and students. 2002”. In: *Philadelphia: SIAM* ().

[70] Ariel L Escobar et al. “Kinetic properties of DM-nitrophen and calcium indicators: rapid transient response to flash photolysis”. In: *Pflügers Archiv* 434.5 (1997), pp. 615–631.

[71] Developed with the special contribution of the European Heart Rhythm Association (EHRA) et al. “Guidelines for the management of atrial fibrillation: the Task Force for the Management of Atrial Fibrillation of the European Society of Cardiology (ESC)”. In: *European heart journal* 31.19 (2010), pp. 2369–2429.

[72] Gregory M Faber and Yoram Rudy. “Calsequestrin mutation and catecholaminergic polymorphic ventricular tachycardia: a simulation study of cellular mechanism”. In: *Cardiovascular research* 75.1 (2007), pp. 79–88.

[73] Alexandre Fabiato. “Calcium-induced release of calcium from the cardiac sarcoplasmic reticulum”. In: *American Journal of Physiology-Cell Physiology* 245.1 (1983), pp. C1–C14.

[74] Alexandre Fabiato and Franfoise Fabiato. “Calcium and cardiac excitation-contraction coupling”. In: *Annual Review of Physiology* 41.1 (1979), pp. 473–484.

[75] Martin Falcke. “On the role of stochastic channel behavior in intracellular Ca 2+ dynamics”. In: *Biophysical journal* 84.1 (2003), pp. 42–56.

[76] John L Farber. “The role of calcium in cell death”. In: *Life sciences* 29.13 (1981), pp. 1289–1295.

[77] Joäo Ferreira-Martins et al. “Spontaneous calcium oscillations regulate human cardiac progenitor cell growth”. In: *Circulation research* 105.8 (2009), pp. 764–774.

[78] LE Ford and RJ Podolsky. “Calcium uptake and force development by skinned muscle fibres in EGTA buffered solutions”. In: *The Journal of physiology* 223.1 (1972), p. 1.

[79] Konrad F Frank et al. “Modulation of SERCA: implications for the failing human heart”. In: *Basic research in cardiology* 97.1 (2002), pp. I72–I78.

[80] Clara Franzini-Armstrong, Linda J Kenney, and Elizabeth Varriano-Marston. "The structure of calsequestrin in triads of vertebrate skeletal muscle: a deep-etch study." In: *The Journal of cell biology* 105.1 (1987), pp. 49–56.

[81] Clara Franzini-Armstrong and Feliciano Protasi. "Ryanodine receptors of striated muscles: a complex channel capable of multiple interactions". In: *Physiological Reviews* 77.3 (1997), pp. 699–729.

[82] Clara Franzini-Armstrong, Feliciano Protasi, and Venkat Ramesh. "Shape, size, and distribution of Ca2+ release units and couplons in skeletal and cardiac muscles". In: *Biophysical journal* 77.3 (1999), pp. 1528–1539.

[83] Michael Frisk et al. "Variable t-tubule organization and Ca2+ homeostasis across the atria". In: *American Journal of Physiology-Heart and Circulatory Physiology* 307.4 (2014), H609–H620.

[84] Hanne C Gadeberg et al. "Heterogeneity of T-tubules in pig hearts". In: *PLoS One* 11.6 (2016), e0156862.

[85] Samuel Galice et al. "Size matters: Ryanodine receptor cluster size affects arrhythmogenic sarcoplasmic reticulum calcium release". In: *Journal of the American Heart Association* 7.13 (2018), e008724.

[86] Patricia Garcia-Canadilla et al. "Complex congenital heart disease associated with disordered myocardial architecture in a midtrimester human fetus". In: *Circulation: Cardiovascular Imaging* 11.10 (2018), e007753.

[87] Davide Gianni et al. "SERCA2a in heart failure: role and therapeutic prospects". In: *Journal of bioenergetics and biomembranes* 37.6 (2005), pp. 375–380.

[88] Daniel T Gillespie. "Exact stochastic simulation of coupled chemical reactions". In: *The journal of physical chemistry* 81.25 (1977), pp. 2340–2361.

[89] Edward Glasscock et al. "Expression and function of Kv1. 1 potassium channels in human atria from patients with atrial fibrillation". In: *Basic research in cardiology* 110.5 (2015), p. 47.

[90] Pranay Goel, James Sneyd, and Avner Friedman. "Homogenization of the cell cytoplasm: the calcium bidomain equations". In: *Multiscale Modeling & Simulation* 5.4 (2006), pp. 1045–1062.

[91] Ary L Goldberger et al. "PhysioBank, PhysioToolkit, and PhysioNet: components of a new research resource for complex physiologic signals". In: *circulation* 101.23 (2000), e215–e220.

[92] AM Gomez et al. "Defective excitation-contraction coupling in experimental cardiac hypertrophy and heart failure". In: *Science* 276.5313 (1997), pp. 800–806.

[93] AM Gomez et al. "Heart failure after myocardial infarction: altered excitation-contraction coupling". In: *Circulation* 104.6 (2001), pp. 688–693.

[94] Eleonora Grandi et al. "Human atrial action potential and Ca2+ model: sinus rhythm and chronic atrial fibrillation". In: *Circulation research* (2011), CIRCRESAHA–111.

[95] Michel Grouselle et al. "Digital-imaging microscopy analysis of calcium release from sarcoplasmic reticulum in single rat cardiac myocytes". In: *Pflügers Archiv* 418.1-2 (1991), pp. 109–119.

[96] Grzegorz Grynkiewicz, Martin Poenie, and Roger Y Tsien. "A new generation of Ca2+ indicators with greatly improved fluorescence properties." In: *Journal of biological chemistry* 260.6 (1985), pp. 3440–3450.

[97] Ang Guo and Long-Sheng Song. "AutoTT: automated detection and analysis of T-tubule architecture in cardiomyocytes". In: *Biophysical journal* 106.12 (2014), pp. 2729–2736.

[98] Ang Guo et al. "Emerging mechanisms of T-tubule remodelling in heart failure". In: *Cardiovascular research* 98.2 (2013), pp. 204–215.

[99] Inna Györke et al. "The role of calsequestrin, triadin, and junctin in conferring cardiac ryanodine receptor responsiveness to luminal calcium". In: *Biophysical journal* 86.4 (2004), pp. 2121–2128.

[100] S Gyorke et al. "Regulation of sarcoplasmic reticulum calcium release by luminal calcium in cardiac muscle". In: *Front Biosci* 7.1 (2002), pp. d1454–1463.

[101] Sandor Györke and Dmitry Terentyev. "Modulation of ryanodine receptor by luminal calcium and accessory proteins in health and cardiac disease". In: *Cardiovascular research* 77.2 (2007), pp. 245–255.

[102] Sandor Györke et al. "Chain-reaction Ca 2+ signaling in the heart". In: *The Journal of clinical investigation* 117.7 (2007), pp. 1758–1762.

[103] Jürgen Hain et al. "Phosphorylation modulates the function of the calcium release channel of sarcoplasmic reticulum from cardiac muscle". In: *Journal of Biological Chemistry* 270.5 (1995), pp. 2074–2081.

[104] Yasuhiro Hakamata et al. "Primary structure and distribution of a novel ryanodine receptor/calcium release channel from rabbit brain". In: *FEBS letters* 312.2-3 (1992), pp. 229–235.

[105] Jordi Heijman et al. "Function and regulation of serine/threonine phosphatases in the healthy and diseased heart". In: *Journal of molecular and cellular cardiology* 64 (2013), pp. 90–98.

[106] Frank R Heinzel et al. "Dyssynchrony of Ca2+ release from the sarcoplasmic reticulum as subcellular mechanism of cardiac contractile dysfunction". In: *Journal of molecular and cellular cardiology* 50.3 (2011), pp. 390–400.

[107] Stefan W Hell and Jan Wichmann. "Breaking the diffraction resolution limit by stimulated emission: stimulated-emission-depletion fluorescence microscopy". In: *Optics letters* 19.11 (1994), pp. 780–782.

[108] Gonzalo Hernandez-Hernandez, Enric Alvarez-Lacalle, and Yohannes Shiferaw. "Role of connectivity and fluctuations in the nucleation of calcium waves in cardiac cells". In: *Physical Review E* 92.5 (2015), p. 052715.

[109] Richard G Hibbs and Victor J Ferrans. "An ultrastructural and histochemical study of rat atrial myocardium". In: *American Journal of Anatomy* 124.3 (1969), pp. 251–279.

[110] DW Hilgemann and Denis Noble. "Excitation-contraction coupling and extracellular calcium transients in rabbit atrium: reconstruction of basic cellular mechanisms". In: *Proceedings of the Royal society of London. Series B. Biological sciences* 230.1259 (1987), pp. 163–205.

[111] Robert Hinch et al. "A simplified local control model of calcium-induced calcium release in cardiac ventricular myocytes". In: *Biophysical journal* 87.6 (2004), pp. 3723–3736.

[112] Allan L Hodgkin and Andrew F Huxley. "The components of membrane conductance in the giant axon of Loligo". In: *The Journal of physiology* 116.4 (1952), pp. 473–496.

[113] Gregory S Hoeker et al. "Spontaneous calcium release in tissue from the failing canine heart". In: *American Journal of Physiology-Heart and Circulatory Physiology* 297.4 (2009), H1235–H1242.

[114] Yufeng Hou et al. "Nanoscale analysis of ryanodine receptor clusters in dyadic couplings of rat cardiac myocytes". In: *Journal of molecular and cellular cardiology* 80 (2015), pp. 45–55.

[115] Leif Hove-Madsen et al. "Atrial fibrillation is associated with increased spontaneous calcium release from the sarcoplasmic reticulum in human atrial myocytes". In: *Circulation* 110.11 (2004), pp. 1358–1363.

[116] Heikki V Huikuri, Agustin Castellanos, and Robert J Myerburg. "Sudden death due to cardiac arrhythmias". In: *New England Journal of Medicine* 345.20 (2001), pp. 1473–1482.

[117] J Hüser, SL Lipsius, and LA Blatter. "Calcium gradients during excitation-contraction coupling in cat atrial myocytes." In: *The Journal of Physiology* 494.Pt 3 (1996), p. 641.

[118] Jörg Hüser et al. "Functional coupling between glycolysis and excitation—contraction coupling underlies alternans in cat heart cells". In: *The Journal of physiology* 524.3 (2000), pp. 795–806.

[119] Anna Huttenlocher et al. "Regulation of cell migration by the calcium-dependent protease calpain". In: *Journal of Biological Chemistry* 272.52 (1997), pp. 32719–32722.

[120] Michael Ibrahim et al. "Mechanical unloading reverses transverse tubule remodelling and normalizes local Ca2+-induced Ca2+ release in a rodent model of heart failure". In: *European journal of heart failure* 14.6 (2012), pp. 571–580.

[121] Ml Inui, Akitsugu Saito, and Sidney Fleischer. "Purification of the ryanodine receptor and identity with feet structures of junctional terminal cisternae of sarcoplasmic reticulum from fast skeletal muscle." In: *Journal of Biological Chemistry* 262.4 (1987), pp. 1740–1747.

[122] Vivek Iyer, Roger J Hajjar, and Antonis A Armoundas. "Mechanisms of abnormal calcium homeostasis in mutations responsible for catecholaminergic polymorphic ventricular tachycardia". In: *Circulation research* 100.2 (2007), e22–e31.

[123] Leighton T Izu, W Gil Wier, and C William Balke. "Evolution of cardiac calcium waves from stochastic calcium sparks". In: *Biophysical journal* 80.1 (2001), pp. 103–120.

[124] Leighton T Izu et al. "Ca2+ waves in the heart". In: *Journal of molecular and cellular cardiology* 58 (2013), pp. 118–124.

[125] Leighton T Izu et al. "Interplay of ryanodine receptor distribution and calcium dynamics". In: *Biophysical journal* 91.1 (2006), pp. 95–112.

[126] Vincent Jacquemet. "Steady-state solutions in mathematical models of atrial cell electrophysiology and their stability". In: *Mathematical biosciences* 208.1 (2007), pp. 241–269.

[127] M Saleet Jafri, J Jeremy Rice, and Raimond L Winslow. "Cardiac Ca2+ dynamics: the roles of ryanodine receptor adaptation and sarcoplasmic reticulum load". In: *Biophysical journal* 74.3 (1998), pp. 1149–1168.

[128] MS Jafri and J Keizer. "On the roles of Ca2+ diffusion, Ca2+ buffers, and the endoplasmic reticulum in IP3-induced Ca2+ waves". In: *Biophysical journal* 69.5 (1995), pp. 2139–2153.

[129] José Jalife. "Introduction to the Series on Computational Approaches to Cardiac Arrhythmias: Translation Into Diagnostics and Therapy". In: *Circulation research* 112.5 (2013), pp. 831–833.

[130] Isuru Jayasinghe et al. "True molecular scale visualization of variable clustering properties of ryanodine receptors". In: *Cell reports* 22.2 (2018), pp. 557–567.

[131] Larry R Jones et al. "Regulation of Ca2+ signaling in transgenic mouse cardiac myocytes overexpressing calsequestrin." In: *The Journal of clinical investigation* 101.7 (1998), pp. 1385–1393.

[132] Annelise O Jorgensen and Kevin P Campbell. "Evidence for the presence of calsequestrin in two structurally different regions of myocardial sarcoplasmic reticulum." In: *The Journal of cell biology* 98.4 (1984), pp. 1597–1602.

[133] Rodolphe P Katra and Kenneth R Laurita. "Cellular mechanism of calcium-mediated triggered activity in the heart". In: *Circulation research* 96.5 (2005), pp. 535–542.

[134] Rodolphe P Katra et al. “Ryanodine receptor dysfunction and triggered activity in the heart”. In: *American Journal of Physiology-Heart and Circulatory Physiology* 292.5 (2007), H2144–H2151.

[135] M Tognon Kaufman and B Roizman. “Calcium Mobilization and Exocyt osis After One”. In: *Virology* 172 (1989), p. 435.

[136] Makoto Kawai, Munir Hussain, and Clive H Orchard. “Excitation-contraction coupling in rat ventricular myocytes after formamide-induced detubulation”. In: *American Journal of Physiology-Heart and Circulatory Physiology* 277.2 (1999), H603–H609.

[137] James P Keener and James Sneyd. *Mathematical physiology*. Vol. 1. Springer, 1998.

[138] Joel Keizer and Gary W De Young. “Two roles of Ca2+ in agonist stimulated Ca2+ oscillations”. In: *Biophysical journal* 61.3 (1992), pp. 649–660.

[139] Joel Keizer and Leslie Levine. “Ryanodine receptor adaptation and Ca2+ (-) induced Ca2+ release-dependent Ca2+ oscillations”. In: *Biophysical journal* 71.6 (1996), pp. 3477–3487.

[140] Joel Keizer and Gregory D Smith. “Spark-to-wave transition: saltatory transmission of calcium waves in cardiac myocytes”. In: *Biophysical chemistry* 72.1-2 (1998), pp. 87–100.

[141] Malcolm M Kirk et al. “Role of the transverse-axial tubule system in generating calcium sparks and calcium transients in rat atrial myocytes”. In: *The Journal of physiology* 547.2 (2003), pp. 441–451.

[142] James Kneller et al. “Remodeling of Ca2+-handling by atrial tachycardia: evidence for a role in loss of rate-adaptation”. In: *Cardiovascular research* 54.2 (2002), pp. 416–426.

[143] Björn C Knollmann et al. “Casq2 deletion causes sarcoplasmic reticulum volume increase, premature Ca 2+ release, and catecholaminergic polymorphic ventricular tachycardia”. In: *The Journal of clinical investigation* 116.9 (2006), pp. 2510–2520.

[144] Jens Kockskämper et al. “Activation and propagation of Ca 2+ release during excitation-contraction coupling in atrial myocytes”. In: *Biophysical journal* 81.5 (2001), pp. 2590–2605.

[145] Michael Kohlhaas et al. “Increased sarcoplasmic reticulum calcium leak but unaltered contractility by acute CaMKII overexpression in isolated rabbit cardiac myocytes”. In: *Circulation research* 98.2 (2006), pp. 235–244.

[146] Jussi T Koivumäki, Topi Korhonen, and Pasi Tavi. “Impact of sarcoplasmic reticulum calcium release on calcium dynamics and action potential morphology in human atrial myocytes: a computational study”. In: *PLoS computational biology* 7.1 (2011), e1001067.

[147] Arthur A Kort and Edward G Lakatta. “Calcium-dependent mechanical oscillations occur spontaneously in unstimulated mammalian cardiac tissues.” In: *Circulation research* 54.4 (1984), pp. 396–404.

[148] Bouwe P Krijthe et al. “Projections on the number of individuals with atrial fibrillation in the European Union, from 2000 to 2060”. In: *European heart journal* 34.35 (2013), pp. 2746–2751.

[149] Ursula Kummer et al. “Transition from stochastic to deterministic behavior in calcium oscillations”. In: *Biophysical journal* 89.3 (2005), pp. 1603–1611.

[150] F Anthony Lai et al. “Purification and reconstitution of the calcium release channel from skeletal muscle”. In: *Nature* 331.6154 (1988), pp. 315–319.

[151] Edward G Lakatta, Victor A Maltsev, and Tatiana M Vinogradova. “A coupled SYSTEM of intracellular Ca2+ clocks and surface membrane voltage clocks controls the timekeeping mechanism of the heart’s pacemaker”. In: *Circulation research* 106.4 (2010), pp. 659–673.

[152] Derek R Laver. “Ca2+ stores regulate ryanodine receptor Ca2+ release channels via luminal and cytosolic Ca2+ sites”. In: *Biophysical journal* 92.10 (2007), pp. 3541–3555.

[153] Young-Seon Lee and James P Keener. “A calcium-induced calcium release mechanism mediated by calsequestrin”. In: *Journal of theoretical biology* 253.4 (2008), pp. 668–679.

[154] Ilse Lenaerts et al. “Ultrastructural and functional remodeling of the coupling between Ca2+ influx and sarcoplasmic reticulum Ca2+ release in right atrial myocytes from experimental persistent atrial fibrillation”. In: *Circulation research* 105.9 (2009), pp. 876–885.

[155] Qince Li et al. “Mechanisms by which cytoplasmic calcium wave propagation and alternans are generated in cardiac atrial myocytes lacking t-tubules—insights from a simulation study”. In: *Biophysical journal* 102.7 (2012), pp. 1471–1482.

[156] Benjamin Lindner et al. “Effects of noise in excitable systems”. In: *Physics reports* 392.6 (2004), pp. 321–424.

[157] P Lipp et al. “Spatially non-uniform Ca2+ signals induced by the reduction of transverse tubules in citrate-loaded guinea-pig ventricular myocytes in culture.” In: *The Journal of physiology* 497.3 (1996), pp. 589–597.

[158] Tao Liu et al. “Altered calcium handling produces reentry-promoting action potential alternans in atrial fibrillation–remodeled hearts”. In: *JCI insight* 5.8 (2020).

[159] Anna Llach et al. “Sarcoplasmic reticulum and L-type Ca2+ channel activity regulate the beat-to-beat stability of calcium handling in human atrial myocytes”. In: *The Journal of physiology* 589.13 (2011), pp. 3247–3262.

[160] Qing Lou et al. "Alternating membrane potential/calcium interplay underlies repetitive focal activity in a genetic model of calcium-dependent atrial arrhythmias". In: *The Journal of physiology* 593.6 (2015), pp. 1443–1458.

[161] William E Louch et al. "Control of Ca2+ release by action potential configuration in normal and failing murine cardiomyocytes". In: *Biophysical journal* 99.5 (2010), pp. 1377–1386.

[162] William E Louch et al. "T-tubule disorganization and reduced synchrony of Ca2+ release in murine cardiomyocytes following myocardial infarction". In: *The Journal of physiology* 574.2 (2006), pp. 519–533.

[163] Valeriy Lukyanenko and Sandor Györke. "Ca2+ sparks and Ca2+ waves in saponin-permeabilized rat ventricular myocytes". In: *The Journal of physiology* 521.3 (1999), pp. 575–585.

[164] Valeriy Lukyanenko et al. "The role of luminal Ca2+ in the generation of Ca2+ waves in rat ventricular myocytes". In: *The Journal of Physiology* 518.1 (1999), pp. 173–186.

[165] Ching-hsing Luo and Yoram Rudy. "A dynamic model of the cardiac ventricular action potential. I. Simulations of ionic currents and concentration changes." In: *Circulation research* 74.6 (1994), pp. 1071–1096.

[166] Ching-Hsing Luo and Yoram Rudy. "A dynamic model of the cardiac ventricular action potential. II. Afterdepolarizations, triggered activity, and potentiation." In: *Circulation research* 74.6 (1994), pp. 1097–1113.

[167] Ching-hsing Luo and Yoram Rudy. "A model of the ventricular cardiac action potential. Depolarization, repolarization, and their interaction." In: *Circulation research* 68.6 (1991), pp. 1501–1526.

[168] Alexander R Lyon et al. "Loss of T-tubules and other changes to surface topography in ventricular myocytes from failing human and rat heart". In: *Proceedings of the National Academy of Sciences* 106.16 (2009), pp. 6854–6859.

[169] Lauren Mackenzie et al. "Predetermined recruitment of calcium release sites underlies excitation-contraction coupling in rat atrial myocytes". In: *The Journal of Physiology* 530.3 (2001), pp. 417–429.

[170] Lauren Mackenzie et al. "The spatial pattern of atrial cardiomyocyte calcium signalling modulates contraction". In: *Journal of cell science* 117.26 (2004), pp. 6327–6337.

[171] David H MacLennan and SR Wayne Chen. "Store overload-induced Ca2+ release as a triggering mechanism for CPVT and MH episodes caused by mutations in RYR and CASQ genes". In: *The Journal of physiology* 587.13 (2009), pp. 3113–3115.

[172] David H MacLennan and PTS Wong. "Isolation of a calcium-sequestering protein from sarcoplasmic reticulum". In: *Proceedings of the National Academy of Sciences* 68.6 (1971), pp. 1231–1235.

[173] DH MacLennan, KP Campbell, and RA Reithmeier. *Calsequestrin In Calcium and Cell Function. WY Cheung, editor*. 1983.

[174] Niall Macquaide, J Dempster, and GL Smith. “Measurement and modeling of Ca2+ waves in isolated rabbit ventricular cardiomyocytes”. In: *Biophysical journal* 93.7 (2007), pp. 2581–2595.

[175] Niall Macquaide et al. “Ryanodine receptor cluster fragmentation and redistribution in persistent atrial fibrillation enhance calcium release”. In: *Cardiovascular research* 108.3 (2015), pp. 387–398.

[176] Aman Mahajan et al. “A rabbit ventricular action potential model replicating cardiac dynamics at rapid heart rates”. In: *Biophysical journal* 94.2 (2008), pp. 392–410.

[177] Lars S Maier et al. “Ca2+ handling in isolated human atrial myocardium”. In: *American Journal of Physiology-Heart and Circulatory Physiology* 279.3 (2000), H952–H958.

[178] Jonathan S Marchant and Ian Parker. “Role of elementary Ca 2+ puffs in generating repetitive Ca 2+ oscillations”. In: *The EMBO Journal* 20.1-2 (2001), pp. 65–76.

[179] Echebarria B. Shiferaw Y. & Alvarez-Lacalle E. Marchena M. “Buffering and total calcium levels determine the presence of oscillatory regimes in cardiac cells”. In: *Under revision* - (2020), pp. –.

[180] Miquel Marchena and Blas Echebarria. “Computational model of calcium signaling in cardiac atrial cells at the submicron scale”. In: *Frontiers in Physiology* 9 (2018), p. 1760.

[181] Miquel Marchena and Blas Echebarria. “Influence of the tubular network on the characteristics of calcium transients in cardiac myocytes”. In: *Plos one* 15.4 (2020), e0231056.

[182] Andrew R Marks. “Calcium cycling proteins and heart failure: mechanisms and therapeutics”. In: *The Journal of clinical investigation* 123.1 (2013), pp. 46–52.

[183] Steven O Marx et al. “PKA phosphorylation dissociates FKBP12. 6 from the calcium release channel (ryanodine receptor): defective regulation in failing hearts”. In: *Cell* 101.4 (2000), pp. 365–376.

[184] Ro E McAllister, D Noble, and RW Tsien. “Reconstruction of the electrical activity of cardiac Purkinje fibres.” In: *The Journal of physiology* 251.1 (1975), pp. 1–59.

[185] Mark D McCauley and Xander HT Wehrens. “Ryanodine receptor phosphorylation, calcium/calmodulin-dependent protein kinase II, and life-threatening ventricular arrhythmias”. In: *Trends in cardiovascular medicine* 21.2 (2011), pp. 48–51.

[186] Thomas G McNary et al. “Mechanical modulation of the transverse tubular system of ventricular cardiomyocytes”. In: *Progress in biophysics and molecular biology* 110.2-3 (2012), pp. 218–225.

[187] Sivan Vadakkadath Meethal et al. “Structure–function relationships of Ca spark activity in normal and failing cardiac myocytes as revealed by flash photography”. In: *Cell calcium* 41.2 (2007), pp. 123–134.

[188] Shanthi Mendis et al. *Global atlas on cardiovascular disease prevention and control.* Geneva: World Health Organization, 2011.

[189] Viorel Mihalef et al. “Patient-specific modelling of whole heart anatomy, dynamics and haemodynamics from four-dimensional cardiac CT images”. In: *Interface Focus* 1.3 (2011), pp. 286–296.

[190] George Ralph Mines. “On circulating excitations in heart muscle and their possible relation to tachycardia and fibrillation”. In: *Trans R Soc Can* 8 (1914), pp. 43–52.

[191] George Ralph Mines. “On dynamic equilibrium in the heart”. In: *The Journal of physiology* 46.4-5 (1913), pp. 349–383.

[192] Robert D Mitchell, HK Simmerman, and LR Jones. “Ca2+ binding effects on protein conformation and protein interactions of canine cardiac calsequestrin.” In: *Journal of Biological Chemistry* 263.3 (1988), pp. 1376–1381.

[193] Masahito Miura, Penelope A Boyden, and Henk EDJ ter Keurs. “Ca2+ waves during triggered propagated contractions in intact trabeculae: determinants of the velocity of propagation”. In: *Circulation research* 84.12 (1999), pp. 1459–1468.

[194] Kenneth J Mukamal et al. “Alcohol consumption and risk of atrial fibrillation in men and women: the Copenhagen City Heart Study”. In: *Circulation* 112.12 (2005), pp. 1736–1742.

[195] Michael P Murphy. “How mitochondria produce reactive oxygen species”. In: *Biochemical journal* 417.1 (2009), pp. 1–13.

[196] Junichi Nakai et al. “Primary structure and functional expression from cDN A of the cardiac ryanodine receptor/calcium release channel”. In: *FEBS letters* 271.1-2 (1990), pp. 169–177.

[197] Stanley Nattel and Dobromir Dobrev. “The multidimensional role of calcium in atrial fibrillation pathophysiology: mechanistic insights and therapeutic opportunities”. In: *European heart journal* 33.15 (2012), pp. 1870–1877.

[198] Michael Nivala et al. “Computational modeling and numerical methods for spatiotemporal calcium cycling in ventricular myocytes”. In: *Frontiers in physiology* 3 (2012).

[199] Michael Nivala et al. “T-tubule disruption promotes calcium alternans in failing ventricular myocytes: mechanistic insights from computational modeling”. In: *Journal of molecular and cellular cardiology* 79 (2015), pp. 32–41.

[200] Denis Noble. “A modification of the Hodgkin—Huxley equations applicable to Purkinje fibre action and pacemaker potentials”. In: *The Journal of physiology* 160.2 (1962), pp. 317–352.

[201] DA Nordsletten et al. “Coupling multi-physics models to cardiac mechanics”. In: *Progress in biophysics and molecular biology* 104.1-3 (2011), pp. 77–88.

[202] Anders Nygren et al. “Mathematical model of an adult human atrial cell: the role of K+ currents in repolarization”. In: *Circulation research* 82.1 (1998), pp. 63–81.

[203] Thomas O’Hara et al. “Simulation of the undiseased human cardiac ventricular action potential: model formulation and experimental validation”. In: *PLoS computational biology* 7.5 (2011).

[204] CH Orchard, DA Eisner, and DG Allen. “Oscillations of intracellular Ca2+ in mammalian cardiac muscle”. In: *Nature* 304.5928 (1983), pp. 735–738.

[205] World Health Organization et al. “Causes of death 2008: data sources and methods”. In: *Geneva: World Health Organization* (2011).

[206] Leiv Øyehaug et al. “Synchrony of cardiomyocyte Ca2+ release is controlled by T-tubule organization, SR Ca2+ content, and ryanodine receptor Ca2+ sensitivity”. In: *Biophysical journal* 104.8 (2013), pp. 1685–1697.

[207] Sandeep V Pandit and José Jalife. “AGING AND AF RESEARCH: WHERE WE ARE AND WHERE WE SHOULD GO”. In: *Heart rhythm: the official journal of the Heart Rhythm Society* 4.2 (2007), p. 186.

[208] Côme Pasqualin et al. “Automatic quantitative analysis of t-tubule organization in cardiac myocytes using ImageJ”. In: *American Journal of Physiology-Cell Physiology* 308.3 (2014), pp. C237–C245.

[209] Isaac N Pessah, ROXANNE A Stambuk, and JOHN E Casida. “Ca2+-activated ryanodine binding: mechanisms of sensitivity and intensity modulation by Mg2+, caffeine, and adenine nucleotides.” In: *Molecular pharmacology* 31.3 (1987), pp. 232–238.

[210] Bradley N Plummer et al. “Spontaneous calcium oscillations during diastole in the whole heart: the influence of ryanodine reception function and gap junction coupling”. In: *American Journal of Physiology-Heart and Circulatory Physiology* 300.5 (2011), H1822–H1828.

[211] Martin Poenie et al. “Changes of free calcium levels with stages of the cell division cycle”. In: *Nature* 315.6015 (1985), pp. 147–149.

[212] Steven M Pogwizd, John P McKenzie, and Michael E Cain. “Mechanisms underlying spontaneous and induced ventricular arrhythmias in patients with idiopathic dilated cardiomyopathy”. In: *Circulation* 98.22 (1998), pp. 2404–2414.

[213] Steven M Pogwizd et al. “Arrhythmogenesis and contractile dysfunction in heart failure: roles of sodium-calcium exchange, inward rectifier potassium current, and residual β-adrenergic responsiveness”. In: *Circulation research* 88.11 (2001), pp. 1159–1167.

[214] Silvia G Priori et al. “Mutations in the cardiac ryanodine receptor gene (hRyR2) underlie catecholaminergic polymorphic ventricular tachycardia”. In: *Circulation* 103.2 (2001), pp. 196–200.

[215] Xiao-Yan Qi et al. “Role of small-conductance calcium-activated potassium channels in atrial electrophysiology and fibrillation in the dog”. In: *Circulation* 129.4 (2014), pp. 430–440.

[216] Zhilin Qu and James N Weiss. “Mechanisms of ventricular arrhythmias: from molecular fluctuations to electrical turbulence”. In: *Annual review of physiology* 77 (2015), pp. 29–55.

[217] Rafael J Ramirez, Stanley Nattel, and Marc Courtemanche. “Mathematical analysis of canine atrial action potentials: rate, regional factors, and electrical remodeling”. In: *American Journal of Physiology-Heart and Circulatory Physiology* 279.4 (2000), H1767–H1785.

[218] RL Rasmusson et al. “A mathematical model of electrophysiological activity in a bullfrog atrial cell”. In: *American Journal of Physiology-Heart and Circulatory Physiology* 259.2 (1990), H370–H389.

[219] John J Rice, M Saleet Jafri, and Raimond L Winslow. “Modeling gain and gradedness of Ca2+ release in the functional unit of the cardiac diadic space”. In: *Biophysical journal* 77.4 (1999), pp. 1871–1884.

[220] Mark Antony Richards et al. “Transverse tubules are a common feature in large mammalian atrial myocytes including human”. In: *American Journal of Physiology-Heart and Circulatory Physiology* 301.5 (2011), H1996–H2005.

[221] Nicoletta Rizzi et al. “Unexpected structural and functional consequences of the R33Q homozygous mutation in cardiac calsequestrin: a complex arrhythmogenic cascade in a knock in mouse model”. In: *Circulation research* 103.3 (2008), pp. 298–306.

[222] SP Robertson, J DAVID Johnson, and JD Potter. “The time-course of Ca2+ exchange with calmodulin, troponin, parvalbumin, and myosin in response to transient increases in Ca2+”. In: *Biophysical journal* 34.3 (1981), pp. 559–569.

[223] Elena Saftenku, Alan J Williams, and Rebecca Sitsapesan. “Markovian models of low and high activity levels of cardiac ryanodine receptors”. In: *Biophysical journal* 80.6 (2001), pp. 2727–2741.

[224] Alfonso Santiago et al. “Fully coupled fluid-electro-mechanical model of the human heart for supercomputers”. In: *International journal for numerical methods in biomedical engineering* 34.12 (2018), e3140.

[225] Gerardo J Escalera Santos et al. “Effects of noise near a homoclinic bifurcation in an electrochemical system”. In: *Physical Review E* 70.2 (2004), p. 021103.

[226] Philipp Sasse et al. “Intracellular Ca2+ oscillations, a potential pacemaking mechanism in early embryonic heart cells”. In: *The Journal of general physiology* 130.2 (2007), pp. 133–144.

[227] Yoji Sato et al. “Cardiac-specific overexpression of mouse cardiac calsequestrin is associated with depressed cardiovascular function and hypertrophy in transgenic mice”. In: *Journal of Biological Chemistry* 273.43 (1998), pp. 28470–28477.

[228] FA Schanne et al. “Calcium dependence of toxic cell death: a final common pathway”. In: *Science* 206.4419 (1979), pp. 700–702.

[229] Torsten Schenkel et al. “MRI-based CFD analysis of flow in a human left ventricle: methodology and application to a healthy heart”. In: *Annals of biomedical engineering* 37.3 (2009), pp. 503–515.

[230] Gerhard Schmid, Igor Goychuk, and Peter Hänggi. “Stochastic resonance as a collective property of ion channel assemblies”. In: *EPL (Europhysics Letters)* 56.1 (2001), p. 22.

[231] Tilmann Schober et al. “Myofilament Ca sensitization increases cytosolic Ca binding affinity, alters intracellular Ca homeostasis, and causes pause-dependent Ca-triggered arrhythmia”. In: *Circulation research* 111.2 (2012), pp. 170–179.

[232] Bas A Schoonderwoerd et al. “New risk factors for atrial fibrillation: causes of ‘not-so-lone atrial fibrillation’”. In: *Europace* 10.6 (2008), pp. 668–673.

[233] Ulrich Schotten et al. “Atrial fibrillation-induced atrial contractile dysfunction: a tachycardiomyopathy of a different sort”. In: *Cardiovascular research* 53.1 (2002), pp. 192–201.

[234] Thomas R Shannon, Kenneth S Ginsburg, and Donald M Bers. “Potentiation of fractional sarcoplasmic reticulum calcium release by total and free intra-sarcoplasmic reticulum calcium concentration”. In: *Biophysical journal* 78.1 (2000), pp. 334–343.

[235] Thomas R Shannon, Kenneth S Ginsburg, and Donald M Bers. “Quantitative assessment of the SR Ca2+ leak-load relationship”. In: *Circulation research* 91.7 (2002), pp. 594–600.

[236] Thomas R Shannon, Kenneth S Ginsburg, and Donald M Bers. “Reverse mode of the sarcoplasmic reticulum calcium pump and load-dependent cytosolic calcium decline in voltage-clamped cardiac ventricular myocytes”. In: *Biophysical Journal* 78.1 (2000), pp. 322–333.

[237] Thomas R Shannon, Fei Wang, and Donald M Bers. “Regulation of cardiac sarcoplasmic reticulum Ca release by luminal [Ca] and altered gating assessed with a mathematical model”. In: *Biophysical journal* 89.6 (2005), pp. 4096–4110.

[238] Thomas R Shannon et al. “A mathematical treatment of integrated Ca dynamics within the ventricular myocyte”. In: *Biophysical journal* 87.5 (2004), pp. 3351–3371.

[239] Xin Shen et al. “3D dSTORM imaging reveals novel detail of ryanodine receptor localization in rat cardiac myocytes”. In: *The Journal of physiology* 597.2 (2019), pp. 399–418.

[240] Yohannes Shiferaw. “Nonlinear onset of calcium wave propagation in cardiac cells”. In: *Physical Review E* 94.3 (2016), p. 032405.

[241] Yohannes Shiferaw, Gary L Aistrup, and J Andrew Wasserstrom. *Intracellular Ca2+ waves, afterdepolarizations, and triggered arrhythmias*. 2012.

[242] Vyacheslav M Shkryl et al. “Refractoriness of sarcoplasmic reticulum Ca2+ release determines Ca2+ alternans in atrial myocytes”. In: *American Journal of Physiology-Heart and Circulatory Physiology* 302.11 (2012), H2310–H2320.

[243] R Sitsapesan and AJ Williams. “Regulation of current flow through ryanodine receptors by luminal Ca 2+”. In: *Journal of Membrane Biology* 159.3 (1997), pp. 179–185.

[244] Ioannis Smyrnias et al. “Comparison of the T-tubule system in adult rat ventricular and atrial myocytes, and its role in excitation–contraction coupling and inotropic stimulation”. In: *Cell calcium* 47.3 (2010), pp. 210–223.

[245] James Sneyd et al. “On the dynamical structure of calcium oscillations”. In: *Proceedings of the National Academy of Sciences* 114.7 (2017), pp. 1456–1461.

[246] Steven M Snyder, Bradley M Palmer, and Russell L Moore. “A mathematical model of cardiocyte Ca2+ dynamics with a novel representation of sarcoplasmic reticular Ca2+ control”. In: *Biophysical journal* 79.1 (2000), pp. 94–115.

[247] Eric A Sobie et al. “Termination of cardiac Ca2+ sparks: an investigative mathematical model of calcium-induced calcium release”. In: *Biophysical journal* 83.1 (2002), pp. 59–78.

[248] C Soeller and MB Cannell. “Examination of the transverse tubular system in living cardiac rat myocytes by 2-photon microscopy and digital image–processing techniques”. In: *Circulation research* 84.3 (1999), pp. 266–275.

[249] Christian Soeller and David Baddeley. “Super-resolution imaging of EC coupling protein distribution in the heart”. In: *Journal of molecular and cellular cardiology* 58 (2013), pp. 32–40.

[250] Christian Soeller et al. “Analysis of ryanodine receptor clusters in rat and human cardiac myocytes”. In: *Proceedings of the National Academy of Sciences* 104.38 (2007), pp. 14958–14963.

[251] Christian Soeller et al. “Three-dimensional high-resolution imaging of cardiac proteins to construct models of intracellular Ca2+ signalling in rat ventricular myocytes”. In: *Experimental physiology* 94.5 (2009), pp. 496–508.

[252] Lei Song et al. “Calsequestrin 2 (CASQ2) mutations increase expression of calreticulin and ryanodine receptors, causing catecholaminergic polymorphic ventricular tachycardia”. In: *The Journal of clinical investigation* 117.7 (2007), pp. 1814–1823.

[253] Long-Sheng Song et al. “Orphaned ryanodine receptors in the failing heart”. In: *Proceedings of the National Academy of Sciences* 103.11 (2006), pp. 4305–4310.

[254] Zhen Song, Michael B Liu, and Zhilin Qu. “Transverse tubular network structures in the genesis of intracellular calcium alternans and triggered activity in cardiac cells”. In: *Journal of molecular and cellular cardiology* 114 (2018), pp. 288–299.

[255] Zhen Song, Zhilin Qu, and Alain Karma. “Stochastic initiation and termination of calcium-mediated triggered activity in cardiac myocytes”. In: *Proceedings of the National Academy of Sciences* 114.3 (2017), E270–E279.

[256] Zhen Song et al. “Long-Lasting Sparks: Multi-Metastability and Release Competition in the Calcium Release Unit Network”. In: *PLoS Comput Biol* 12.1 (2016), e1004671.

[257] MD Stern, MC Capogrossi, and EG Lakatta. “Spontaneous calcium release from the sarcoplasmic reticulum in myocardial cells: mechanisms and consequences”. In: *Cell calcium* 9.5-6 (1988), pp. 247–256.

[258] Michael D Stern. “Theory of excitation-contraction coupling in cardiac muscle”. In: *Biophysical journal* 63.2 (1992), pp. 497–517.

[259] Michael D Stern et al. “Local control models of cardiac excitation–contraction coupling: a possible role for allosteric interactions between ryanodine receptors”. In: *The Journal of general physiology* 113.3 (1999), pp. 469–489.

[260] Sarah CW Stevens et al. “Intra-sarcoplasmic reticulum Ca2+ oscillations are driven by dynamic regulation of ryanodine receptor function by luminal Ca2+ in cardiomyocytes”. In: *The Journal of physiology* 587.20 (2009), pp. 4863–4872.

[261] Bruno D Stuyvers, Penelope A Boyden, and Henk EDJ ter Keurs. *Calcium waves: physiological relevance in cardiac function.* 2000.

[262] Henry Sutanto et al. “The subcellular distribution of ryanodine receptors and L-type Ca2+ channels modulates Ca2+-transient properties and spontaneous Ca2+-release events in atrial cardiomyocytes”. In: *Frontiers in physiology* 9 (2018), p. 1108.

[263] T Takamatsu and WG Wier. “Calcium waves in mammalian heart: quantification of origin, magnitude, waveform, and velocity.” In: *The FASEB journal* 4.5 (1990), pp. 1519–1525.

[264] Toshiyuki Takasage et al. “Regulation of the cardiac ryanodine receptor by protein kinase-dependent phosphorylation”. In: *The Journal of Biochemistry* 109.1 (1991), pp. 163–170.

[265] Hiroshi Takeshima et al. “Primary structure and expression from complementary DNA of skeletal muscle ryanodine receptor”. In: *Nature* 339.6224 (1989), pp. 439–445.

[266] Takeo Tanaami et al. “Difference in propagation of Ca2+ release in atrial and ventricular myocytes”. In: *The Japanese journal of physiology* (2005), pp. 0504270003–0504270003.

[267] Dalin Tang et al. “Image-based patient-specific ventricle models with fluid–structure interaction for cardiac function assessment and surgical design optimization”. In: *Progress in pediatric cardiology* 30.1-2 (2010), pp. 51–62.

[268] Vallmitjana A. Llach A. Herraiz A.-Jímenez-Sabado V. Godoy-Marín-H. Nolla-Colomer C. Echebarria B. Marchena M. Cabello N. Ferrero-Gregori A. Ginel A. Viñolas X. Montiel J. Ciruela F. Benítez R. Cinca J. & Hove-Madsen L. Tarifa C. “Preferential subsarcolemmal calcium spark distribution potentiates arrhythmogenic electrical activity in patients with atrial fibrillation”. In: *In preparation* - (2020), pp. –.

[269] Dmitry Terentyev et al. “Abnormal interactions of calsequestrin with the ryanodine receptor calcium release channel complex linked to exercise-induced sudden cardiac death”. In: *Circulation research* 98.9 (2006), pp. 1151–1158.

[270] Dmitry Terentyev et al. “Calsequestrin determines the functional size and stability of cardiac intracellular calcium stores: mechanism for hereditary arrhythmia”. In: *Proceedings of the National Academy of Sciences* 100.20 (2003), pp. 11759–11764.

[271] Rüdiger Thul et al. “Subcellular calcium dynamics in a whole-cell model of an atrial myocyte”. In: *Proceedings of the National Academy of Sciences* 109.6 (2012), pp. 2150–2155.

[272] Ruediger Thul et al. “Unifying principles of calcium wave propagation—insights from a three-dimensional model for atrial myocytes”. In: *Biochimica et Biophysica Acta (BBA)-Molecular Cell Research* 1853.9 (2015), pp. 2131–2143.

[273] AW Trafford, ME Diaz, and DA Eisner. “A novel, rapid and reversible method to measure Ca buffering and time-course of total sarcoplasmic reticulum Ca content in cardiac ventricular myocytes”. In: *Pflügers Archiv* 437.3 (1999), pp. 501–503.

[274] AW Trafford et al. “Comparison of subsarcolemmal and bulk calcium concentration during spontaneous calcium release in rat ventricular myocytes.” In: *The Journal of Physiology* 488.3 (1995), pp. 577–586.

[275] AW Trafford et al. “Propagating calcium waves initiated by local caffeine application in rat ventricular myocytes.” In: *The Journal of physiology* 489.2 (1995), pp. 319–326.

[276] Natalia A Trayanova. “Whole-heart modeling: applications to cardiac electrophysiology and electromechanics”. In: *Circulation research* 108.1 (2011), pp. 113–128.

[277] RY Tsien, T Pozzan, and TJ Rink. “Calcium homeostasis in intact lymphocytes: cytoplasmic free calcium monitored with a new, intracellularly trapped fluorescent indicator.” In: *The Journal of cell biology* 94.2 (1982), pp. 325–334.

[278] Aslak Tveito et al. “Instabilities of the resting state in a mathematical model of calcium handling in cardiac myocytes”. In: *Mathematical biosciences* 236.2 (2012), pp. 97–107.

[279] Per Uhlén and Nicolas Fritz. “Biochemistry of calcium oscillations”. In: *Biochemical and biophysical research communications* 396.1 (2010), pp. 28–32.

[280] Filip Van Petegem. “Ryanodine receptors: structure and function”. In: *Journal of Biological Chemistry* 287.38 (2012), pp. 31624–31632.

[281] David R Van Wagoner et al. “Atrial L-type Ca2+ currents and human atrial fibrillation”. In: *Circulation research* 85.5 (1999), pp. 428–436.

[282] Anthony Varghese and Raimond L Winslow. “Dynamics of abnormal pacemaking activity in cardiac Purkinje fibers”. In: *Journal of theoretical biology* 168.4 (1994), pp. 407–420.

[283] Anthony Varghese and Raimond L Winslow. “Dynamics of the calcium subsystem in cardiac Purkinje fibers”. In: *Physica D: Nonlinear Phenomena* 68.3-4 (1993), pp. 364–386.

[284] Mariano Vázquez et al. “Alya: Multiphysics engineering simulation toward exascale”. In: *Journal of computational science* 14 (2016), pp. 15–27.

[285] John A Vest et al. “Defective cardiac ryanodine receptor regulation during atrial fibrillation”. In: *Circulation* 111.16 (2005), pp. 2025–2032.

[286] S Viatchenko-Karpinski et al. “Intracellular Ca2+ oscillations drive spontaneous contractions in cardiomyocytes during early development”. In: *Proceedings of the National Academy of Sciences* 96.14 (1999), pp. 8259–8264.

[287] Serge Viatchenko-Karpinski et al. “Abnormal calcium signaling and sudden cardiac death associated with mutation of calsequestrin”. In: *Circulation research* 94.4 (2004), pp. 471–477.

[288] Tatiana M Vinogradova et al. “High basal protein kinase A–dependent phosphorylation drives rhythmic internal Ca2+ store oscillations and spontaneous beating of cardiac pacemaker cells”. In: *Circulation research* 98.4 (2006), pp. 505–514.

[289] Tatiana M Vinogradova et al. "Rhythmic ryanodine receptor Ca2+ releases during diastolic depolarization of sinoatrial pacemaker cells do not require membrane depolarization". In: *Circulation research* 94.6 (2004), pp. 802–809.

[290] Niels Voigt et al. "Cellular and molecular mechanisms of atrial arrhythmogenesis in patients with paroxysmal atrial fibrillation". In: *Circulation* (2013), CIRCULATIONAHA–113.

[291] Niels Voigt et al. "Enhanced sarcoplasmic reticulum Ca2+ leak and increased Na+-Ca2+ exchanger function underlie delayed afterdepolarizations in patients with chronic atrial fibrillation". In: *Circulation* 125.17 (2012), pp. 2059–2070.

[292] John Wagner and Joel Keizer. "Effects of rapid buffers on Ca2+ diffusion and Ca2+ oscillations." In: *Biophysical Journal* 67.1 (1994), p. 447.

[293] AP Walden, KM Dibb, and AW Trafford. "Differences in intracellular calcium homeostasis between atrial and ventricular myocytes". In: *Journal of molecular and cellular cardiology* 46.4 (2009), pp. 463–473.

[294] Xander HT Wehrens et al. "Ca2+/calmodulin-dependent protein kinase II phosphorylation regulates the cardiac ryanodine receptor". In: *Circulation research* 94.6 (2004), e61–e70.

[295] Xander HT Wehrens et al. "Enhancing calstabin binding to ryanodine receptors improves cardiac and skeletal muscle function in heart failure". In: *Proceedings of the National Academy of Sciences* 102.27 (2005), pp. 9607–9612.

[296] Sheng Wei et al. "T-Tubule Remodeling During Transition From Hypertrophy to Heart Failure. Novelty and Significance". In: *Circulation research* 107.4 (2010), pp. 520–531.

[297] James N Weiss et al. "Early afterdepolarizations and cardiac arrhythmias". In: *Heart rhythm* 7.12 (2010), pp. 1891–1899.

[298] James N Weiss et al. "The dynamics of cardiac fibrillation". In: *Circulation* 112.8 (2005), pp. 1232–1240.

[299] James N Weiss et al. "Ventricular fibrillation: how do we stop the waves from breaking?" In: *Circulation research* 87.12 (2000), pp. 1103–1107.

[300] NRA Wiener. "The mathematical formulation of the problem of conduction of impulses in a network of connected excitable elements, specifically in cardiac muscle". In: *Arch Inst Cardiol Mex* 16 (1946), pp. 1–61.

[301] Maurits CEF Wijffels et al. "Atrial fibrillation begets atrial fibrillation: a study in awake chronically instrumented goats". In: *Circulation* 92.7 (1995), pp. 1954–1968.

[302] Mathias Wilhelms et al. "Benchmarking electrophysiological models of human atrial myocytes". In: *Frontiers in physiology* 3 (2013), p. 487.

[303] Raimond L Winslow et al. “Generation and propagation of ectopic beats induced by spatially localized Na–K pump inhibition in atrial network models”. In: *Proceedings of the Royal Society of London. Series B: Biological Sciences* 254.1339 (1993), pp. 55–61.

[304] Raimond L Winslow et al. “Mechanisms of altered excitation-contraction coupling in canine tachycardia-induced heart failure, II: model studies”. In: *Circulation research* 84.5 (1999), pp. 571–586.

[305] Lai-Hua Xie and James N Weiss. “Arrhythmogenic consequences of intracellular calcium waves”. In: *American Journal of Physiology-Heart and Circulatory Physiology* 297.3 (2009), H997–H1002.

[306] Yung-Hsin Yeh et al. “Calcium-handling abnormalities underlying atrial arrhythmogenesis and contractile dysfunction in dogs with congestive heart failure”. In: *Circulation: Arrhythmia and Electrophysiology* 1.2 (2008), pp. 93–102.

[307] Lixia Yue et al. “Ionic remodeling underlying action potential changes in a canine model of atrial fibrillation”. In: *Circulation research* 81.4 (1997), pp. 512–525.

[308] Guang Qin Zhang et al. “Identification and characterization of calcium sparks in cardiomyocytes derived from human induced pluripotent stem cells”. In: *PloS one* 8.2 (2013).

[309] Shengmei Zhou et al. “Nonreentrant focal activations in pulmonary veins in canine model of sustained atrial fibrillation”. In: *American Journal of Physiology-Heart and Circulatory Physiology* 283.3 (2002), H1244–H1252.

Part V

Appendixes

Appendix A

Model parameters

In this appendix one can find the parameters of the subcellular model.

General parameters		
Δt	ms	0.007
Δx	μm	0.1
L_x	μm	80
L_y	μm	12
T	K	308
V_{rest}	mV	-85
V_{max}	mV	10
D_i	$\mu\text{m}^2/\text{ms}$	280
D_{sr}	$\mu\text{m}^2/\text{ms}$	90
Release parameters		
g_{rel}	ms^{-1}	8
N_{RyR}		9
k_{oc}	ms^{-1}	0.04
k_a	$\mu\text{M}^{-3}/\text{ms}$	10^{-3}
k_c	$\mu\text{M}^{-1}/\text{ms}$	10^{-3}
k_b	$\mu\text{M}^{-3}/\text{ms}$	10^{-3}
k_{ic}	ms^{-1}	$5{\cdot}10^{-3}$
Max_{SR}		15
Min_{SR}		1
H		10
EC_{50-SR}		450
LCC parameters		
g_{CaL}	ms^{-1}	$7.86{\cdot}10^{15}$
N_{LCC}		5
K_{LCC}	μM	5

TABLE A.1: Parameters of the subcellular model (part 1).

SERCA parameters		
g_{up}	μM/ms	$3{\cdot}10^{-1}$
K_i	μM	0.1
K_{sr}	μM	1300
NCX parameters		
g_{NCX}	μM/ms	12
$[\mathrm{Ca}]_\mathrm{o}$	μM	1800
$[\mathrm{Na}]_\mathrm{o}$	μM	136000
$[\mathrm{Na}]_\mathrm{i}$	μM	10000
k_{sat}		0.27
η		0.35
K_{mNao}	μM	87500
K_{mCao}	μM	1300
K_{mNai}	μM	12300
K_{mCai}	μM	3.6
Buffer parameters		
B_{TnC}	μM	70
$k_{on,TnC}$	$\mu\mathrm{M}^{-1}\mathrm{ms}^{-1}$	0.00327
$k_{off,TnC}$	ms^{-1}	0.00196
B_{CaM}	μM	24
$k_{on,CaM}$	$\mu\mathrm{M}^{-1}\mathrm{ms}^{-1}$	0.003
$k_{off,CaM}$	ms^{-1}	0.02
B_{SR}	μM	23.5
$k_{on,SR}$	$\mu\mathrm{M}^{-1}\mathrm{ms}^{-1}$	0.01
$k_{off,SR}$	ms^{-1}	0.006
B_{Rhod}	μM	5
$k_{on,Rhod}$	$\mu\mathrm{M}^{-1}\mathrm{ms}^{-1}$	0.069
$k_{off,Rhod}$	ms^{-1}	0.13
B_{CSQ}	μM	2400
K_{CSQ}	μM	2000

TABLE A.2: Parameters of the subcellular model (part 2).

Appendix B

Deterministic compartment model of a CaRU

In this appendix I show how to derive the simplified model in Eqs. (8.2)-(8.4) from a detailed deterministic model of calcium handling. We consider cytosolic and luminal spaces, each separated into different compartments, i.e, dyadic and cytosolic by the one side, and junctional and network SR, by the other. We also consider the effect of two buffers in the cytosol, TnC and SR, and CSQ in the SR. The effect of the buffers is actually very relevant, as they change the structure of possible solutions of the system.

With this, the dynamics can be described by the following set of deterministic equations for the calcium concentration at the different compartments

$$\frac{dc_d}{dt} = gP_o(c_j - c_d) - \frac{c_d - c_i}{\tau_i} \tag{B.1}$$

$$\frac{dc_{sr}}{dt} = \frac{v_i}{v_{sr}} g_{up} \frac{c_i^2}{K_s^2 + c_i^2} - \frac{c_{sr} - c_j}{\tau_{sr}} \tag{B.2}$$

$$\frac{dc_j}{dt} = \frac{v_{sr}}{v_{jsr}} \frac{c_{sr} - c_j}{\tau_{sr}} - \frac{v_d}{v_{jsr}} gP_o(c_j - c_d) - \tag{B.3}$$

$$- \; k_{onSQ}\, c_j(B_{SQ} - C_{bSQ}) + k_{offSQ} C_{bSQ} \tag{B.4}$$

where c_d, c_j, c_{sr}, c_i stand for the concentration in dyadic space, free luminal, SR network and cytosol, P_o is the fraction of RyR2s in the open state, τ_i and τ_{sr} are the diffusion time constants out of the dyadic space and SR network, v_i, v_d, v_{jsr} and v_{sr} are the volumes associated with each compartment, g_{up} is the strength of SERCA pump, K_s is the concentration at which SERCA closes and g is the strength of the release current. The dynamics of the buffers are given by linear reactions with the following set of ODEs

$$\frac{dC_{bTnC}}{dt} = k_{onTnC} c_i(B_{TnC} - C_{bTnC}) - k_{offnTnC} C_{bTnC} \tag{B.5}$$

$$\frac{dC_{bSR}}{dt} = k_{onSR} c_i(B_{SR} - C_{bSR}) - k_{offSR} C_{bSR} \tag{B.6}$$

$$\frac{dC_{bSQ}}{dt} = k_{onSQ} c_j(B_{SQ} - C_{bSQ}) - k_{offSQ} C_{bSQ} \tag{B.7}$$

Since the total amount of calcium has just a variation of about by a 5% or 10% over a calcium cycle, I assume that the total calcium concentration, $\bar{c}_T$, is fixed. In this way, one does not have to solve a differential equation for the calcium concentration in the cytosol. Rather, it is derived from the algebraic equation:

$$\bar{c}_T = \frac{v_i}{v_i + v_{sr}}(c_i + c_{b,TnC} + c_{b,SR} + c_{b,CaM}) + \frac{v_{sr}}{v_i + v_{sr}}(c_{sr} + c_{bSQ}) \tag{B.8}$$

Homeostatic behavior of the cell will eventually load the system more or less, increasing or decreasing $\bar{c}_T$.

Gating of the RyR2 can been described by Markov models that describe the transitions among different conformations of the channel. Thus, for the dynamics of the RyR2 I consider a phenomenological four state model (Fig. 2.1c) [259].

$$\frac{dP_R}{dt} = -k_p c_d^2 P_R - k_i c_d P_R + k_r P_{I_A} + k_m P_o \tag{B.9}$$

$$\frac{dP_o}{dt} = k_p c_d^2 P_R - k_i c_d P_o + k_r P_{I_B} - k_m P_o \tag{B.10}$$

$$\frac{dP_{I_A}}{dt} = -k_p c_d^2 P_{I_A} + k_i c_d P_R - k_r P_{I_A} + k_m P_{I_B} \tag{B.11}$$

with the last equation given by the condition that the sum of probabilities is equal to 1

$$P_{I_B} = 1 - P_R - P_o - P_{I_A} \tag{B.12}$$

P_R and P_o are the ratios of local RyR2 in the recovered and open states. P_{I_A} and P_{I_B} stand for the terminated states.

To make model treatable I assume several hypothesis.

1. We consider rapid equilibrium of c_j ($\dot{c}_j = 0$). Thus

$$\dot{c}_j = 0 = \frac{v_{sr}}{v_{jsr}} \frac{c_{sr} - c_j}{\tau_{sr}} - \frac{v_d}{v_{jsr}} g P_o (c_j - c_d) - k_{onSQ}\, c_j (B_{SQ} - C_{bSQ}) + k_{offSQ} C_{bSQ} \tag{B.13}$$

then

$$c_j = c_{sr} - \tau_{sr} \left[\frac{v_d}{v_{sr}} g P_o (c_j - c_d) - \frac{v_{jsr}}{v_{sr}} \left(k_{onSQ} c_j (B_{SQ} - C_{bSQ}) - k_{offSQ} C_{bSQ} \right) \right] \tag{B.14}$$

2. At first order, I approximate c_j as c_{sr} in the right hand side of Eq. (B.14). This approximation is valid when $\tau_{sr}\frac{v_d}{v_{sr}} g P_o \ll 1$ and $\tau_{sr}\frac{v_d}{v_{sr}} g P_o \ll 1$. Then, the ODE for c_{sr} in Eq. (B.4) reads as

$$\frac{dc_{sr}}{dt} = \frac{v_i}{v_{sr}} g_{up} \frac{c_i^2}{K_s^2 + c_i^2} - \frac{v_d}{v_{jsr}} g P_o (c_{sr} - c_d) - \tag{B.15}$$

$$- \frac{v_{jsr}}{v_{sr}} \left[k_{onSQ} c_{sr} (B_{SQ} - C_{bSQ}) - k_{offSQ} C_{bSQ} \right] \tag{B.16}$$

where I have eliminated the dependence with c_j.

3. We apply the rapid buffer approximation in the SR because CSQ is very fast [222, 38]. The derivation of c_{sr} in terms of c_{sr}^{tot} have been already shown in the main text (see Eqs. 3.25-3.30).

4. We assume that all the buffers in the cytosol are in equilibrium. Then

$$C_{bTnC} = \frac{B_{TnC} c_i}{K_{TnC} + c_i}, \quad C_{bSR} = \frac{B_{SR} c_i}{K_{SR} + c_i} \tag{B.17}$$

5. Besides, I combine both TnC and SR buffers in only one buffer with a total concentration of B_b and an affinity of K_b, which will be

$$C_b = \frac{B_b c_i}{K_b + c_i} \tag{B.18}$$

6. Finally, since in our simulations the inactivated states of the RyR2s are not determinant to produce oscillations (see Fig. B.1), for simplicity I have neglected them. I consider that the inactivated states of the RyR2s do not play a role in the mechanisms that produce oscillations. For that reason, I reduce the four state model to a two state model

$$\mathrm{C} \underset{\mathrm{k}_m}{\overset{\mathrm{k}_p \mathrm{c_d}^2}{\rightleftharpoons}} \mathrm{O}$$

where k_m sets the mean open time $\tau_{rec} = 1/k_m$ of a RyR2 while k_p gives the open probability. Then, the ODE for the open probability P_o is

$$\frac{dP_o}{dt} = -k_m P_o + k_p c_d^2 (1 - P_o) \tag{B.19}$$

The parameters of these equations are taken from the literature where, except for those of the RyR2, are well documented. The ratio of SR to cytosol in the cell is roughly 1 to 20-30. The order of magnitude of the volume of the cleft where calcium is released is around 10^{-3} μm^3 [238]. SERCA is roughly activated at around 0.2-0.5 μM and closed at around 15-20 μM and the amount of buffers which is relevant to the absorption is around 50-100 μM, taking an average affinity of around 0.5 μM [238]. The whole set of parameters is given in Table B.1.

Parameters		
Parameter	Units	Value
v_d	μm^3	0.001
v_i	μm^3	0.45
v_{sr}	μm^3	0.01
τ_i	ms	0.01
g_{up}	$\mu M/ms$	0.5
K_s	μM	0.2
g	ms^{-1}	20
k_p	$\mu M^{-2} ms^{-1}$	10^{-3}
k_m	ms^{-1}	0.25
K_o	μM	15
B_b	μM	80
K_b	μM	0.5

TABLE B.1: Parameters of the model.

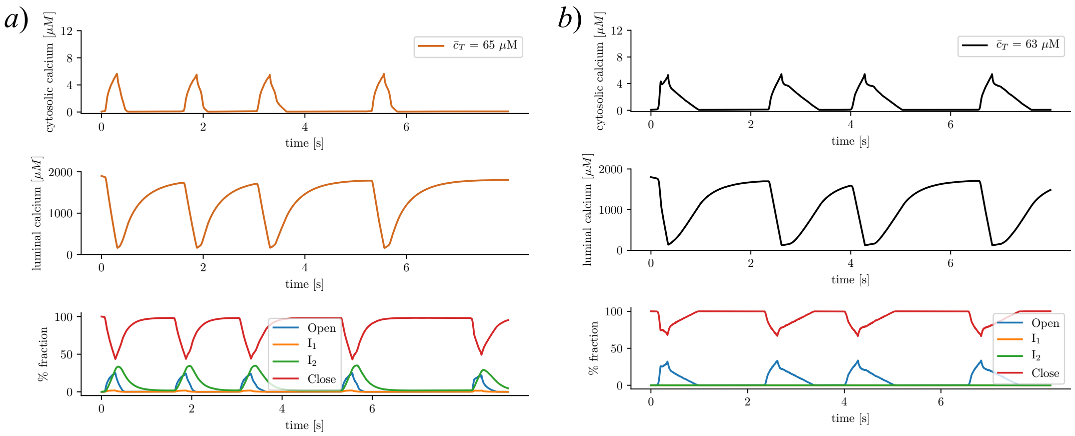

FIGURE B.1: **Role of inactivation in the onset of oscillations.** Periodic calcium waves in the subcellular model with (a) and without (b) inactivation. In the lower panel I show the fraction of RyR2s in the different states shown in Fig. 3.3. For the simulations in (b) I have set all the inactivation rates equal to zero.

List of publications and research activity

List of publications

- Marchena, M., & Echebarria, B. (2018). Computational model of calcium signaling in cardiac atrial cells at the submicron scale. Frontiers in physiology, 9, 1760.
- Marchena, M., & Echebarria, B. (2020). Influence of the tubular network on the characteristics of calcium transients in cardiac myocytes. PloS one, 15(4), e0231056.
- Marchena, M., Echebarria, B., Shiferaw, Y., & Alvarez-Lacalle, E. (2020). Buffering and total calcium levels determine the presence of oscillatory regimes in cardiac cells. bioRxiv. *Under revision*
- Tarifa, C., Vallmitjana, A., Llach, A., Herraiz, A., Jímenez-Sabado, V., Godoy-Marín, H., Nolla-Colomer, C., Echebarria, B., Marchena, M., Cabello, N., Ferrero-Gregori, A., Ginel, A., Viñolas, X., Montiel, J., Ciruela, F., Benítez, R., Cinca, J., & Hove-Madsen, L. (2020). Preferential subsarcolemmal calcium spark distribution potentiates arrhythmogenic electrical activity in patients with atrial fibrillation. *In preparation*
- Catala, M., Pino, D., Marchena, M., Palacios, P., Urdiales, T., Cardona, P., Alonso, S., Lopez-Codina, D., Prats, C. & Alvarez-Lacalle E. (2020). Robust estimation of diagnostic rate and real incidence of COVID-19 for European policymakers. medRxiv. *Under revision*
- Catala, M., Marchena, M., Conesa, D., Palacios, P., Urdiales, T., Alonso, S., Alvarez-Lacalle, E., Lopez-Codina, D., Cardona, P. & Prats, C. (2020). Short-term predictions and indexes to study covid19 pandemic evolution. *In preparation*

Research stays

- APRIL-MAY 2017: **California State University, Northridge (CSUN)**, Physics Department, in the group headed by Prof. Yohannes Shiferaw.

The transition to atrial fibrillation is a complex problem that involves many aspects. In particular, how a cluster communicates with other clusters is a crucial process that heavily determines the wave propagation conditions. With this in mind, we worked in a model to understand the onset of the wave propagation on a z-plane modelling the calcium dynamics.

- April-May 2018: **California State University, Northridge (CSUN)**, Physics Department, in the group headed by Prof. Yohannes Shiferaw.

  During the stay, I learned about theoretical techniques to treat the appearance of subcellular calcium waves and I developed a computational model to study the influence of these calcium waves on the initiation of arrhythmias.

Conferences

- September 1-2, 2016: **Workshop on Nonlinear Dynamics in Biological Systems**, Basque Center for Applied Mathematics (BCAM).

  The meeting will consist of sessions focusing on different topics: Heart Dynamics, Complex Chemical Systems, Cell Dynamics and Communication, Cell Motility and Active Particles, Complex Networks. Each session will include mathematical modelling as well as experimental or applied research.

- January 15-18, 2017: **1st Biology For Physics: Is There New Physics in Living Matter?**, Barcelona Biomedical Research Park (BBRP).

  The contents of the workshop were organized under the umbrella of a few selected themes which all shared the underlying playground of nonequilibrium physics which was at the core of living matter. Topics included: Physical principles of mechanochemical networks: new challenges for soft matter physics, Systems biology and self-organization: from active matter to cells and tissues, Stochastic thermodynamics: from single molecules to complex machinery, Physics of biological evolution: from the second law to the selection of structures.

- March 30 - April 1, 2017: **XXI Conference on Statistical Physics (FisEs'17)**, University of Sevilla.

  The conference covered a wide range of topics including traditional aspects of statistical mechanics, such as applications to hard and soft condensed matter, phase transitions, disordered systems and non-equilibrium physics, as well as emergent and modern applications such as turbulence, signal processing, complex systems and mathematics.

- June 19-22, 2017: **9th International Conference "ENGINNERING OF CHEMICAL COMPLEXITY"**, University of Barcelona, IN2UB.

  Chemical complexity in live systems.

- NOVEMBER 3-4, 2017: **Atrial Fibrillation (AF) Symposium: From Mechanisms to Population Science**, Centro Nacional de Investigaciones Cardiovasculares (CNIC).

  The main objective of the conference was to join together some of the leading experts in atrial fibrillation in Europe and the USA to present and discuss the latest developments in fundamental, translational, clinical and population sciences and technological advances in this field. On this occasion, the experts exchanged the latest data and knowledge on the advances in population genetics which have shown that there are genes closely related to the disease, which opens new perspectives in the knowledge of the molecular basis of atrial fibrillation, the most common heart rhythm disease in the world, which has a great impact on public health.

- OCTOBER 18-20, 2018: **XXII Conference on Statistical Physics (FisEs'18)**, Polytechnic University of Madrid.

  The conference covered a wide range of topics including traditional aspects of statistical mechanics, such as applications to hard and soft condensed matter, phase transitions, disordered systems and non-equilibrium physics, as well as emergent and modern applications such as turbulence, signal processing, complex systems and mathematics. *Best poster contribution award over 120 candidates.*

Seminars

- NOVEMBER 10, 2016: **Group seminar in Mathematical and Physical Biology**, Polytechnic University of Catalunya.

  Development of a computational model of calcium signaling in cardiac cells at the submicron scale.

- NOVEMBER 30, 2017: **Group seminar in Mathematical and Physical Biology**, Polytechnic University of Catalunya.

  Introduction to Ipython notebook.

- FEBRUARY 2, 2019: **Meeting of the research group Computational Biology and Complex Systems**, Polytechnic University of Catalunya.

  Influence of microstructure on excitation-contraction coupling in atrial cells.